

**The nerve of facial expression,
impact of its anatomical variations on
iatrogenic surgical injury and a novel
MRI diffusion weighted imaging
technique to image its intra-parotid
course**

2018

M.D.

Dr. Walid El Kininy

B.Dent.Sc, MFDS, MB, BCh, BAO, BA,

MRCS RCSI, Sch TCD

Declaration

I declare that this thesis has not been submitted as an exercise for a degree at this or any other university and it is entirely my own work.

I agree to deposit this thesis in the University's open access institutional repository or allow the library to do so on my behalf, subject to Irish Copyright Legislation and Trinity College Library conditions of use and acknowledgement.

Consent and ethical approval for imaging and research related dissection of cadaveric subjects was implied in the Donor's written approval for their donations to be contributed to teach, research and related imagery within the premises of Trinity College Dublin.

Approval for cadaveric imaging at Trinity College Dublin was sought and obtained from Trinity College Institute of Neuroscience management committee.

As part of our collaboration with the on-going REDEEM trial, all live subjects partaking in the study were enrolled onto the REDEEM trial for non-invasive diffusion weighted magnetic resonance imaging of the brain. Consent was obtained for extension of scanning to the head and neck to enable analysis of the parotid gland and facial nerve course. All images were analysed and signed off by the Professor of Radiology at Tallaght University Hospital, a TCD affiliated teaching hospital.

Summary

This doctorate in clinical medicine set out to assess how variations in facial nerve anatomy to the intra-parotid venous system could impact on surgical access to the parotid gland or the mandible, and explored methods to help reduce the risk of iatrogenic facial nerve injury. The vast majority of surgical descriptions in parotid or extra-oral mandibular surgery rely on the normally described relationship of the facial nerve to predefined surgical landmarks and intra-parotid venous structures.

Published reports on the incidence of the iatrogenic facial nerve injury vary widely according to speciality and institutions. What is known is that multiple specialities require the skills and knowledge to operate safely in or around the parotid gland where the extra-cranial facial nerve is put at risk. A recent systematic review of maxillofacial extra-oral access to the mandibular condyle, involving eight-multicentre studies showed incidence of iatrogenic facial nerve injury of up to 11%, with some studies suggesting incidence rates of up to 42% with particular approaches.¹ The impact of anatomical variation on surgical technique was not considered in any of the reports and neither was the potential for preoperative imaging of the facial nerve.

Imaging of the extra-cranial facial nerve has historically been extremely difficult despite the wide availability of imaging methods available today. Diffusion weighted magnetic resonance imaging of intracranial white-matter tracts has shown great success in recent years. The application of this method of imaging of extra- central nervous system neural tracts is now being explored. This doctorate aims to assess the feasibility of reproducing the facial nerve white-matter tract as it courses through the parotid gland.

The first arm of this doctorate research project involved detailed dissections of the facial nerve in a cohort of cadaveric subjects donated to the anatomy department of Trinity College Dublin. Facial nerve variation to predefined surgical landmarks and intra-parotid venous structures was analysed with respect to potential impact on surgical technique. A novel, previously unreported variation of the facial nerve and the superficial temporal vein was discovered, and subsequently published.

The second arm of this doctorate research project involved the collaboration between this Doctorate research project in the department of anatomy and the neuroscience Institute's PhD level REDEEM trial, Trinity College Dublin. As part of this collaboration, cadaveric diffusion weighted magnetic resonance imaging of the head and neck was undertaken, followed by detailed dissections of the facial nerve. Extra-cranial facial nerve tracts were identified and anatomically validated. The imaging parameters used were successfully applied to live subjects with disease free parotid glands, thereby proving the feasibility of imaging the extra-cranial facial nerve tract. The profound clinical implications of this are elaborated, especially in the context of helping avoid iatrogenic facial nerve injury, where prevention far outweighs the limited and arduous possibility of nerve repair and cure.

Acknowledgements

First and foremost, I would like to thank God for the wisdom, patience and the foresight to enable completion of this project. I would like to thank my wife, Mary for her continued support throughout this busy period while pregnant herself and subsequently for taking full care of our new-born son, Adam, to enable my completion of the project. Additionally, I would like to thank my parents for their full and unwavering support, especially my Father, who underwent major surgery during the time of this project, but while still, was fully supportive and in constant prayer for me.

I would like to thank my supervisor, Dr. Denis Stephen Barry, whose support and help was available throughout the project. Additionally, I would like to thank Professor Leo F A Stassen, Professor / Chair of Oral & Maxillofacial Surgery, Trinity College Dublin for the help with initial plan to undertake this project, and guidance throughout.

From the department of Anatomy of Trinity College Dublin, I would like to thank the head of the department, Dr. Nick Mahony for allowing successful collaboration with another department, and scanning of the donors outwith the Anatomy building. I would also like to mention my gratitude to the senior technical staff of the department, Siobhan and Phil, who were of great help with timings of dissections, budgetary matters and facilitating the training of the TCIN staff to enable scanning at the Neuroscience Institute and arranging the transfer of the donors across for scanning. Additionally, a great thank you to Mary and Claire who were instrumental for the daily running of the project at ground level without any delays.

I would also like to thank a close colleague and personal friend, Dr. Shane Davy, who was instrumental in assisting with the project throughout all its stages. His assistance in the dissections, the transfers of donors to and from the Anatomy department to the Neuroscience institute and the MRI data reading and analysis was greatly appreciated.

I would also like to thank Dr. Aisling O'Mahony, Dr. Daniel Shanley and Dr. Lylas Aljohmani for their continued support throughout the project and for volunteering to participate in the scanning process for the imaging feasibility study.

From the Neuroscience institute's REDEEM trial, with whom a successful and fruitful collaboration was created, I would like to particularly like to thank Dr. Darren Roddy, PhD student of the DWI arm of the trial, for his help and support with setting up the collaboration, facilitating the approval from TCIN management committee, arranging the scanning dates with the relevant staff and helping with the post processing of the imaging data. In addition, I would also like to thank Dr. Erik O'Hanlon, postdoctoral researcher and image analyst for his help with the scanning parameters and imaging process. Overall thanks to Professor Veronica O'Keene, supervisor of the REDEEM trial and TCIN management committee member, who was in favour of, and allowed the successful collaboration to bear fruit.

Great appreciation is extended to Professor William Torregiani of Tallaght University Hospital Radiology Department and Dr. Alison Hurley, principal neuroradiologist of the same department for their guidance and corroboration of the imaging results.

Publications resulting from this work

Peer reviewed publication

Novel variations in spatial relations between the facial nerve and superficial temporal and maxillary veins

Walid El Kininy, Shane Davy, Leo Stassen, Denis Stephen Barry
Folia Morphol (Warsz). 2018. doi: 10.5603/FM.a2018.0019

Variations in the relationship of the retromandibular vein to the facial nerve have been widely reported due to their relevance for surgical approaches in parotid, osteotomy and mandibular condyle surgery. In the context of the retromandibular retroparotid approach, remaining deep to the retromandibular vein is advised to decrease the likelihood of encountering the facial nerve during mandibular condyle surgery.

In the present report, an unusual variant of the superficial temporal vein lying superficial to the facial nerve is described. This represents a variation of the venous branching pattern within the parotid gland, whereby the superficial temporal vein joins the maxillary vein inferior to its usual communication. These findings are discussed in the context of commonly used surgical approaches to the mandible for condylar trauma, or osteotomy surgery.

Abstract publication

Spatial variations in the arrangement of the facial nerve within the parotid gland and its relationship to the retromandibular vein, and the analysis of its anatomic significance to the extra-oral surgical approaches to the mandibular condyle

W. El Kininy, S. Davy, D. Barry and L. F. A. Stassen
(2017), *Anatomical Society Winter meeting, King's College London, London 2016*. *J. Anat.*, 231: 445-468. doi:10.1111/joa.12637

B14, Trinity College Dublin Anatomy Department, Ireland

The mandibular condyle presents a surgical region fraught with risks to the facial nerve. In traumatic settings, the mandibular condyle fracture is a controversial area of discussion in terms of the most appropriate management – either open or closed reduction. Historically, the majority of these fractures were managed with closed reduction; however, there is a growing body of evidence to support open treatment.

A gap exists in the literature as to the impact of facial nerve variations or variations of the facial nerve to the retromandibular vein on the various approaches to the mandibular condyle. The current extra-oral surgical approaches grossly rely on the normal position and divisions of the facial nerve and the retromandibular vein as a landmark and guide.

As part of an MD on the impact of facial nerve variation in mandibular condyle surgery, using 13 donors (eight female, five male) donated as part of the anatomy teaching programme in the Department of Anatomy, TCD –twenty six parotid glands will be dissected to elucidate any variations within this Irish population of donors. Fourteen parotid glands dissections have already been performed.

Provisional results have shown significant variations: 21% have shown variation in the relationship of the facial nerve to the intra-parotid venous structures. In one case, the facial nerve main trunk was found deep to the superficial temporal vein (STV), exiting between it and the maxillary vein (MV), continuing superficial to the MV. This particular variation has not been reported previously in the literature.

We report on the current literature and discuss our provisional results on facial nerve variation.

Consent for dissection of the human donors with imagery of their facial nerves was obtained for each individual donor under the voluntary consent process provided by each donor when signing onto the Trinity College Anatomy Department donor programme prior to their death. The consent form explicitly states that dissections for teaching and research along with appropriate imagery are allowed.

Presentations resulting from this work

Oral Presentations

3-Dimensional tractography of the extracranial facial nerve course using diffusion weighted Magnetic Resonance Imaging

*El Kininy W, Roddy D, Davy S, O'Keane V, O'Hanlon E, Stassen LFA & Barry D
ABAOMS Annual Conference, Liverpool, 15th -17th November 2017*

3-Dimensional tractography of the extracranial facial nerve course using diffusion weighted Magnetic Resonance Imaging

*El Kininy W, Roddy D, Davy S, O'Keane V, O'Hanlon E, Stassen LFA & Barry D
Anatomical Society Meeting, 18-20th December, Dundee, Scotland*

Table of Contents

Declaration.....	i
Summary.....	ii
Acknowledgements.....	iv
Publications resulting from this work.....	v
Presentations resulting from this work.....	vi
Table of Contents.....	vii
List of Figures.....	xi
List of Tables.....	xiii
Abbreviations.....	xiv
Chapter 1. Background.....	1
Chapter 2. Facial nerve positional variation, its surgical identification and the variation to intra-parotid venous structures.....	8
2.1 Introduction.....	8
2.2 Materials and method.....	13
2.3 Results.....	17
2.3.1 ‘Safe zone’ pre-auricular approach.....	18
2.3.2. Tragal pointer to main trunk.....	19
2.3.3 Results – Angle of mandible to main trunk.....	21
2.3.4 Intra-parotid venous variation to the facial nerve.....	22
2.4 Discussion.....	30
2.4.1 ‘Safe zone’ – temporal branch to pre-auricular line.....	30

2.4.2 Tragal pointer.....	31
2.4.3 Angle of mandible to main trunk.....	34
2.4.4 Intra-parotid venous variation to the facial nerve	36
2.4.6 Conclusion.....	45

Chapter 3 – Diffusion Weighted Tractography of the extra-cranial facial nerve course.....46

3.1 Background.....	46
3.1.1 Extra-cranial facial nerve imaging.....	46
3.1.2 Clinical Implications.....	47
3.1.3 Diffusion Imaging.....	50
3.1.4 Aims and Objectives.....	52
3.2 Materials and Methods.....	53
3.2.1 Cadaveric scan & dissection.....	53
3.2.2 Donor embalming technique.....	54
3.2.3 Dissection technique.....	56
3.2.4 Imaging protocol used and post-processing analyses.....	57
3.2.4.1 Anatomical (T1) imaging.....	57
3.2.4.2 Diffusion Weighted Imaging (DWI).....	57
3.2.4.3 DTI data pre-processing.....	58
3.2.4.4 Post-processing Head and Neck tractography.....	59
3.3 Results.....	60
3.3.1 Cadaveric scan 1 - right facial nerve.....	60

3.3.1.1 Dissection.....	60
3.3.1.2 Diffusion tractography.....	61
3.3.2 Cadaveric scan 2 – right facial nerve tractography.....	67
3.3.2.1 Dissection.....	67
3.3.2.2 Diffusion tractography.....	70
3.3.3 Cadaveric scan 2 – left facial nerve tractography.....	73
3.3.3.1 Dissection.....	73
3.3.3.2 Diffusion Imaging.....	75
3.3.4 Live subject scan results.....	80
3.3.4.1 Live subject A.....	80
3.3.4.2 Live subject B.....	85
3.4 Discussion.....	88
3.4.1 Cadaveric scan 1 – right facial nerve.....	88
3.4.2 Cadaveric scan 2 – right facial nerve.....	96
3.4.3 Cadaveric scan 2 – left facial nerve.....	101
3.4.4 Clinical applicability to live subject scans.....	104
Chapter 4 - Conclusion.....	110
References.....	117
Appendix 1 Peer Reviewed Publication.....	123
Appendix 2 Dodge Dis-Spray.....	135
Appendix 3 Dodge Metaflow.....	138
Appendix 4 Dodge Rectifiant.....	140
Appendix 5 Dodge Introfiant Arterial.....	142

Appendix 6 Dodge Restorative.....	146
Appendix 7 DWI Data pre processing.....	148

List of Figures

Figure 1 Labeled auricle (left). Tragal pointer highlighted with red hat pin (right).....	11
Figure 2 Facial nerve dissection technique.....	15
a) Extended pre-auricular incision marked,	
b) Subcutaneous tissue plane superficial to SMAS layer,	
c) Terminal buccal branch identification,	
d) Retrograde dissection to main trunk and 2 divisions,	
e) Completed dissection of facial nerve	
Figure 3 Measured distances in mm between point of crossing of most posterior branch of temporal branch of facial nerve on malar arch to pre auricular line on malar arch.....	18
Figure 4 Measured distances in mm from the tragal pointer to the point of bifurcation of the main trunk of the facial nerve.....	19
Figure 5	20
a. Top left – Bifurcation of facial nerve (FN) posterior to tragal pointer	
b. Top right – Bifurcation of FN in line with tragal pointer in sagittal plane	
c. Right – Bifurcation of FN anterior to tragal pointer in sagittal plane	
Figure 6 Distance of angle of mandible to point of bifurcation of main trunk of facial nerve.....	21
Figure 7 Retromandibular vein superficial to one or more branches of facial nerve.....	23
a) Cervicofacial division of facial nerve (FN) deep to retromandibular vein	
b) Cervicofacial division of facial nerve (black) deep to retromandibular vein (blue) schematic	
c) Cervicofacial division of facial nerve deep to RMV	
d) Cervicofacial division of FN (black) deep to RMV (blue) schematic	
Figure 8 Neural ring of facial nerve around retromandibular vein.....	24
a) Main trunk of facial nerve deep to RMV	
b) Schematic of relation of vein to nerve	
c) RMV reflected anteriorly to show FN trunk superficial to vein	
d) RMV reflected posteriorly in fig 7d (right) to demonstrate FN trunk deep to vein	
Figure 9 Superficial temporal vein superficial to temporal branch of facial nerve.....	25
a) Superficial temporal vein runs superficial to temporal branch of facial nerve	
b) Schematic showing the venous structures (blue) with the STV superficial to the temporal branch of the facial nerve (black)	
Figure 10 STV superficial to main trunk.....	26
a. Superficial temporal vein superficial to facial nerve main trunk	
b. Schematic showing facial nerve (black) and venous structures (blue).	
c. Superficial temporal vein superficial to main trunk of FN (opposite side of same cadaver)	
d. Schematic showing FN (black), intra parotid venous system (blue).	
Figure 11 STV superficial and tightly adherent to FN main trunk (a-d depicting one cadaver)...	27
a. STV superficial to all facial nerve branches. Confluence of STV and MV shown	
b. STV lifted showing superficial nature of vein to the facial nerve	
c. STV removed showing facial nerve main trunk	
d. Schematic of FN in black and venous structures in blue	
Figure 12 STV superficial and tightly adherent to FN main trunk (a-f depicting one cadaver).....	28
a. Labeled superficial parotid dissection of variation with scale	
b. Unlabeled sided schematic of facial nerve variation	
c. Schematic of facial nerve variation	
d. Labeled dissection showing the FN variation with STV reflected inferiorly	
e. Unlabeled dissection showing the FN variation with STV reflected inferiorly	
f. Enhanced image of superficial parotid dissection	
Figure 13 ExploreDTI data conversion tool.....	59
Figure 14 Scan cadaver scan 1 right dissection technique.....	61
a. Extended pre auricular approach to parotid gland	
b. Skin & subcutaneous tissue was lifted & identification of the buccal division	
c. TF division of facial nerve exposed showing zygomatic and temporal branches.	
d. Entire facial nerve with five terminal divisions.	
Figure 15 Scan cadaver 1 right T2 MRI with tractography overlay.....	62

a. ROI in blue drawn at the stylomastoid foramen anatomical site on a T2 overlay	
b. Cervicofacial division of the facial nerve isolated using ROI seed gate (blue).	
c. Sagittal view of cervicofacial trunk of facial nerve	
Figure 16 Scan cadaver 1 right comparable segment of tract to anatomic dissection.....	63
• Comparable segment (red) of cervicofacial trunk – coronal view	
• Sagittal view of cervicofacial trunk comparable segment (red)	
Figure 17 Scan cadaver 1 right temporofacial division tractography.....	64
a. Sagittal view of temporofacial ROI gate	
b. Coronal view of full facial nerve tract (CF and TF divisions) with both stylomastoid and temporofacial ROI seed gates (blue).	
c. Coronal view of temporofacial tract only with temporofacial ROI seed gate (blue)	
Figure 18 Sagittal view of TF ROI gate. Tract showing evidence of both CF and TF trunks.....	65
Figure 19 Both TF and CF tracts superimposed.....	66
a. Sagittal view	
b. Coronal view	
Figure 20 Scan cadaver 2 right dissection technique.....	68
a. Extended pre auricular incision pre marked	
b. Plane superficial to SMAS – terminal buccal branch identified	
c. Retrograde dissection of buccal terminal branch	
d. Completed dissection of facial nerve showing both divisions	
Figure 21 Scan cadaver 2 right fully labelled completed dissection.....	69
Figure 22 Scan cadaver 2 right axial and sagittal views of ROI gate placed at SM foramen.....	70
Figure 23 Scan cadaver 2 right coronal and sagittal views of tracts analysed through SM gate.	
‘And’ ROI gate placed to isolate most dense, anatomically relevant portion of tract.....	71
Figure 24 Scan cadaver 2 right corono-sagittal & axial view of isolated cervicofacial tract.....	72
Figure 25 Scan cadaver 2 left dissection technique.....	73
a. Extended pre auricular incision marked	
b. Subcutaneous tissue plane superficial to SMAS layer	
c. Terminal buccal branch identification	
d. Retrograde dissection to main trunk and 2 divisions	
Figure 26 Scan cadaver 2 left completed dissection.....	74
Figure 27 Scan cadaver 2 left ROI & tract superimposed on T1 overlay.....	75
a. Axial view of stylomastoid foramen ROI gate (blue)	
b. Coronal view of analysed tract involving stylomastoid foramen ROI gate	
c. Lateral corono-sagittal view of tracts	
d. Medial corono-sagittal view of tracts	
Figure 28 Scan cadaver 2 left ‘NOT’ gates.....	76
a. ‘NOT’ ROI (red) placed along sagittal axis	
b. Medial aspect of ‘NOT’ ROI gate in red	
Figure 29 Scan cadaver 2 left post ‘NOT’ analysis.....	77
a. Sagittal view of tract not involving sagittal ‘NOT’ ROI	
b. Coronal view of tract not involving sagittal ‘NOT’ ROI	
Figure 30 Scan cadaver 2 left filtration of ‘SEED’ ROI.....	78
a. ‘SEED’ ROI gates (blue) consolidated to 2 separate gates to isolate the 2 main tracts traversing SMF.	
b. Coronal view of new (blue) tracts analysed through consolidated SM ‘SEED’ ROI. White tracts – remaining spurious tracts through original ‘SEED’ ROI.	
c. Sagittal view of new (blue) consolidated tracts through revised ‘SEED’ ROI. White – spurious	
Figure 31 Scan cadaver 2 left facial nerve tract post processing of DWI image.....	79
Figure 32 Live subject A stylomastoid ROI.....	80
a. Posterior coronal view of SM foramen ‘seed’ ROI (blue)	
b. Posterior coronal view with axial slice to show 3D location of SM foramen	
Figure 33 Live subject A initial tracts.....	81
a. Sagittal view of resultant tracts emerging through stylomastoid (SM) ROI gate (blue)	
b. Coronal view of same tracts – dense appearing tracts with large medial extension	
c. Axial view of subsampled tracts of the order of 2:1 showing large element of tracts coursing medial to mandibular ramus (shown). SM foramen ROI gate (blue) also shown	
Figure 34 Live subject A ‘NOT’ gate.....	83
a. Axial view of tract with ‘seed’ ROI (blue) and two ‘not’ ROI gates (red)	
b. Coronal view of anterior ‘not’ ROI gate to exclude tracts coursing medial to mandible	
c. Axial view of new tract (coloured) superimposed on old white tract.	
Figure 35 Live subject A fully analysed tracts.....	84

a. Axial section of fully analysed, labeled facial nerve tract.	
b. Sagittal section of fully analysed, labeled tract	
Figure 36 Live subject B.....	86
a. Axial view of stylomastoid foramen seed ROI (blue).	
b. Axial view of ROI with tracts in situ	
Figure 37 Live subject B tracts.....	87
• Sagittal section of resultant tract	
• Coronal section of resultant tract	
Figure 38 Scan cadaver 1 right point to point calibrated anatomical measurement.....	89
Figure 39 Scan cadaver 1 right coronal view of tract measurement.....	90
Figure 40 Scan cadaver 1 right TF anatomical analysis.....	93
Figure 41 Scan cadaver 1 right TF tract analysis.....	94
Figure 42 Scan cadaver 1 right all tracts combined.....	95
Figure 43 Scan cadaver 2 right tract analysis.....	97
a. Labelled tractography image of bifurcation and cervicofacial division	
b. Red segment signifies portion of CF division from point of bifurcation to turn of tract	
Figure 44 Scan cadaver 2 right anatomical validation.....	99
Figure 45 Scan cadaver 2 right tract compared to anatomical dissection.....	100
a. Highlighted anatomic dissection of CF division with scale, correlated to imaging tract	
b. Corresponding diffusion imaging tract highlighted in red	
Figure 46 Scan cadaver 2 left tract analysis.....	101
a. Complete facial nerve as per DWI analysis	
b. CF division only colour coded to signify different measurements made from bifurcation	
c. Sagittal view of CF division only with colour coded measured segments	
Figure 47 Scan cadaver 2 left anatomical validation.....	103
Figure 1 (publication) Variant facial nerve to STV.....	133
Figure 2 (publication) Normal facial nerve.....	134

List of Tables

Table 1 Tource & Vacher classification.....	10
Table 2 Demographic data of cadaveric donors included in the study.....	13
Table 3 Relationships of the point of bifurcation of the dissected facial nerve trunk to the tragal pointer and respective percentages.....	20
Table 4 Variation of intra parotid venous structures to the facial nerve.....	22
Table 5 Facial nerve and retromandibular vein variants classification.....	37
Table 6 Scan cadaver 1 right anatomical measurement.....	88
Table 7 Scan cadaver 1 right tract metrics.....	91
Table 8 Scan cadaver 1 right both tract FA values.....	95
Table 9 Scan cadaver 2 right tract metrics.....	98
Table 10 Scan cadaver 2 left tract metrics.....	102
Table 11 Scan cadaver 2 left anatomical measurement.....	103
Table 1 (publication) Facial nerve and retromandibular vein variants classification.....	132

Abbreviations

A.B, Anastomosing branch.
ADC, Apparent Diffusion Coefficient
B, Buccal branch
C, Cervical branch
CF, Cervicofacial
CSD, Constrained Spherical Deconvolution
DICOM, Digital Imaging and Communications in Medicine
DTI, Diffusion Tensor Imaging
DWI, Diffusion Weighted Imaging
EAM, External Auditory Meatus
EPI, echo-planar imaging
FA, Fractional Anisotropy
FOD, Fibre Orientation Distribution
HARDI, High Angular Resolution Diffusion Imaging
J, Junction of STV and MV
M or MM, Marginal mandibular branch
Matlab, Matrix Laboratory
MRI, Magnetic Resonance Imaging
MV, Maxillary vein
NifTI, Neuroimaging Informatics Technology Initiative
PMI, Post-mortem interval
REDEEM,
ROI, Region Of Interest
RV / RMV, Retromandibular vein
RV(r), Retromandibular vein reflected
SE EPI, spin-echo echo-planar imaging
SI, Scan interval
SMAS, Superficial Masseteric Aponeurosis System
SMF, Stylomastoid foramen
STV, Superficial Temporal Vein
T, Temporal branch
 T_2 vs T_2^* , True T_2 relaxation vs Observed T_2 relaxation
TF, Temporofacial
TP, Tragial Pointer
XML, Extensible Markup Language
Z, Zygomatic branch

Chapter 1. Background

The facial nerve is the seventh cranial nerve, whose motor branches are predominantly within its distal, extra- cranial segment. The extra-cranial segment, after exiting through the stylomastoid foramen, quickly enters the parotid gland after giving off the nerves to the stylohyoid muscle and posterior belly of digastric muscle. From here, the facial nerve courses as a main trunk in the tightly encapsulated parotid gland, and divides initially into two main divisions – the temporo-facial and cervico-facial divisions. These upper and lower divisions respectively, further subdivide in varying patterns to provide the five terminal branch bundles – temporal, zygomatic, buccal, marginal mandibular and cervical, that provide motor innervation to the muscles of facial expression. Within the gland the branches of the facial nerve run in different directions corresponding with their destinations, i.e. scalp, eyelids, mid-face, lower face and neck, and they do so in superficial and deep planes. There is no specific, developmentally determined plane in which the facial nerve branches pass between superficial and deep lobes of the gland. Within the gland the nerve branches communicate with each other, forming a plexiform arrangement that lies superficial to the retromandibular vein, which in turn is superficial to the external carotid artery.

The retromandibular vein is formed within the parotid by the confluence of the superficial temporal and maxillary veins. The retromandibular vein emerges from the lower part (pole) of the gland and divides into an anterior branch, which joins the facial vein, and a posterior branch, which joins the posterior auricular vein to form the external jugular vein. However, the retromandibular division may occur within the gland with the two branches emerging from the lower pole.

Multiple specialities and surgeries require the skills to operate on and through the parotid gland. The myriad of procedures that require access to facial areas, where a facial nerve injury can be a complication, include maxillofacial procedures to access the mandible extra orally in traumatic settings to reduce fractures of the condylar head or neck and in elective settings to replace the temporomandibular joint or carry out orthognathic mandibular movements.^{1,2} Head and neck procedures involving varying depths of parotidectomy in order to

remove parotid pathologies, whether benign or malignant also pose risk of iatrogenic facial nerve injury.^{1,3} Otologic surgery in the form of tympanomastoidecomy can be a risk to the facial nerve main trunk.^{1,4} Another realm of surgeries that require care of the facial nerve is cosmetic surgeries where facelifts can be performed via deep plane rhytidectomies, where flap elevation is required over the anterior border of the parotid gland and the large facial nerve branches are exposed and placed at risk.^{1,5,6}

Iatrogenic surgical facial nerve injury is a devastating complication that results in an inability to perform volitional mimetic facial expression movements which can provoke considerable anxiety.⁷ Emotions are conveyed through facial expression, a motor function of the facial nerve. Happiness can be expressed by the use of subtle smiles using the orbicularis oris muscle. Confusion can be expressed by a subtle eye brow shift using the occipitofrontalis muscle. Frustration can be expressed by the slight wrinkling of the nose.⁸ A more pressing concern in facial nerve injury is the ipsilateral diminished blink reflex, meaning that the cornea may dry, and ultimately ulcerate. Without a regain in function of the facial nerve, the patient will have to wear an eye patch for a lengthy period and may require upper-lid weights or canthopexy surgery to allow closure of the upper eyelid.⁸ Repair of the facial nerve, if attempted in these cases, is not always guaranteed. The mimetic facial expression muscles undergo atrophy and fibrosis roughly twelve months

after denervation.⁵ Considering that nerves regrow at a rate of approximately 1 mm per day⁹, and that the distance between an injured main trunk and a distal motor endplate may be 12 cm or more – the lack of expedient management may result in life long sequelae.¹ Hence, the overall message is one of prevention, rather than cure of iatrogenic injury.

The incidence of iatrogenic facial nerve injury in the respective surgeries is overall, poorly reported in the literature. Hohman et al. in 2014¹, reported a decade's worth of retrospective analysis of iatrogenic facial nerve injury that was referred to their centre – the Massachussets Eye and Ear Infirmary Facial Nerve Centre, Boston, Massachussets. The aim of their retrospective study was to assess the procedure-specific incidence, risk factors, and injury patterns in patients with iatrogenic facial nerve injury as seen at a tertiary care facial nerve center. Of 1810 patient records analysed, one hundred and two were deemed to have suffered iatrogenic facial nerve injury during surgery that required tertiary referral for repair.

The most common reason for injury of the facial nerve were within the category of TMJ, congenital and traumatic deformity surgical procedures, accounting for 40% of all the facial nerve iatrogenic injuries. A large proportion of these injuries were related to TMJ replacement operations, comprising 68% of injuries within this category, with the majority of these injuries affecting the frontal branch. Half of all the TMJ operations in the series were revision surgeries. Repair of mandibular fractures resulted in 20% of maxillofacial surgical facial nerve injuries; orthognathic surgery and procedures for congenital deformities each accounted for 5%, and a single case of ameloblastoma extirpation comprised the remaining 2% of iatrogenic facial nerve injury in the category of TMJ/traumatic deformity.

Resection of benign head and neck lesions accounted for the second most common cause of iatrogenic facial nerve injuries, resulting in 25% of all the referred injuries.¹ Parotidectomy for benign lesions was the most common cause of injuries within this category, resulting most frequently in complete hemifacial weakness. Other benign lesions that contributed to iatrogenic facial nerve injury within the Head and Neck category included resection of congenital anomalies such as lymphatic and vascular malformations, haemangiomas, and branchial cleft cysts, resulting in 20% of injuries. Lymphadenectomies, lipoma excisions and submandibular gland removal accounted for the rest. Malignant head and neck lesions were excluded from the study as it was found that most had undergone contingency planning for primary neuroorrhaphy or interposition grafting, thereby eliminating the need for referral to a tertiary referral centre.

Otologic surgery resulted in 17% of all referred facial nerve injuries, a hundred percent of which affected the full hemiface. Mastoid surgery in general, comprising tympanomastoidectomy procedures, cochlear implantation, mastoid obliteration, endolymphatic sac shunting, labyrinthectomy, and glomus tumor resections, accounted for the majority of facial nerve injury in this category.

Cosmetic surgery, accounted for 11% of all injuries in the studied series. The majority of these cases were rhytidectomy procedures, but did also include neck liposuction in a female, chin implant placement in a male, chin implant removal in a male, and mandibular feminization after gender reassignment. Most of the cosmetic surgery facial nerve injuries were specific to one of the main branch bundles of the facial nerve to where the surgery was localised.

While the above study is in no way conclusive in its level of evidence, what it does show is that facial nerve injury is a common phenomenon across the surgical spectrum. It identifies that as a whole, unintentional facial nerve injury due to surgical intervention is poorly studied, and is overall more common than expected. Most of the literature on the subject is specialty specific, and hence does not provide an overall appreciation of the risks involved and does not provide the opportunity for inter specialty communication and education. Additionally, the study highlights the increased risks of injury in revision surgeries – at times double the risk as shown in other studies.^{4, 10, 11} The reason is the scarring and the resultant disordered anatomy which can be confusing and dangerous to surrounding vital structures, intra operatively.¹

One of the reasons cited for the alarmingly high rate of facial nerve injury in maxillofacial procedures to access the mandible is due to the fact that the literature does not routinely advocate identification of the facial nerve, but rather its avoidance by dissection along fascial planes.¹² In addition, the small 1-2cm retromandibular incisions used to access the mandibular condyle or body would make it difficult to appreciate the facial nerve branching pattern and thereby poses risk to branches that may not be visible.¹³ These surgical approaches tend to rely on conventional anatomy of the facial nerve and its relationship with the surrounding venous structures.^{13, 14} Any variation to the facial nerve or its relationship to the surrounding venous system could therefore pose a considerable risk of unintended facial weakness to patients undergoing emergency traumatic or elective extra-oral surgery to the mandibular condyle.^{13, 14}

Extra-oral surgical access to fractured mandibular condyles – a treatment that is becoming increasingly popular due to the development of rigid fixation techniques¹⁵⁻¹⁷, is one of the most common extra-oral procedures to the mandible seeing as the condyle is the most frequently fractured segment in mandibular trauma¹⁵⁻¹⁹. A recent meta-analysis by E.A.

Al-Moraissi et al, in 2018 ¹⁶ assessing the rate of facial nerve injury in a total of 3873 patients across 96 studies of mandibular condylar fixation after trauma found an overall rate of injury of 8 – 14% with the more traditional surgical approaches to the mandibular condyle. These include the submandibular, pre-auricular and retromandibular transparotid approaches.

Through this Doctorate in Clinical Medicine, we investigate whether anatomical variation in the relationship of the facial nerve to surrounding venous structures could have an impact on surgical technique – both for Maxillofacial and Head and Neck procedures, by the use of venous landmarks. The variations found in a cohort of Irish cadaveric donors to the department of Anatomy, Trinity College Dublin were investigated and compared to the variations already described in the literature. We describe a novel variation of the superficial temporal vein to the facial nerve, which has not been described in the literature or in existing venous variation classification systems to the facial nerve. We include a case review describing this variant and its importance to surgical approaches, especially in parotidectomy procedures. ¹³ Our results of anatomic dissection of a cohort of Irish cadaveric donors of distances between some of the most accessible hard and soft tissue landmarks to the facial nerve main trunk were compared to the distances already established in the literature to identify whether such landmarks could help prevent facial nerve injury during anterograde parotidectomy procedures.

This Doctorate presents a novel approach to imaging the extra-cranial course of the facial nerve using diffusion weighted magnetic resonance imaging. By imaging and tracking the course of the extra-cranial path of the facial nerve, a case is made for the use of this increasingly popular imaging technique for pre-operative diagnosis and three dimensional planning, so as to prevent iatrogenic facial nerve injury during surgery. This may be

especially useful during revision surgery, where the standard anatomical landmarks may not be as visible or reliable. A detailed analysis of the cadaveric scanning procedure and the resultant radiological facial nerve tracts are compared to meticulous facial nerve dissections of the same cadaveric specimens. The scanning parameters most successful were then used in disease free parotid, healthy individuals to assess and produce accurate in-vivo tractography of the extra-cranial course of the facial nerve, and thereby derive a simple imaging protocol that can be clinically applied to most magnetic resonance scanners to produce the facial nerve tract as it courses through the parotid – an imaging function that has historically difficult to achieve.²⁰

Chapter 2: Facial nerve positional variation, its surgical identification and the variation to intra-parotid venous structures

2.1 Introduction

A precise knowledge of facial nerve anatomy and its varied branching patterns is critical to successful parotid and mandibular condyle surgery, both traumatic and elective. However, the facial nerve branching patterns and its relationship with the retromandibular vein has shown considerable variation in published reports ^{14, 21-23}. The observed relationship between the retromandibular vein and facial nerve has been classified into six types ²³ (Table 1). The retromandibular vein was found to be situated medial/deep to the facial nerve in the majority of the cases (Type 1 – the normal configuration) and lateral/superficial to it in up to 28% of cases (Type 2 – the ‘variant patterns’). Types 3 to 6 of this classification system constituted subtypes of Type 2.

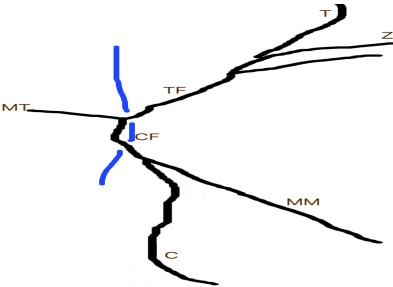
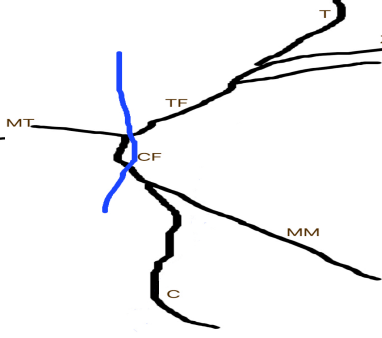
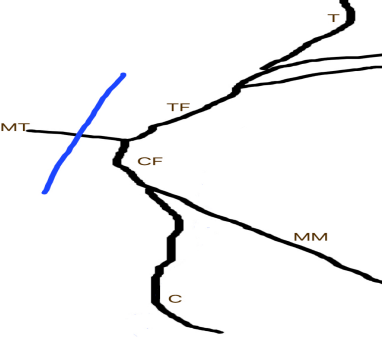
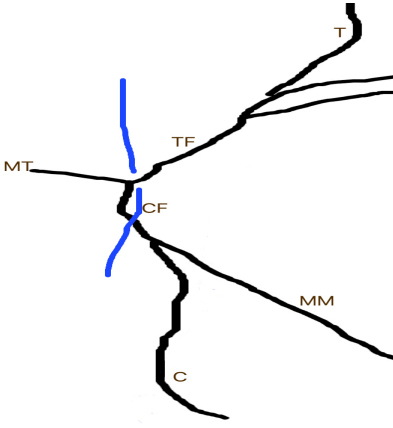
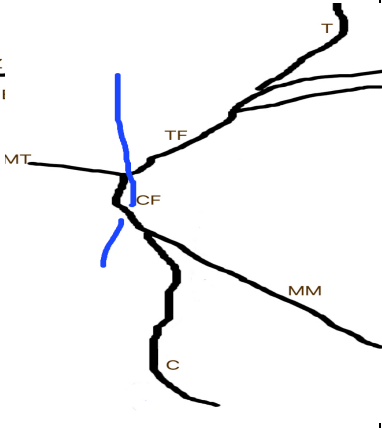
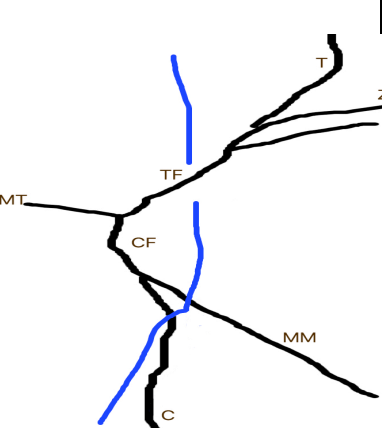
<p>Type 1: RMV (blue) lies medial to the whole facial nerve (facial nerve main trunk and its branches)</p> 	<p>Type 2: RMV lateral to the facial nerve</p> 	<p>Type 3: RMV is lateral to the main trunk</p> 
<p>Type 4: RMV is lateral to the cervicofacial division only</p> 	<p>Type 5: RMV is lateral to the temporofacial division only</p> 	<p>Type 6: RMV is lateral to some of the branches of the cervicofacial division</p> 

Table 1 – Toure & Vacher classification – MT, main trunk, TF, temporofacial, CF, cervicofacial. T,Z,B,MM,C – distal branches

During mandibular condyle or ramus surgeries, multiple approaches can be used and the choice often depends on the location of the fracture site on the mandible in traumatic settings or the area of surgical interest of the ramus in elective settings.²⁴ The surgical approach is often dictated by the level of confidence of the operating surgeon with a particular approach.²⁵ No consensus has been reached as to the most appropriate approach to the mandibular condyle, with each one posing a risk to the facial nerve or one of its branches.² Most techniques rely on an incision that is considered to be safe, and free of facial nerve morbidity. Most commonly, this may be the reliance on the ‘safe zone’ as shown by Alkayat & Bramley²⁶ in 1979 during the pre-auricular approach, or the position

of the retromandibular vein, which is expected to be deep to the facial nerve.²⁷⁻²⁹ By remaining deep to the retromandibular vein during, for example, the commonly used retromandibular approach to the mandibular condyle, it is expected that you will remain deep to the facial nerve.¹⁴ Overall the current extra-oral surgical approaches grossly rely on the normal position and divisions of the facial nerve and the retromandibular vein as a landmark and guide.³⁰

For the purposes of parotid resections, early recognition of the facial nerve is paramount so as to avoid inadvertent injury. With the advantage of the ‘wide front’ views provided by raising the skin flap to expose the parotid gland, the facial nerve can be exposed in its entirety by careful dissection, thereby reducing the risk of damage to the facial nerve – an advantage of direct visualization of the nerve.¹ However, the initial identification of the facial nerve can be difficult with several different approaches and landmarks widely described solely for the initial identification of the facial nerve trunk.^{31, 32} Despite this, there is no consensus as to the best possible landmark to help identify the main trunk of the facial nerve during the commonly used anterograde approach. These landmarks include the tragal pointer, angle of mandible, attachment of the posterior belly of digastric muscle, tympanomastoid suture, external auditory canal, transverse process of the axis and styloid process.³¹

In this study, twenty six facial halves were dissected and analysed with specific focus given to the most commonly used landmarks for both parotid and mandibular surgeries and to the variations of the facial nerve to the retromandibular vein. The tragal pointer is assessed as a commonly used and an easily accessible soft tissue landmark to direct the surgeon easily and effectively to the facial nerve main trunk. The angle of the mandible is also assessed as an easily accessible hard tissue landmark.

The tragal pointer is best understood through an in depth understanding of the auricle of the external ear. ²⁹ The external ear comprises two structures, the external acoustic meatus and the auricle (pinna). The lateral surface of the auricle points somewhat anteriorly and has irregular concavities along its surface along with multiple depressions and projections. The helix is the outermost prominent curved rim, which often has a small tubercle posterosuperiorly - Darwin's tubercle. Anterior and parallel to the helix is the antihelix, which superiorly divides into two crura, creating a triangular fossa. Between the helix and anti-helix is a long depression – the scaphoid fossa. The concha of the auricle lies anterior to the anti-helix, which is encircled anteriorly by the anterior projection of the helix, creating two depressions – the cyma concha superiorly and the cavum concha inferior to the cyma concha.

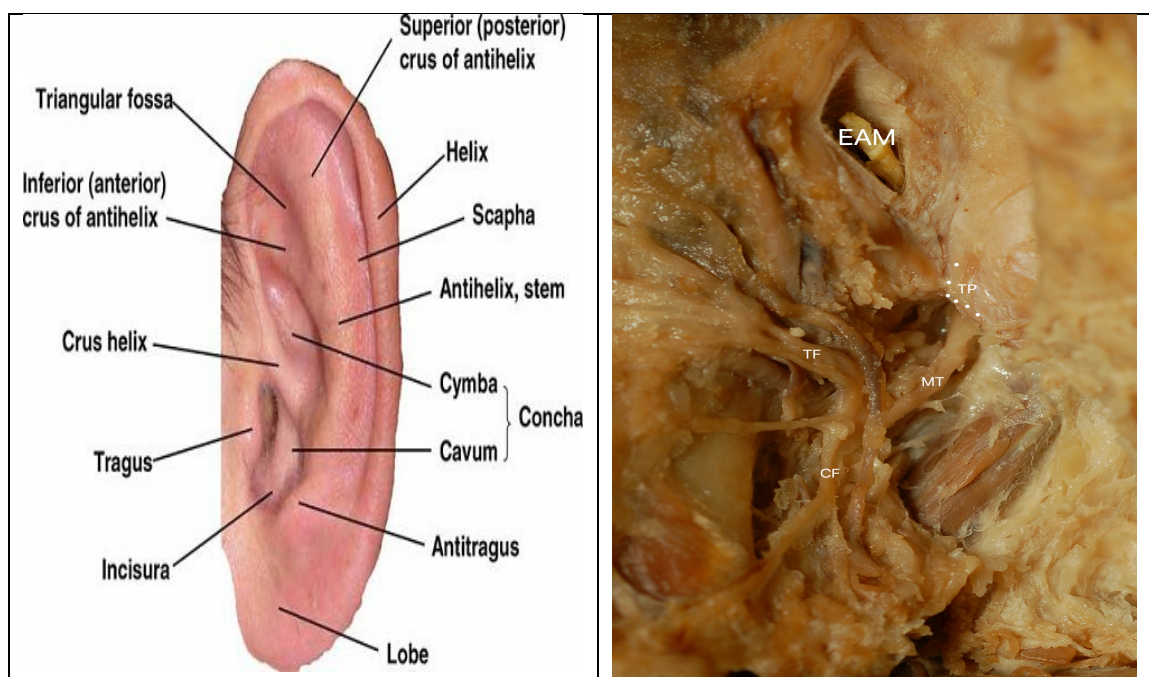


Figure 1. Left - Labeled auricle (left). Right - Tragal pointer highlighted with angulation of pointer marked. Auricle resected to show depth of TP. EAM marked as is the main trunk and the two main divisions of the facial nerve.

The tragus lies anterior to the conchae and inferior to the crus helix. It is a small curved flap of tissue comprised of cartilage. The anterior portion of the tragus points anteriorly and inferiorly and deep. The end of this anterior portion takes a bluntly pointed shape on its medial aspect – this is commonly termed the tragal pointer and is highlighted in (Fig.

1), where the auricle has been resected to show the depth of the pointer and that the angulation of the cartilage tip is in the general direction of the facial nerve trunk.

The reliability of the tragal pointer and others as markers to the facial nerve trunk, and the position of the retromandibular vein as a guide is scrutinised in how variations can affect these surgical guides, and thereby the success of the surgical approaches upon which they rely. We hypothesise that variations in the distances of anatomical landmarks to the facial nerve main trunk and variations in the arrangement of the intra-parotid venous structures to the facial nerve could impact on standard surgical approaches for both parotidectomy and mandibular access procedures.

2.2 Materials and methods

Consent and ethical approval was implied in the Anatomy Department donor consent for dissection and imagery related to research projects within Trinity College Dublin.

Twenty six cadaveric facial halves were dissected, seventeen female and nine male, all of Irish Caucasian descent. The age ranges were 58 – 99 years of age with a mean of 78 years and 3 months of age (Table 2).

Gender	Age	Dissected facial halves	Cause of death
Male 1	66	1	Cholangiocarcinoma
Male 2	73	2	Pancreatic cancer
Male 3	79	2	Lung cancer
Male 4	69	2	Acute leukaemia
Male 5	65	2	Thymic neuroendocrine tumour
Female 1	83	1	Metastatic leiomyosarcoma
Female 2	81	1	Oesophageal cancer
Female 3	79	1	Bladder cancer
Female 4	91	2	Myocardial infarction
Female 5	58	2	Small cell lung cancer
Female 6	70	2	Breast cancer
Female 7	96	2	Heart failure
Female 8	93	2	Intracerebral haemorrhage
Female 9	99	2	Bronchopneumonia
Female 10	90	2	Pneumonia
Mean age / Total facial halves	78	26	

Table 2 - Demographic data of cadaveric donors included in the study

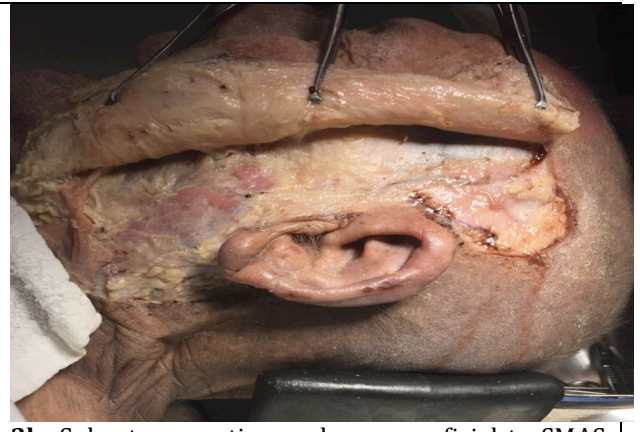
None of the cadavers had any recorded medical history of any head or neck malignancies, pathology, or any visible evidence of facial or neck surgery, or any parotid pathology.

However, one of the male facial halves showed evidence of a deep lobe enlarged lymph node during dissection, with no affect on the facial nerve. The cause of death in this particular donor was documented to be a thymic neuroendocrine tumour. Since, the metastatic node did not impact on the facial nerve or its dissection, the results of the dissection were included.

The dissection of the facial nerve was performed using an extended pre-auricular approach with extension to the mastoid process posteriorly and to the neck inferiorly (Lazy S incision) to expose the entire parotid to allow complete visualization of the main trunk and all the facial nerve branches (Fig. 2a). Skin and subcutaneous tissue were lifted and a plane developed subcutaneously, superior to superficial masseteric aponeurosis system (SMAS) layer (Fig. 2b). The facial nerve was followed using a retrograde approach, often initially by identifying the terminal aspect of the buccal branch and subsequently following this back to the upper division or main trunk (Fig. 2c). Subsequent to this, a superficial parotidectomy was performed by following the divisions and branches of the entire facial nerve from the main trunk (Fig. 2d). Once clearly dissected, the relationship of the facial nerve with the intra parotid venous structures was clearly delineated (Fig. 2e).



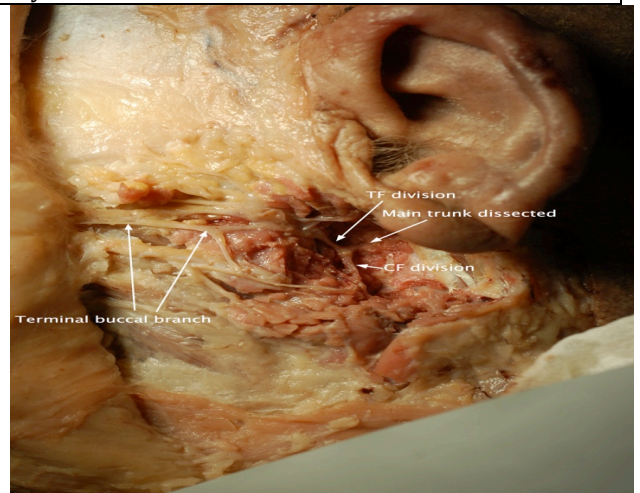
2a. Extended pre auricular incision marked



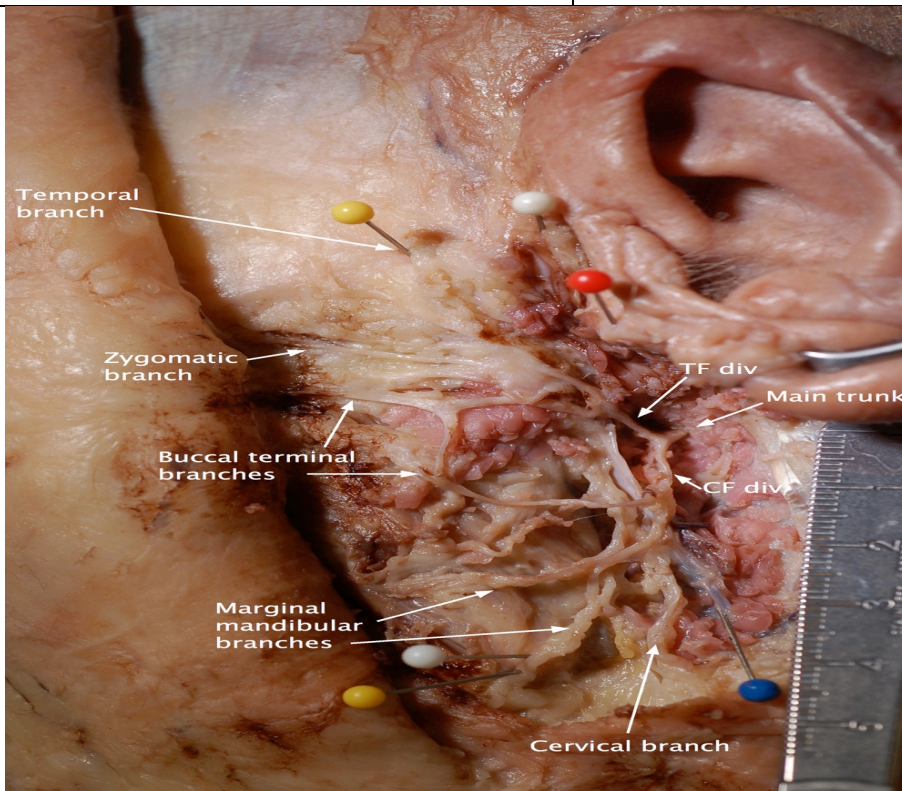
2b. Subcutaneous tissue plane superficial to SMAS layer



2c. Terminal buccal branch identification



2d. Retrograde dissection to main trunk and 2 divisions



2e. Completed dissection of facial nerve. Main trunk shown with the two divisions (cervicofacial / CF & temporofacial / TF). Pins - White: bony landmarks - superior - outermost border of external acoustic meatus, inferior - angle of mandible. Yellow - superior - temporal branch as it crosses zygomatic arch, inferior - marginal mandibular as it crosses lower mandibular border. Red - Tragal pointer. Blue - Retromandibular vein

High quality and high definition images were captured using a Nikon D50 Digital SLR camera throughout the model surgeries and dissections, at a constant distance of approximately 50 cm from the donor.

Measurements and relationships were noted as follows:

1. The distance between the point of division of the main trunk to tragal pointer – a commonly used soft tissue landmark for identification of the facial nerve in anterograde parotidectomy.
2. The distance from the point of division of the main trunk to the angle of the mandible – an easily accessible hard tissue landmark in anterograde parotidectomy.
3. The distance between the temporal division of the facial nerve as it crosses the malar arch to the most anterior point of the external acoustic meatus (pre-auricular line) – to measure the minimum safe distance for incision making in all pre-auricular surgical approaches
4. The point of crossing of the retromandibular vein to the facial nerve and the classification of the relationship.

Measurements were made and digitally calibrated using the software 'Image J' 1.5i, on an apple mac computer, with a local scale calibrated to millimeter distances.

2.3 Results

We highlight the results of our own dissections with the aim of contributing this to the existing literature. Three distances and two venous variations are illustrated.

The distances comprise the distance between the pre auricular line illustrated as the most anterior point of the external acoustic meatus to the most posterior branch of the temporal bundle of the facial nerve. This is known as the ‘safe zone’ utilized in the commonly used pre auricular approach to both the parotid and the mandibular condyle. The ‘safe zone’ pre auricular incision as modified and suggested by AlKayat & Bramley²⁶ in 1979, is based on the minimum distance between the most posterior branch of the temporal bundle of the facial nerve as it lies in the superficial temporal fascia and the pre-auricular line. This measurement is taken along the malar arch.

Two landmarks are assessed for their distances to the main trunk - one soft tissue (tragal pointer) and one hard tissue (angle of mandible) landmark and the result ranges in millimeters with standard deviations are provided. Wetmore et al.³³ in 1991, first described the tragal pointer as a landmark, that is easily reproducible intra operatively, and medial and inferior to which lies the main trunk of the facial nerve. It is a distance that is a commonly used estimate to identify the main trunk of the facial nerve, during anterograde parotidectomy.

Finally, the venous variations identified to the facial nerve are described. We found the commonly described variations of the retromandibular vein to the facial nerve in three of the twenty-six facial halves in addition to a novel variation of the superficial temporal vein to the facial nerve in five of the twenty-six facial halves.

2.3.1 'Safe zone' pre-auricular approach

Twenty six cadaveric dissections were to be included in the measurement of the distance between the crossing point of the temporal branch of the facial nerve over the malar arch, and the point of intersection of the malar arch to the pre-auricular line, at the reference point of the anterior most point of the concavity of the external acoustic meatus. The distances measured range from 6.18 mm to 23.45 mm, with a resultant 'safe zone' as per our dissections of less than 6.18 mm (Fig. 3). The average distance was 14.08 mm with a standard deviation of ± 5.17 mm to the mean (Fig. 3). There was no statistical significance between males and females in the distances of the 'safe zones', using a standard, 2-tailed *t*-test of unequal variance ($p = 0.38$).

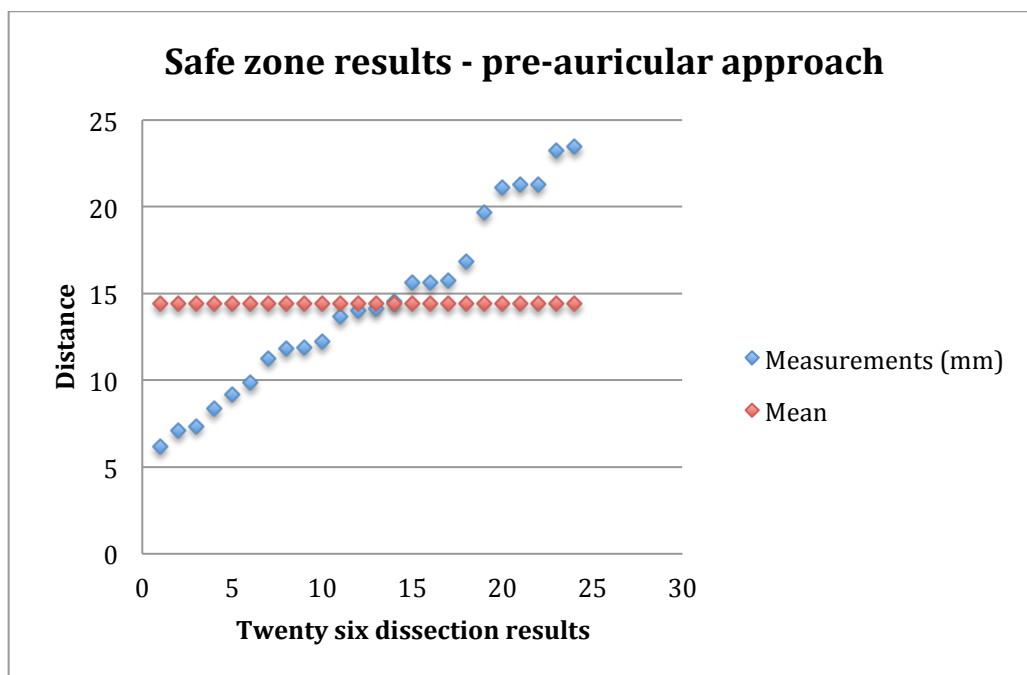


Figure 3. Measured distances in mm between point of crossing of most posterior branch of temporal branch of facial nerve on malar arch to pre auricular line on malar arch. Mean highlighted in red.

2.3.2. Tragal pointer to main trunk

The same twenty-six cadaveric dissections were included in the measurement of the distance between the commonly used surgical landmark ‘the tragal pointer’ to the bifurcation of the main trunk of the facial nerve.

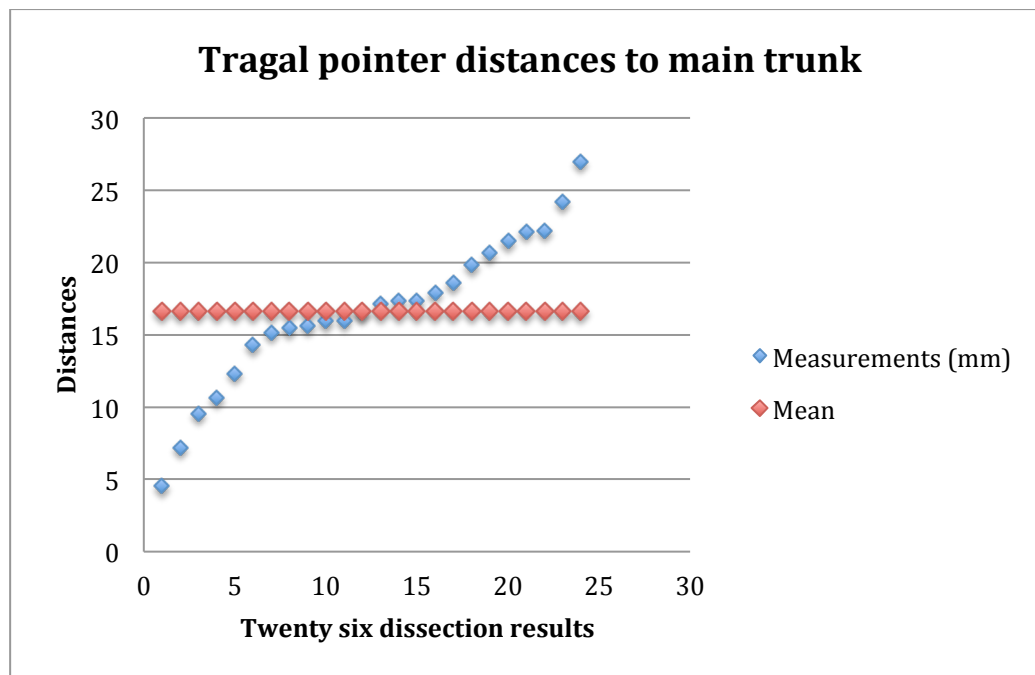


Figure 4. Measured distances in mm from the tragal pointer to the point of bifurcation of the main trunk of the facial nerve. Grey, standard deviation.

The distances of the tragal pointer to the point of bifurcation of the main trunk of the facial nerve range from 4.5 mm to 26.98 mm, with an average distance of 16.89mm and a standard deviation of ± 5.12 mm (Fig. 4). All the dissections showed the point of bifurcation to be medial and inferior to the tragal pointer. Eight of the twenty six dissections showed the point of bifurcation to be posterior and inferior to the tragal pointer, six were anteroinferior and twelve were inferior to the tragal pointer along the same longitudinal axis (Table 3 & Fig. 5).

Antero - inferior	6/26	23%
Inferior	12/26	46.1%
Postero - inferior	8/26	30.7%

Table 3. Relationships of the point of bifurcation of the dissected facial nerve trunk to the tragal pointer and respective percentages.

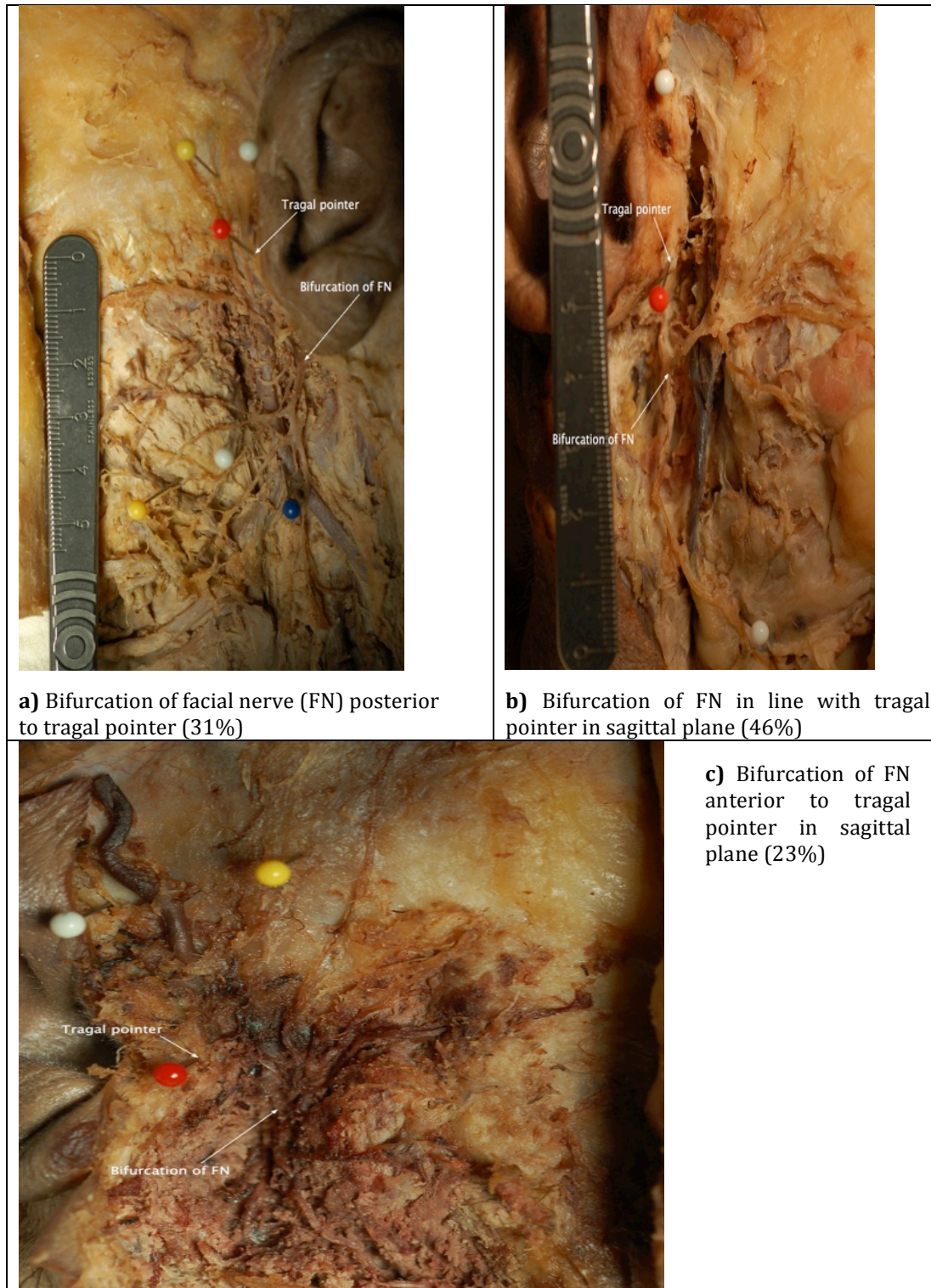


Figure 5 – Antero-posterior relationship of main trunk to tragal pointer

There was no significant difference between male and female cadaver samples.

P value based on a Student *t*-test calculation (2-tailed test of unequal variance) between male and female measurements was 0.347.

2.3.3 Angle of mandible to main trunk

The distance the angle of mandible was in relation to the point of bifurcation of the main trunk of the facial nerve was measured in the same 26 dissections (Fig. 6).

The angle of the mandible was anteroinferior to the main trunk in all cases.

The recorded distances ranged from 5.56 mm to 50.1 mm, with an average distance of 28.26 mm and a standard deviation of ± 9.75 mm to the mean. There were no significant differences between male and female cadavers ($p = 0.316$).

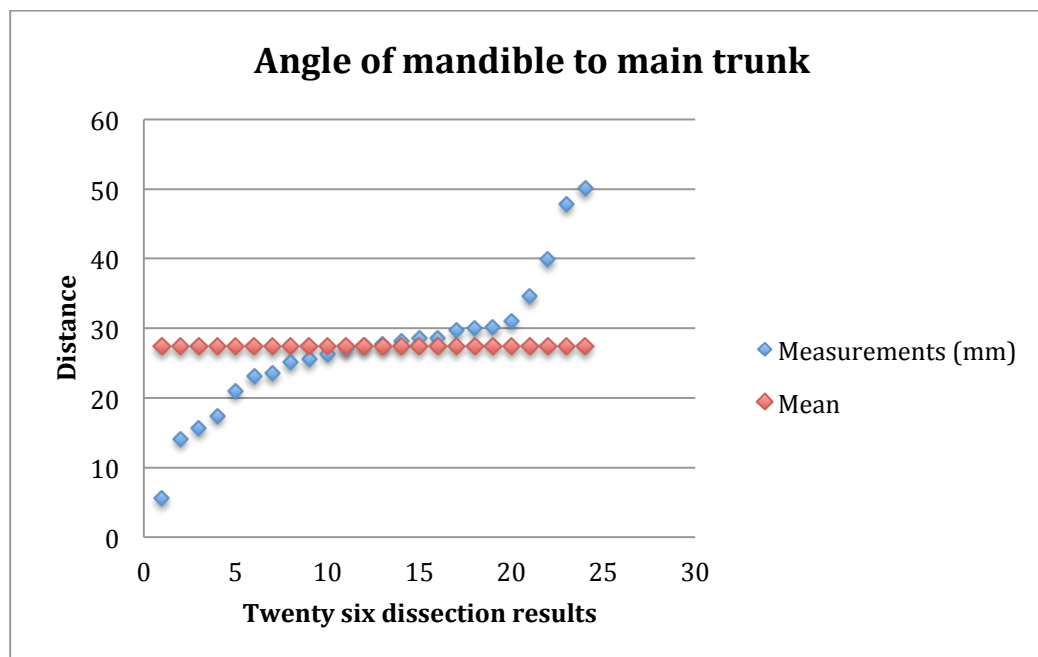


Figure 6. Distance of angle of mandible to point of bifurcation of main trunk of facial nerve in millimeters (blue). Mean (red).

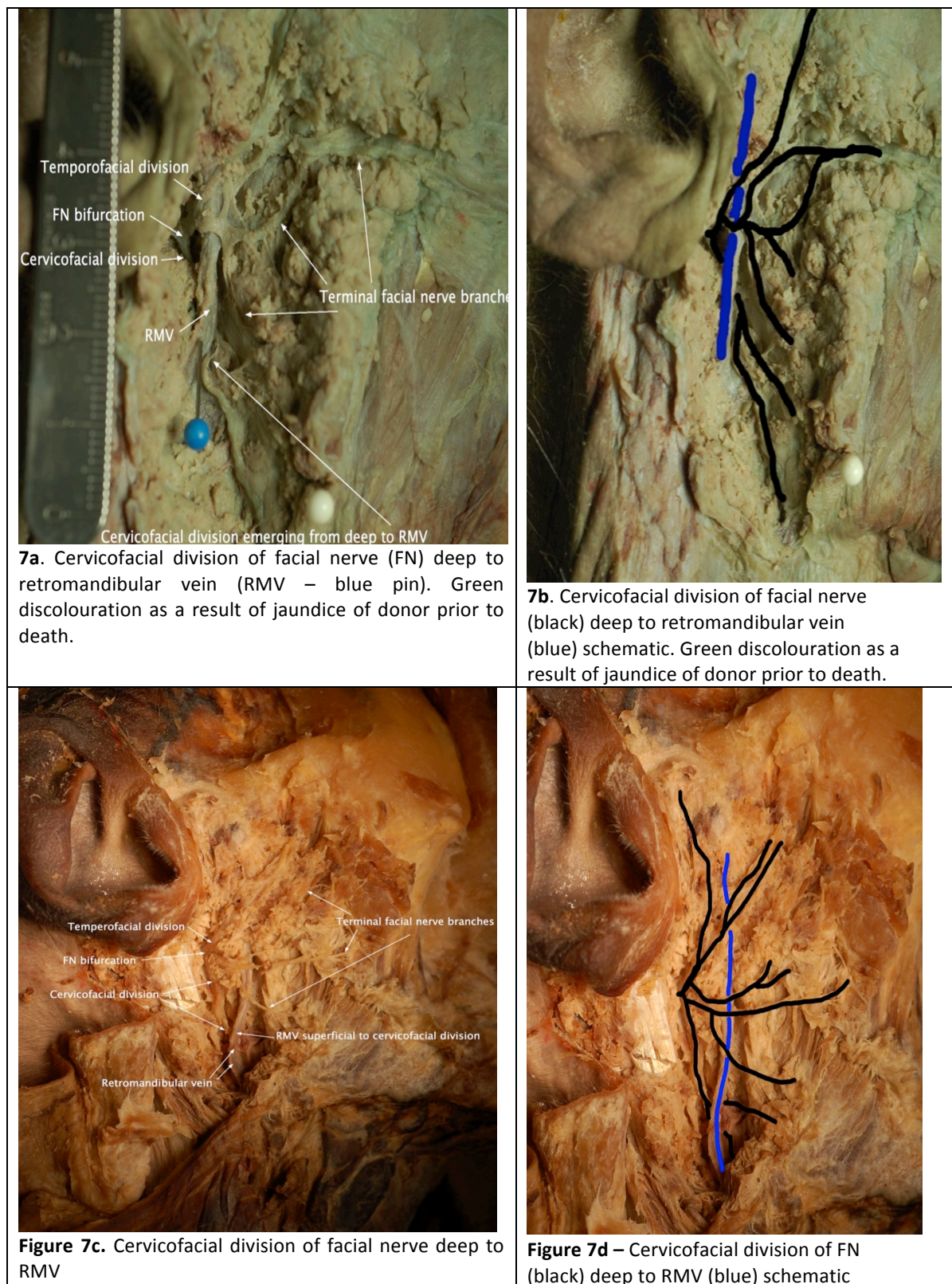
2.3.4 Intra-parotid venous variation to the facial nerve

Deep	Superficial
18	8
	RV superficial to nerve
	3
	STV superficial to nerve
	5

Table 4. Variation of intra-parotid venous structures to the facial nerve. Eight out of 26 of the facial halves dissected were found to have the intra-parotid venous structures (superficial temporal vein / retromandibular vein) superficial to all or part(s) of the facial nerve. Five of 8 variants showed variation of the STV to the facial nerve. Three of 8 showed variation of the RV to the facial nerve.

Twenty-six dissections were carried out of facial halves to investigate the relationship of the facial nerve to the intra-parotid venous structures. Any variation of the usually described relation of the retromandibular vein deep to the facial nerve was classed as a variant, even if the venous structure was superficial to just one or more parts of, or all of the facial nerve.

Eighteen of the 26 facial halves (69%) showed the usually described relationship between vein and nerve, whereby the facial nerve was the most superficial of the intra-parotid structures, followed by the venous structures. The venous structures identified on dissections were the superficial temporal vein joining the maxillary vein superiorly, to become the retromandibular vein within the body of the parotid gland, before dividing again to anterior and posterior branches, which join other veins to form the common facial vein and external jugular vein respectively. Eight of the 26 facial halves (31%) showed variation whereby the facial nerve or one of its branches were deep to an intra-parotid venous structure. Two of the eight (Fig. 7 a-d) showed a variation pattern where the retromandibular vein was superficial to the facial nerve or one of its branches. One of the eight (Fig. 8 a-d) shows a variation where the retromandibular vein is forked by a neural ring where it is both superficial and deep to the facial nerve.



Figs. 8 (a-d) represent a variation of the facial nerve to the retromandibular vein where the main trunk appears to fork around the retromandibular vein, whereby one aspect of the trunk is superficial and one aspect is deep to the vein. This is demonstrated in Figs. 7 (c,

d) where the retromandibular vein is reflected both anteriorly and posteriorly, respectively, to demonstrate this neural forking pattern.

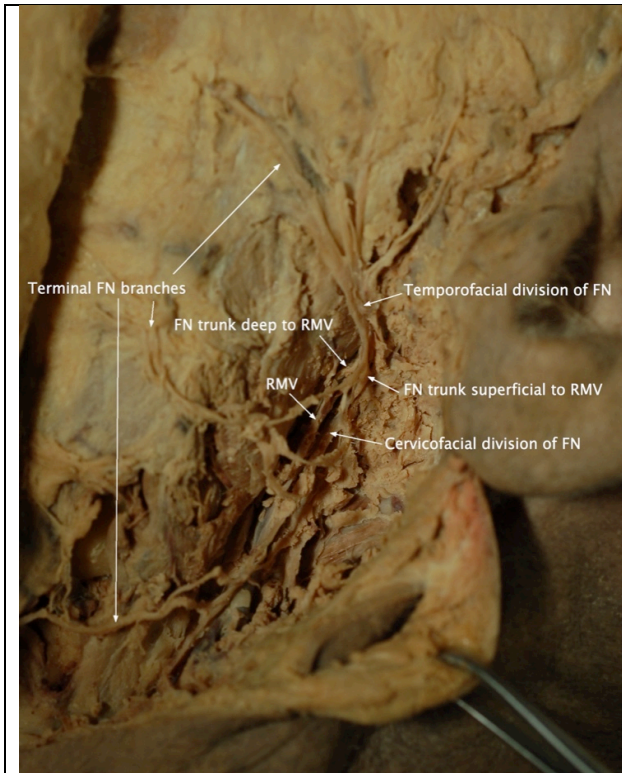


Figure 8a. Main trunk of facial nerve deep to RMV

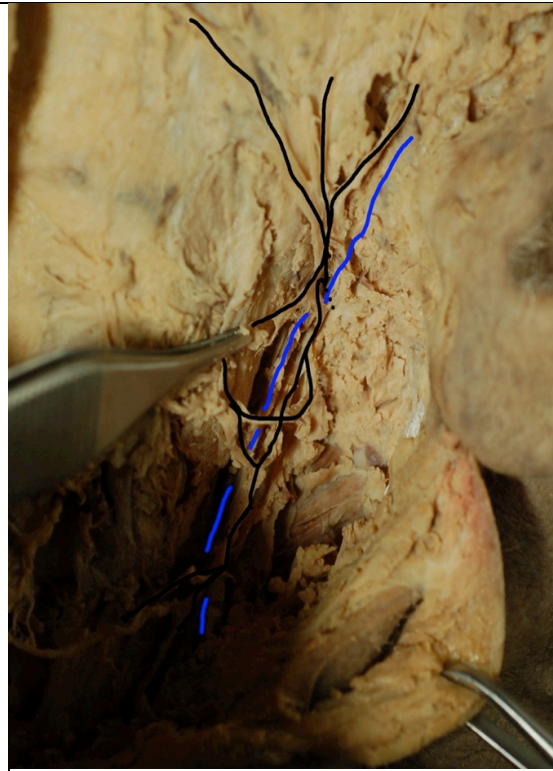
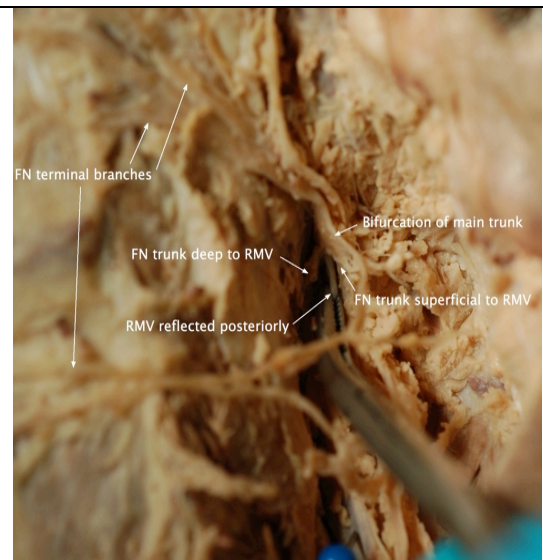
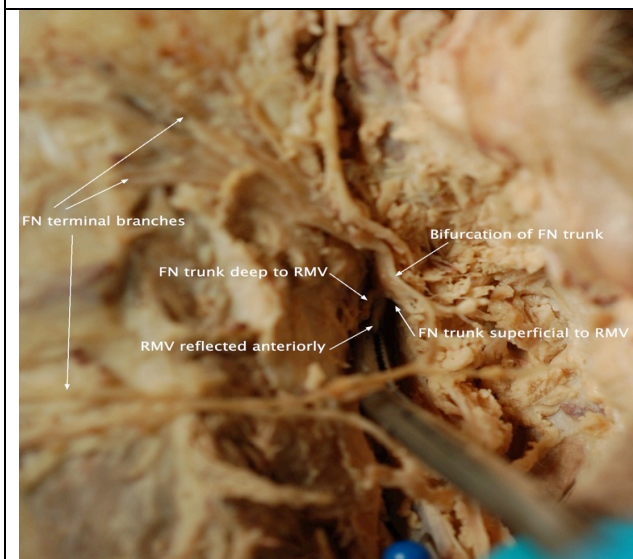


Figure 8b. Schematic of relation of vein to nerve



Figures 8 c & d. RMV reflected anteriorly in fig 7c (left) to show FN trunk superficial to vein and RMV reflected posteriorly in fig 7d (right) to demonstrate FN trunk deep to vein.

Five of the eight variants of intra parotid venous structures to facial nerve were variations of the superficial temporal vein to the facial nerve. The superficial temporal vein was found to be superficial to part of or all of the facial nerve, before joining the deeper maxillary vein to form the retromandibular vein (Figs. 9-12).

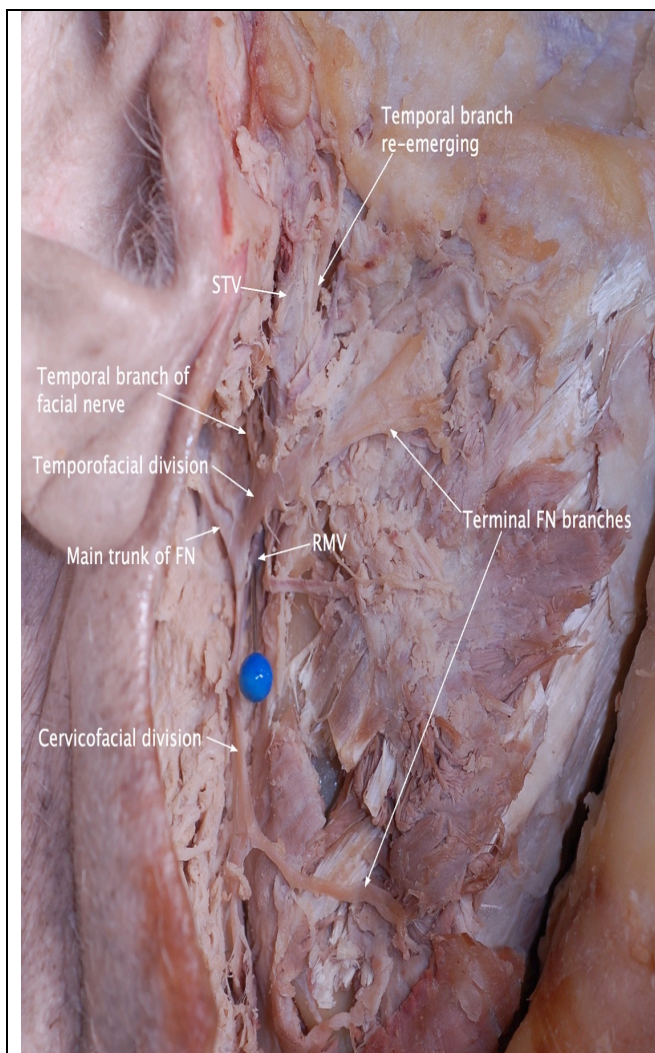


Figure 9a. Superficial temporal vein runs superficial to temporal branch of facial nerve

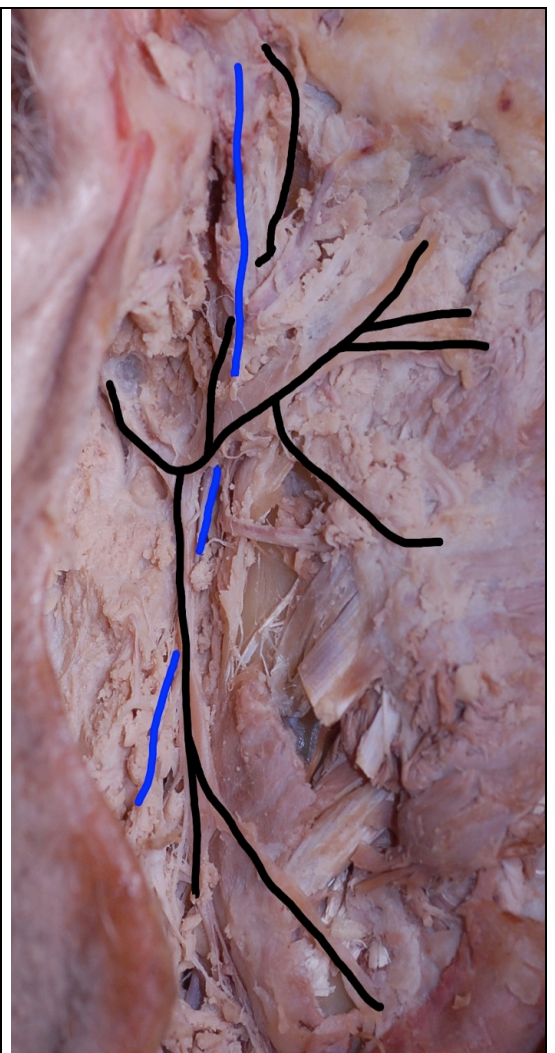


Figure 9b. Schematic showing the venous structures (blue) with the superficial temporal vein superficial to the temporal branch of the facial nerve (black).

Figs. 9 (a & b) show the superficial temporal vein running superficial to the temporal branch of facial nerve in same plane as maxillary vein. Both veins join to form the retromandibular vein deep to the zygomatic branch and temporofacial division of the facial nerve.

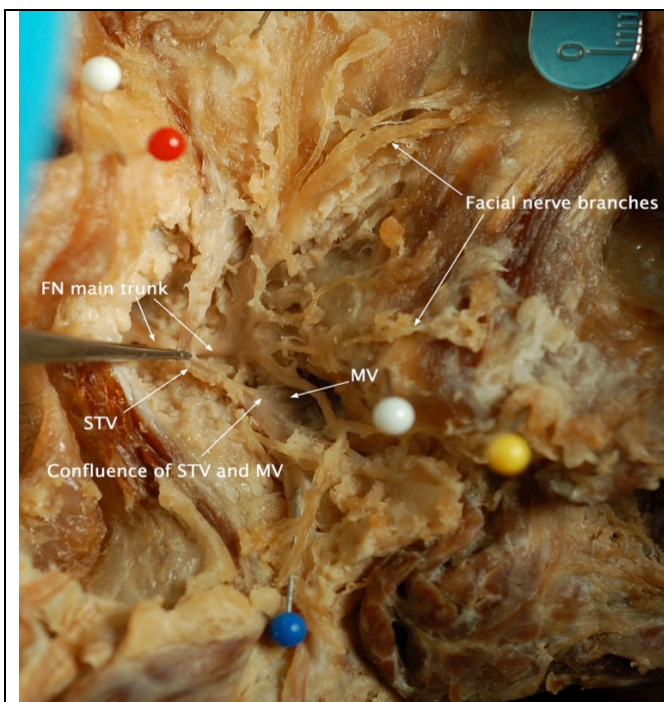


Figure 10a. STV – Superficial temporal vein (superficial to facial nerve main trunk), FN – Facial nerve, MV – Maxillary vein (deep to facial nerve), Confluence of STV and MV to form retromandibular vein

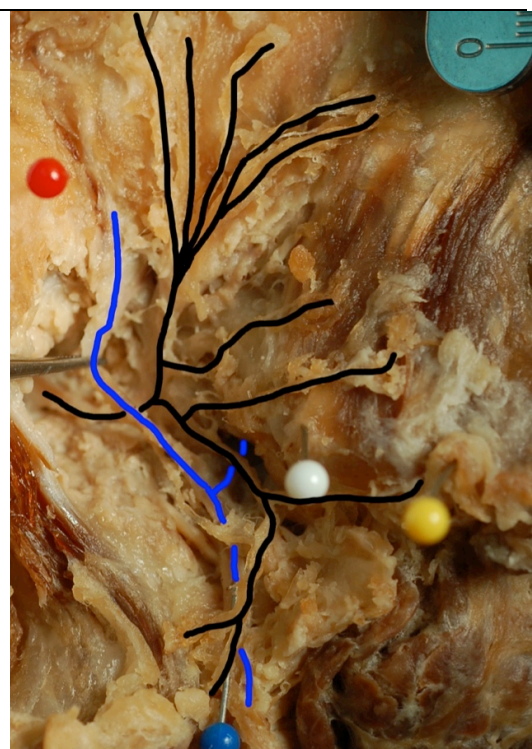


Figure 10b. Schematic showing facial nerve (black) and venous structures (blue).

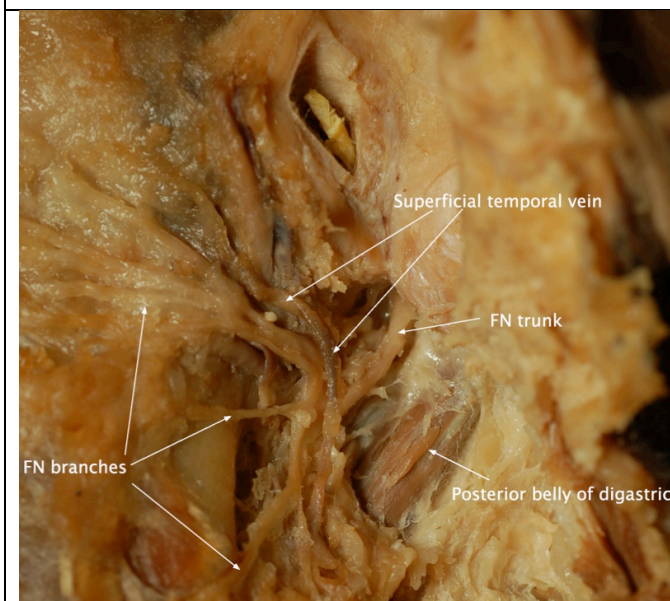


Figure 10c. Facial nerve (FN) trunk and branches evident. Superficial temporal vein superficial to main trunk of FN.

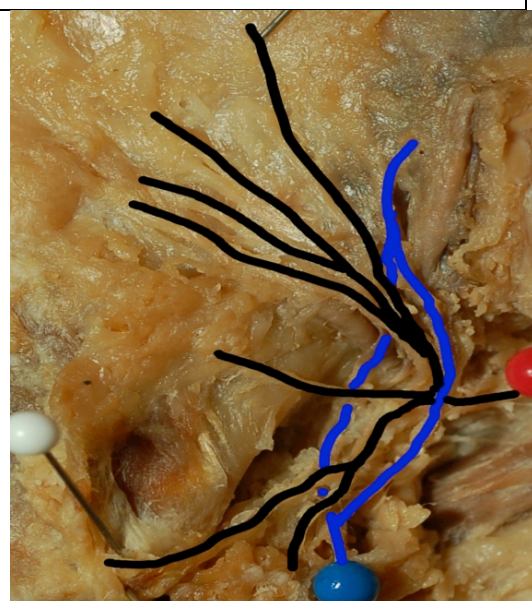


Figure 10d. Schematic showing FN (black), intra parotid venous system (blue). STV superficial to FN and maxillary vein deep.

Figs. 10 (a-d) identify two sides of the same cadaveric donor, with a similar pattern of superficial temporal vein variation to the facial nerve main trunk. In both facial nerve dissections, it is apparent that the superficial temporal vein is superficial to the main trunk, before joining the maxillary vein inferiorly to form the retromandibular vein. This is highlighted in schematics of both variants (Figs. 10 b&d).

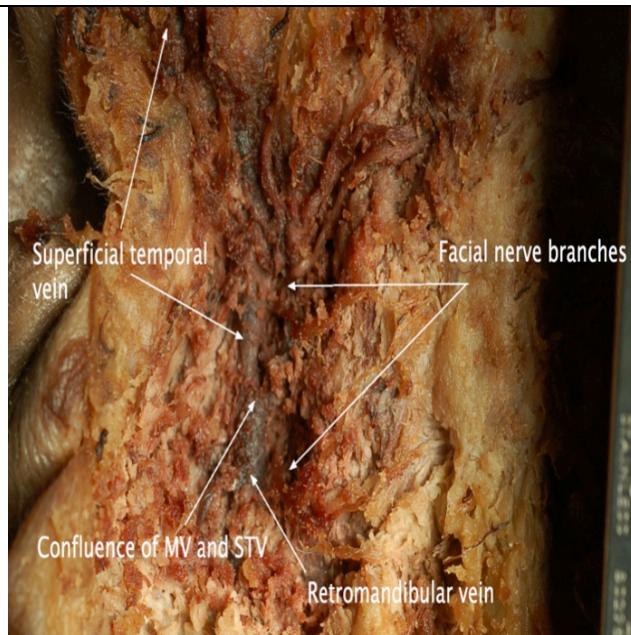


Figure 11a - STV superficial to all facial nerve branches. Confluence of STV and maxillary vein (MV) shown, depicting deep nature of MV. After the confluence of STV and MV, the retromandibular vein is formed. Facial nerve branches shown, arising deep to STV.

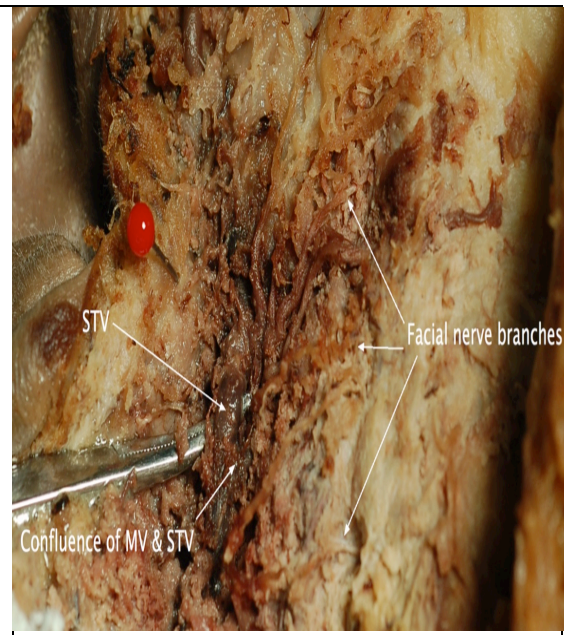


Figure 11b - STV lifted showing superficial nature of vein to the facial nerve.

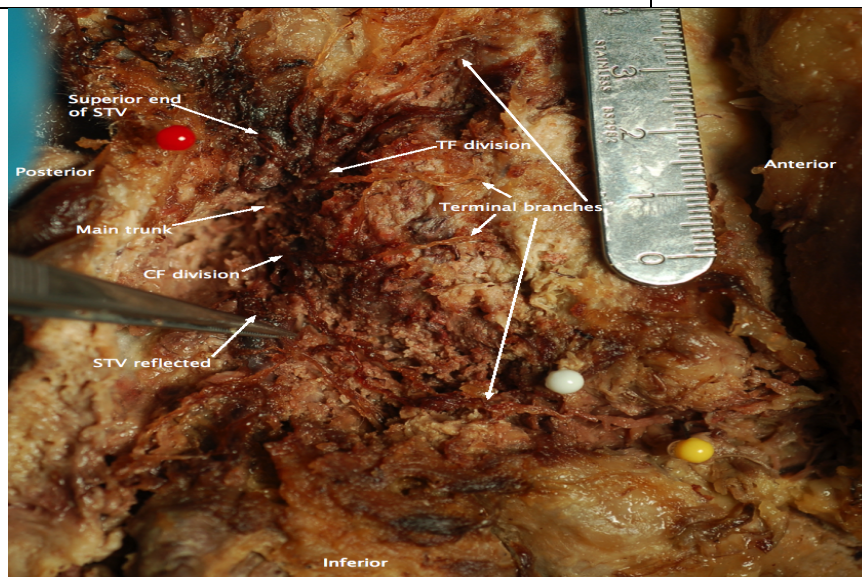


Figure 11c. STV removed showing facial nerve main trunk. White pin - angle of mandible
Yellow pin - marginal mandibular branch crossing lower mandible
Red - tragal pointer.

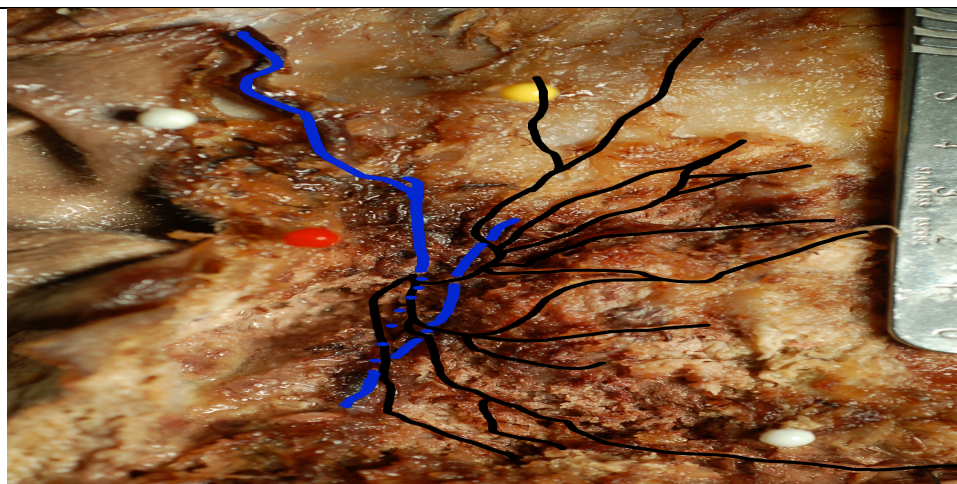


Figure 11d. Schematic of FN in black and venous structures in blue - STV in blue dotted line: removed part of STV. MV joins STV to form RMV.

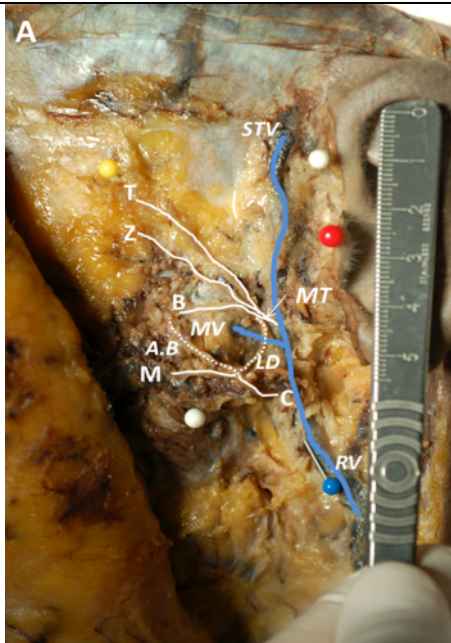


Fig12a Labeled left parotid dissection - facial nerve variation to the superficial temporal and maxillary veins.

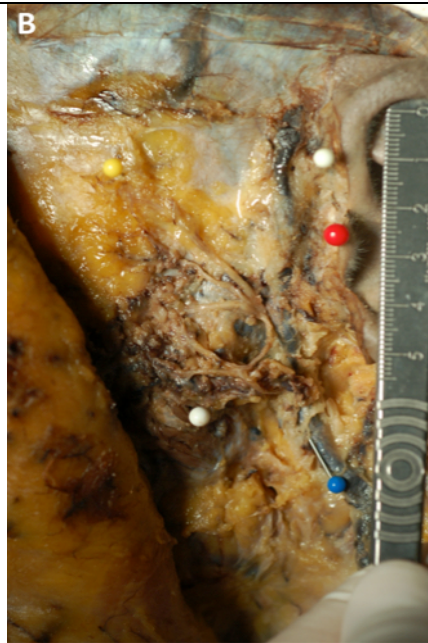


Fig12b Unlabeled left sided schematic of facial nerve variation.

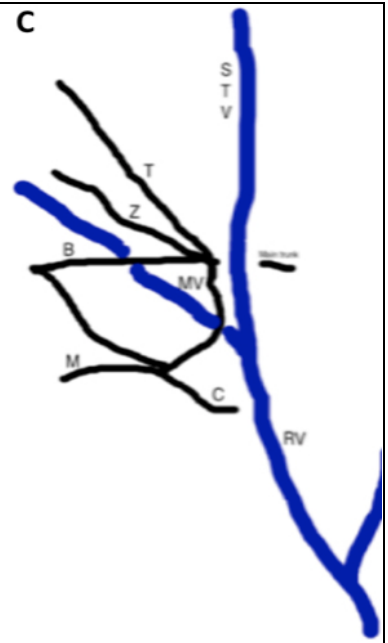


Fig12c Schematic of facial nerve variation.

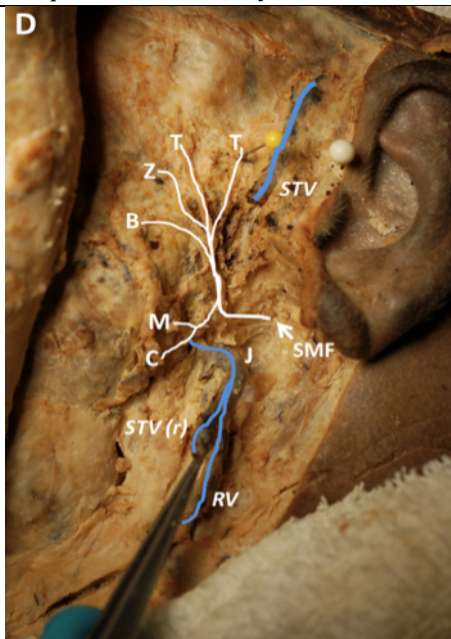


Fig12d Labeled left superficial parotid dissection showing the facial nerve variation with superficial temporal vein reflected inferiorly.



Fig12e Unlabeled left superficial parotid dissection showing the facial nerve variation with superficial temporal vein reflected inferiorly.

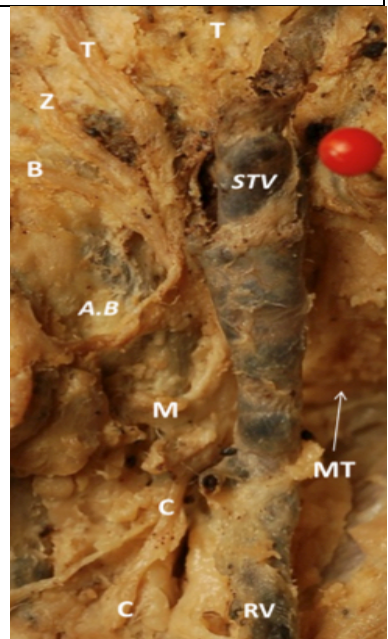


Fig12f Enhanced image of left superficial parotid dissection showing the facial nerve trunk deep to superficial temporal vein.

Figure 12 Pins; Upper white, Junction of zygomatic arch and pre auricular dissection line; Lower white, Angle of mandible; Yellow, Temporal branch crossing zygomatic arch; Red, Tragal pointer; Blue, Retromandibular vein.

Figs. 11 & 12 show two further variants of the superficial temporal vein to the facial nerve. Both have in common that the vein is superficial and tightly adherent to the main trunk of the facial nerve with the trunk bifurcating deep to it and the branches of the nerve appearing from the confluence of the superficial temporal and maxillary veins (Figs. 11 a&b, 12b). Once the superficial temporal vein is reflected (Figs. 11c & 12e), the main trunk becomes visible. Schematics in both figures try to illustrate the variations (Figs. 11d & 12 a,c,d).

2.4 Discussion

2.4.1 'Safe zone' – temporal branch to pre-auricular line

Al Kayat and Bramley ²⁶ in 1979, for many head and neck surgeons revolutionized the approach to the parotid gland and mandibular condyle when they described the 'safe zone', whereby it is unlikely that the temporal branch of the facial nerve will be encountered during surgical approach. Based on dissection of fifty-six facial cadaveric halves, they were able to elucidate that the posterior most ramus of the temporal branch of the facial nerve does not lie any less than 8 mm and anymore than 35 mm from the most anterior point / concavity of the external acoustic meatus with a mean distance of 20 mm. Therefore a pre-auricular incision lying within 8 mm anterior to the most anterior point of the concavity of the external acoustic meatus would be considered safe.

A recent study and review of the literature by Gosain et al. ³⁴ in 1997, assessed the same distance using twelve facial half cadaveric dissections. Their results largely agree with those of Al Kayat and Bramley ²⁶, with a range of 10 – 39 mm (mean 17 mm) from the most posterior ramus of the temporal branch to the same reference point – the most anterior point on the concavity of the external acoustic meatus. Gosain et al ³⁴ created an illustration, based on their findings of the danger zone along the zygomatic arch, spanning 29 mm along the inferior aspect of the zygomatic arch and 36 mm along the superior aspect whereby the temporal rami of the facial nerve are most likely to be found and hence injured. The reason for the difference in lengths along the upper and lower borders of the zygomatic arch takes into consideration the branching pattern of the nerve bundle as it courses the bony arch.

Our study of twenty-six facial halves showed that the most posterior ramus of the temporal nerve ranged from 6.18mm to 23.45mm anterior to the reference point on the external

acoustic meatus, with a resultant 'safe zone' as per our dissections of less than 6.18mm. The average distance was 14.08mm with a standard deviation of ± 5.17 mm to the mean. Less than 6mm implies a smaller safe zone than that advocated by Al Kayat & Bramley²⁶ and Gosain et al³⁴. There was no statistical significance between males and females in our study.

The importance of the figures does not lie in the mean distance, but in the minimal distance. It is disconcerting that the minimal distances do not equate in the three studies, however, we believe that due to variations that may exist, it would not be prudent to rely solely on an absolute figure, but rather rely on the most anterior point of the external acoustic meatus concavity, as a landmark, near which the pre-auricular incision should be placed and not more than 6mm anterior to it. The closer the incision is to the pre-auricular line based on accurate palpation of the external acoustic meatus bony landmark, the less likely that it is to impact on the temporal branch of the facial nerve.

2.4.2 Tragal Pointer

Since Wetmore et al.³³ in 1991, first described the tragal pointer as a surgical landmark for the identification of the facial nerve trunk, it has been widely studied in its distance to the main trunk of the facial nerve prior to its bifurcation^{29, 31, 32}. Pather and Osman³¹ in 2006 examined the relation of the facial nerve trunk to several landmarks including the tragal pointer, tympanomastoid suture, attachment of the posterior belly of the digastric muscle, external auditory meatus, transverse process of the axis, angle of the mandible, and the styloid process. According to their results, the posterior belly of the digastric muscle, the tragal pointer, and the transverse process of the axis are technically good landmarks for the identification of the facial nerve trunk. The mean distance of tragal pointer to the facial nerve was found to be 34 mm \pm 0.67 mm.

They did note, as was noted in other studies ^{29, 32}, the disadvantage of the tragal pointer is its cartilaginous nature, mobility, asymmetry and sometimes irregular tip. Therefore, it was concluded to be a less reliable than these other two landmarks.

Similarly, Rae et al. ³² in 2010, who assessed the precision of four commonly used landmarks on twenty six cadaveric specimens, concluded that their dissections did show variability in the size, shape and the direction the pointer 'pointed' and thereby did not conclude that the tragal pointer should be used as a reliable landmark. Their measured distances of the tragal pointer to the facial nerve trunk showed a comparatively small mean (\pm SD) distance of 6.97 ± 1.8 mm.

The above measured distances in these recent studies differ from the more commonly used results of Conley et al. ³⁵ in 1975 and De Ru et al. ^{36, 37} in 2001, upon which a large number of surgeons rely, whereby they conclude that the distance of the facial nerve lies 1-2cm inferior and deep (medial) to the tragal pointer. Our study has identified a mean distance of 16.89mm and a standard deviation of ± 5.12 mm, largely correlating to these figures, in comparison to the much larger distances found by Pather and Osman ³¹ and the much smaller distances found by Rae et al. ³²

The large inter-study variability can be related to several factors, both related and unrelated to the tragal pointer as a landmark. The soft tissue nature of the tragal pointer, the variability in its size and shape and the direction in which the landmark 'points' are factors already identified in this study and specific to the tragal pointer. However, several other factors can be attributed to the large variability in distances measured across the literature, which may be related to differences in study designs. The post-mortem effects in anatomic

laboratory based studies, such as this one, has the effect of influencing absolute distances by shortening them ³¹, while the effects of port-mortem embalming can lead to fixation artefacts – cartilaginous structures are softer and the fixed position of the landmark may not reflect the true position in real life ³². In addition, the method of point-to-point measurement can lead to variability as no two studies used the same point of reference on the facial nerve trunk. We have decided to use a reproducible point along the facial nerve trunk – its point of bifurcation. However, other studies used the shortest distance between the tragal pointer and the trunk, meaning that reproducibility may be difficult. ^{29, 31, 32, 36}

In relation to male to female comparisons, we found no statistical significance between our cadaveric subjects. This correlates to the findings of other studies, when assessing the distance of the tragal pointer to the facial nerve. ^{31, 32}

In addition to the varying distances of the tragal pointer to the facial nerve trunk, we noticed variations in the sagittal relationship of the two structures. We noted, that in the twenty six facial halves dissected, the point of bifurcation lay, inferior and deep (medial) to the tragal pointer, but in the sagittal plane as shown in table 3, the point of bifurcation was either found posterior to, in line with or anterior to the tragal pointer and to the direction this cartilaginous structure was ‘pointing’.

Forty six percent (12/26 facial halves) showed that the point of bifurcation was in line with the ‘pointer’ in the sagittal plane, meaning that a dissection of 1-2cm inferior and deep to the tragal pointer is likely to lead directly to the main trunk and its bifurcation. This is the commonly described approach when utilizing this surgical landmark. ^{32, 33} However, over half of our dissections showed the bifurcation and the main trunk either anterior or posterior to the tragal pointer in the sagittal plane. This could be of significance, probably

most when in the anterior position, as the risk of inadvertent damage to the trunk could potentially be high if the operating surgeon dissects medially at 1-2cm inferior to the pointer, expecting to find the entire facial nerve trunk and bifurcation either in line with the pointer or even posterior to where the pointer is 'pointing' in the sagittal plane. Of the 23% (6/26) anterior relations that we found, only one was male. This phenomenon has not been considered in previous literature and we feel would warrant further larger scale studies. While the likelihood of damage is low with current advanced methods of nerve stimulation, it remains a potential reason as to how variation in the length of the main trunk or its varying relation to the tragal pointer could mislead the operating surgeon relying on the standard parameters of dissection, when using the tragal pointer as a landmark to identify and therefore protect the facial nerve during anterograde parotidectomy.

2.4.3 Angle of mandible to main trunk

Not a commonly used or advocated landmark, it remains an osseous, easily palpable landmark, which does not require intricate dissection. It has only been minimally studied in its use as a potential landmark to help locate the facial nerve trunk.^{31, 38}

Pather & Osman³¹ in 2006, assessed the distance between the angle of the mandible and the facial nerve trunk in forty cadaveric facial halves, of Caucasian and South African descent. They found the nerve to lie an average distance of 38.1mm (25.3 – 48.69 mm) away from the angle of mandible. There were statistically significant differences between male and female cadaveric specimens, but not between dentate and edentulous mandibles.

Our study revealed an average distance of 28.26 mm to the facial nerve bifurcation with a standard deviation of ± 9.75 mm to the mean. No statistical significance was found in our

study between male and female cadavers in their respective distances from the angle of the mandible to the facial nerve bifurcation.

The variation between our study and that of Pather & Osman's can be due to a multitude of factors. Firstly, their reference point on the facial nerve trunk was not clarified. While we used the reproducible point of bifurcation, their distance was the shortest distance measured between the landmark and the trunk. While it is feasible that the shortest distance to the angle of the mandible would likely correspond to the bifurcation point of the trunk, it cannot be taken conclusively. So a direct comparison between our mean of 28.26 mm and Pather & Osman's mean of 38.1 mm is not possible given the uncertainty in the methods of measurement.

There are known factors in general that would make the angle of the mandible a difficult landmark to use, which could partly explain the discrepancy noted between the two studies. While the angle is an osseous marker, not amenable to the same fixation or decomposition artefacts that soft tissue markers may undergo in embalmed cadavers^{31,32}, it is a mobile point of reference which is amenable to movement artefact, with difficulty in reproducibility between subjects. In addition, the mandible may be of different shapes and sizes, especially between males and females, which showed statistical significance in Pather & Osman's study. The differing size of the mandible could potentially create varying differences in mean lengths both in a sagittal plane from the trunk of the facial nerve, but also in the coronal plane in terms of the depth of dissection required to reach the much deeper facial nerve trunk from the superficial plane the angle of the mandible usually occupies. Therefore, as a landmark for surgical approach, we conclude the angle of the mandible too variable a landmark in its position to enable its use as an effective surgical

reference point. This is the same conclusion reached by the few studies in the literature that did assess this particular reference point.^{31, 38}

2.4.4 Intra-parotid venous variation to facial nerve

Retromandibular vein variation to facial nerve

The parotid gland is unique as it contains a host of neural and vascular structures that enter and exit the gland. From lateral (superficial) to medial (deep), these are the facial nerve, retromandibular vein, external carotid artery, superficial temporal artery, branches of the great auricular nerve, and the maxillary artery. Within the gland the branches of the facial nerve run in different directions corresponding with their destinations, i.e. scalp, eyelids, mid-face, lower face and neck, and they do so in superficial and deep planes. There is no specific, developmentally determined plane in which the facial nerve branches pass between superficial and deep lobes of the gland; the parotid is an integral gland, not divided into lobes. Within the gland the nerve branches communicate with each other, forming a plexiform arrangement that lies superficial to the retromandibular vein, which in turn is superficial to the external carotid artery.

The retromandibular vein generally lies medial to the facial nerve and is formed by the superficial temporal vein and the maxillary vein merging within the superior aspect of the parotid gland at the level of the neck of the mandible.^{14, 23, 29} The vein then courses through the parotid gland between the external carotid artery medially and the facial nerve laterally, which usually gives us an important anatomical landmark in parotid and mandibular surgery.¹⁴ The major risk in these surgeries is injury to the facial nerve due to compression, damage or transection on approach, which has a significant morbidity for the patient.³⁶ Surgical nerve repair, if damage of the nerve is identified, impacts the duration of the operation.³⁶

The retromandibular vein is used as a landmark during pre-operative magnetic resonance imaging (MRI) ³⁹⁻⁴¹, computed tomography (CT) ^{28, 40} and sonography ⁴² to identify the most likely location of the facial nerve within the parotid gland. In addition, the retromandibular vein is used intra-operatively as an important landmark to reveal the facial nerve branches inside the parotid substance as the vein may be traced superiorly into the gland after its identification. The facial nerve is expected to be found superficial to the vein ^{23, 43}. Likewise, the superficial temporal vein has been shown to be a useful indicator during dissection of the upper parotid gland, as its usual superficial and superior location within the parotid gland serves as a guide to the beginning of the retromandibular vein ^{43, 44}.

Variations in the relationships between the intra-parotid venous structures and the facial nerve are widely described ^{21, 22, 43, 44}. While a universally recognised classification system does not exist, Toure and Vacher in 2010 classified six facial nerve and retromandibular vein variants (Tables 1 & 5). ²³

Type 1	Retromandibular vein lay medial (deep) to the facial nerve (65.2%)
Type 2	Retromandibular vein lay lateral (superficial) to the facial nerve (28%)
Types 3-6	Constituted subtypes of type 2.

Table 5. Facial nerve and retromandibular vein variants classification

Variations in the arrangement of the facial nerve and the retromandibular vein is of great surgical significance as the relationship of two structures is of importance pre and intra-operatively in helping to identify the location and preserving the facial nerve. Some studies report that the retromandibular vein topography in relation to facial nerve may be different more usually than it is thought such as in that of Kopuz et al. in 1995, where it was concluded that the retromandibular vein lay deep to the facial nerve temporofacial and

cervicofacial divisions in 90% (45/50), and in 10% (5/50) the retromandibular vein course was deep to the temporofacial and superficial to the cervicofacial divisions, whereas in a single case the retromandibular vein was detected superficial to the nerve, at its bifurcation level.²² Additionally, after examining 85 cadaveric facial halves, Kim et al.²¹ in 2009, observed the standard superficial position of the facial nerve cervicofacial division in relation to the vein in 83%. However, the nerve was found deep to the vein in 17% of the cases, where in 6% it divided after crossing the vein and in 11% before. No significant difference was found according to gender.

The observed relationship between the retromandibular vein and facial nerve was classified in 6 types by Toure and Vacher²³ (Tables 1 & 5). The retromandibular vein was found to be situated deep to the facial nerve in the majority of the cases (Type 1, 65.2%, 86/132) and superficial to it in 28% (Type 2, 37/132). Types 3 to 6 constituted subtypes of Type 2. The retromandibular vein was found superficial to the facial nerve main trunk in 13.6% (Type 3, 18/132), to the cervicofacial division in 7.6% (Type 4, 10/132), to the temporofacial division in 3% (Type 5, 4/132) and to some of the cervicofacial facial nerve branches in 3.8% (Type 6, 5/132). In the rest of the specimens, the retromandibular vein or its branches were present on both sides of the facial nerve trunk in 4.5% (6/132), of the cervicofacial division in 1.5% (2/132) and of the temporofacial division (1/132) in 0.8%. Furthermore, some cases of encountered variants have been reported in the literature independently. Bhattacharyya and Varvares⁴⁵ in 2010, observed a case, in which the inferior division of facial nerve was encountered deep to the retromandibular vein during parotid surgery, whereas cases in which the facial nerve and its branches were found encircled by venous rings²³, or “forked” between the retromandibular vein and its divisions have also been reported, found either during cadaver dissection or surgery⁴³.

A recent review by Piagkou et al. in 2013, tabulates the numbers of facial halves across the literature that showed variations between the facial nerve and retromandibular vein.¹⁴ The

variations reported ranged from 2% to 28%, with a total percentage variation across eight multi centered studies ^{21-23, 46-50} of 11.83% (73 / 617 total facial halves) where the vein is superficial in part, or in full, to the nerve.

Of the twenty-six cadaveric facial halves dissected and examined in our study, eight of the twenty-six showed variation of the relationship of the nerve to the intra parotid venous structures. Three of these eight variants were of the retromandibular vein to the facial nerve (Figs. 7 & 8). Two showed the retromandibular vein coursing superficial to the cervicofacial division of the facial nerve (Fig. 7 a-d). One showed the facial nerve trunk both deep and superficial to the retromandibular vein, suggesting the formation of a neural ring around the vein (Fig. 8).

The former two of our three variants of facial nerve to retromandibular vein (Fig. 7) show the vein coursing the facial nerve at a level anterior to the point of bifurcation. Soon after the bifurcation, the temporofacial division remains at a level superficial to the vein. However, the cervicofacial divisions of both cadaveric halves dive deep to the retromandibular vein before emerging once again at a more caudal position. This is a pattern previously described by several studies ^{21,22}, already mentioned. It corresponds to variant type 4 according to Toure & Vacher's classification ²³.

The third cadaveric variant involving the retromandibular vein and the facial nerve (figs 8 a-d) is an unusual variant not previously described. The retromandibular vein does seem to cross the facial nerve trunk in its course inferiorly through the parotid gland. However, on close inspection, it becomes evident that the trunk of the facial nerve appears to arise both deep and superficial to the retromandibular vein before joining to become one trunk - giving rise to the bifurcation of the facial nerve. The variant is that the facial nerve trunk, as it travels through the parotid gland creates a neural ring around the retromandibular vein. Figures 8 c & d attempt to show this concept by showing the degrees of movement of

the retromandibular vein within the confines of the ring of neural tissue that is the trunk of the facial nerve that lies both deep (medial) and superficial (lateral) to the retromandibular vein. Venous rings through which the facial nerve courses have been described previously²³, however there has never been a description of a neural ring of facial nerve through which the retromandibular vein passes.

In order to confirm this developmental anomaly, histological analysis would be the gold standard. However, due to the time limitations we faced with this particular cadaveric donor before interment, we were unable to perform the necessary histology. However, clinically, it did not seem that the structure deep to the retromandibular nerve was inseparable from the remainder of the trunk of the facial nerve once rejoined, thereby indicating the likelihood that the facial nerve trunk has developed into a neural ring around the retromandibular vein. The significance of this anomaly, although rare, is that the retromandibular vein cannot be used as a landmark surgically as both superficial and deep to it will lie the facial nerve trunk. In addition, any intra operative trauma to the vein requiring ligation, may actually pose risk to the facial nerve trunk.

Clinical significance of RMV variation to FN

A surgical example of where the retromandibular vein is relied upon to lead the surgeon away from the facial nerve is the extra-oral surgical approach to the mandibular condyle. Descriptions of both the transparotid and retroparotid methods of the retromandibular approach to the mandibular condyles stress the importance of remaining superficial to the retromandibular vein.⁵¹ The mandibular condyle poses a surgical region fraught with risks to the facial nerve.² In traumatic settings, the mandibular condyle fracture is a controversial area of discussion in terms of the most appropriate management, whether that constitutes open or closed reduction. Historically, the majority of these fractures were

managed with closed reduction; however, there is a growing body of evidence to support open treatment.^{15, 17} Extra-oral open reduction of the fractured mandibular condyle has many surgical approaches⁵²⁻⁵⁴, all of which provide limited 1-2 cm views of the structures involved, and hence a likelihood of facial nerve damage, as opposed to the wide front (Lazy S) views provided by parotid dissections.¹³ No agreement in the literature has been reached as to most appropriate approach to the mandibular condyle, with each approach possessing its own advantages and disadvantages with respect to posing a risk to the facial nerve or one of its branches.²

The retromandibular approach exposes the entire mandibular ramus from behind the posterior border. It therefore is useful for procedures involving the area on or near the condylar process / head, or the ramus itself. There are two varieties of retromandibular approach used to access the posterior mandible. They differ in the placement of the incision and the anatomic dissection to the mandible. The transparotid approach has the advantage of close proximity of the skin incision to the area of interest. The retroparotid approach has the advantage of not dissecting through the parotid gland. Both surgical approaches rely on conventional knowledge of normal anatomy of the facial nerve and its relationship to the retromandibular vein. In particular, the retroparotid approach relies heavily on the knowledge that the facial nerve lies superficial to the retromandibular vein.⁵¹ Any of the variations discussed above or indeed found within our cadaveric study, would imply that this commonly used surgical approach poses risk to the facial nerve due to its varied location – deep to the retromandibular vein.

Superficial temporal vein variation to facial nerve

Of the eight variant venous relationships to the facial nerve we discovered in our study, five were not variations of the retromandibular vein as described previously, but rather variations of the superficial temporal vein to the facial nerve (Figs. 9 – 12).

The superficial temporal vein was demonstrated in five cadaveric halves to be superficial to either the temporal branch of the facial nerve or indeed the entire facial nerve – the trunk and both the temporofacial and cervicofacial divisions.

This type of venous variation has not been described in any form as extensively as how the plane in which the retromandibular vein is located in relation to the nerve within the parotid has been described. In a case report Piagkou et al ⁵¹, described a variant, in which the superficial temporal vein was encountered lying over both the facial nerve divisions.

The first variant of the superficial temporal vein to the facial nerve we discovered (Fig 9 a & b) was a male cadaveric half, which demonstrated the temporal nerve branch coming off the temporofacial division of the facial nerve, diving deep to the superficial temporal vein and re-emerging more superiorly from deep to the superficial temporal vein. The superficial temporal vein continues inferiorly in the same plane, remaining deep to the temporofacial division coming off the bifurcation of the facial nerve. This particular case probably represents a variation in the direction of the temporal branch of the facial nerve rather than a variation in the intra-parotid venous structures. Nonetheless, the implications of failing to identify that there is a facial nerve branch deep to the superficial temporal vein during dissection could ultimately be significant, especially during access to the zygomatic arch for instance, in traumatic settings.

Figures 10 – 12 represent the most common type of superficial temporal vein variant we found. In these four cadaveric halves, the superficial temporal vein was superficial to the facial nerve trunk / both divisions after the bifurcation, before joining with the deeper maxillary vein, to form the retromandibular vein more caudal than would usually be expected within the parotid gland. The facial nerve branches appear to pass between the

fork of the superficial temporal vein and the maxillary veins in all cases. This relationship has not been described previously in the literature apart from the case reported by Piagkou et al. in 2013.⁵¹ It is a pattern where the superficial temporal vein largely would appear similar to the retromandibular vein in many respects, before joining the deeper maxillary vein. Considering the aberrant location of the superficial temporal vein, lying lateral to the facial nerve trunk in this variant type, and not the expected retromandibular vein the potential for injury to the facial nerve is significant in the context of parotid and condylar surgeries for clinicians who use the retromandibular vein as a landmark deep to which the facial nerve is not expected to be encountered⁵¹. This study demonstrates that the superficial temporal vein may be the first venous landmark encountered during a retromandibular - retroparotid surgical approach to the condyle. It should be noted that this variant pattern on the intra-parotid venous structures most likely represents a variation in the formation of the retromandibular vein, as the superficial temporal vein joins the maxillary vein in the parotid substance inferior to the tragal point, which is much more inferior than is generally recognised by surgeons⁴⁴. It is unlikely that it is the facial nerve that is the varying factor in these cases.

Clinical significance of the STV variation to the FN

However, regardless of the cause of the variation, the significance does not change. One must be aware that if relying on the retromandibular vein as a landmark intra-operatively, that it may not be the retromandibular vein that may be encountered at this caudal level within the parotid, but rather an aberrant superficial temporal vein, deep to which is the facial nerve trunk or its divisions may be forked between it and the maxillary vein.

In our study we have demonstrated that the superficial temporal vein is a structure that must be considered during parotid and peri-parotid surgery. Not only can the temporal

branches of the nerve vary in relation to the superficial temporal vein, but also this vein can be a large variant, extending caudally into the parotid gland to remain superficial to the facial nerve before joining the maxillary vein. Hence, when considering parotid surgery, reference to the retromandibular vein alone, as in most surgical texts can be misleading. Rather, the superficial temporal / maxillary vein complex and the resultant retromandibular vein should be seen as an intra-parotid venous complex that is likely to be as varied in each of its components as much as the facial nerve is likely to vary in each of its components. As part of the work completed in this Doctorate, a peer reviewed publication is included in appendix 1, describing the first superficial temporal vein variant (Fig 12) identified and elaborating the possible clinical implications.¹³

2.4.6 Conclusion

Two main methods of surgical guidance to the facial nerve were assessed in this arm of the Doctorate project. Firstly, the use of hard and soft tissue landmarks to identify the location of the facial nerve – the tragal pointer, the angle of mandible and the ‘safe zone’ along the malar arch, were all assessed for variability to the classical descriptions taught and used by operating surgeons across the spectrum. Secondly, the variations of the retromandibular vein and interestingly, the potential for superficial temporal vein variation was illustrated and described. The use of these venous landmarks may be problematic if variations do exist – both in potentially misleading the interpretation of MRI and CT images where the retromandibular vein is seen as a guide as to whether the facial nerve is involved in pathology or not and intra-operatively where the operating surgeon may be relying on the conventional relationship of the facial nerve to intra parotid venous structures, to help identify and protect the nerve.

Given the extent of variability shown in our study, which largely corresponds to the findings across the literature, the second arm of this Doctorate project seeks to utilize a relatively novel approach to outline the tract of the extra-cranial course of the facial nerve using diffusion weighted magnetic resonance imaging. This can be of great pre-operative benefit as it can allow the surgeon to assess the three dimensional position of the facial nerve by enabling accurate, case specific imagery of the location and direction of travel of the facial nerve, thereby reducing the reliance on surgical guides that may be obsolete, especially if variations do exist. In addition, by visualizing the facial nerve tract on imaging, the potential arises for significant improvements in diagnostic and staging procedures where neural involvement in surrounding pathology can be ascertained and potentially quantified.

Chapter 3 – Diffusion weighted tractography of the extra-cranial facial nerve course

3.1 Background

3.1.1 Extra-cranial facial nerve imaging

Imaging of the facial nerve has historically been difficult and inaccurate, given the complicated course of the facial nerve, and the different media each of the facial nerve sub-sections travel through.²⁰ The choice of imaging technique is tailored to the suspected pathology and its clinical localisation along the course of the nerve. Typically, if the pathology is localised to the cisternal, intracanalicular segments or the pontine nuclei, the indicated imaging technique is contrast-enhanced MRI. If clinical suspicion localises the lesion to the mastoid, tympanic, or labyrinthine segments, the indicated imaging technique is high-resolution temporal bone CT to investigate the fallopian canal. If the locality of the pathology is uncertain, contrast-enhanced MRI is often performed to further investigate. In cases of tumours involving the facial nerve, both MRI and temporal bone CT are recommended for the evaluation.²⁰

The extra-cranial course of the facial nerve is complicated by the tightly encapsulated parotid gland through which it travels. Its location is not fixed within the gland and may vary both in the caudocranial and mediolateral dimensions. The parotid is arbitrarily divided into superficial and deep lobes by the facial nerve.⁵⁵ Historically, the intra-parotid segment of the facial nerve has been best visualised using high resolution T1-weighted MRI images using a microscopic coil.²⁰ This allows for recognition of the facial nerve, but seldom allows for credible ability to track its course. With the use of gadolinium contrast, enhancement of the facial nerve within the parotid raises suspicion of the involvement of

the nerve in inflammatory or neoplastic processes, as usually with contrast, the cisternal, intra canalicular, labyrinthine and parotid segments of the facial nerve do not enhance ⁵⁶. In cases of parotid tumours, a reliable facial nerve map may assist safe and effective tumour resection. To date, morphological MRI techniques to try to produce a facial nerve map remain extremely difficult requiring complex spatial reconstructions, as slice-by-slice analysis is too difficult with these techniques. ^{57, 58}

Diffusion tensor tractography (a relatively new MRI imaging technique) has shown some promise in the identification of the facial nerve course extra-cranially. ⁵⁹⁻⁶¹ This is a relatively new technology in the setting of extra-cranial neural white matter tracts, but has been used extensively in the mapping of intra-cranial white matter tracts and in the setting of the facial nerve, to map and delineate the facial nerve from involved vestibular schwannomas. ^{62, 63} This study assesses the feasibility of applying diffusion tensor imaging techniques to map the extra-cranial facial nerve course.

3.1.2 Clinical implications

Surgical resection in the setting of parotid tumours remains the gold standard treatment, despite the risk to the facial nerve. ⁶⁴ The major risk in these surgeries is injury to the facial nerve due to compression, damage or transection on approach, which has significant morbidity for the patient. ³⁶ Consequences of damage to the facial nerve may impact on quality of life via functional deficits in eating, drinking, speaking and conveying intimate human information and emotion. ⁶⁵ One such deficit is the issue of corneal exposure, leading to desiccation, and ultimately blindness if left untreated ⁵⁹.

One way to considerably reduce the risk of iatrogenic damage to the facial nerve would be to have available a reliable map of the extra-cranial portion of the nerve as it courses

through the parotid gland.⁵⁹ The most obvious setting where this would be advantageous is in the case of a parotid tumour, where a facial nerve map would allow for effective planning of surgery and focused pre-operative counselling to the patient as to the likely risk of facial nerve damage and to which branch the damage is most likely to occur with the specific resultant deformity explained.^{59, 61} Furthermore, from a diagnostic and treatment planning point of view, by using diffusion tractography in the setting of parotid tumours, it has been shown possible to determine radiologically whether there is contact with the facial nerve by a parotid tumour, by measuring the fractional anisotropy (FA) values of the tracts in proximity to the tumour.^{59, 61} Fractional Anisotropy (FA) is a scalar value between zero and one that describes the anisotropy of a tissue undergoing a diffusion imaging process. Zero would mean that diffusion is isotropic – unrestricted in all directions. One would mean that diffusion occurs in only one axis and is restricted in all other directions. FA is a value used in diffusion imaging that is dependent on and reflective of fiber density, axonal diameter and myelination in a white matter tract. A reduction of FA values in facial nerve tracts approximating parotid tumours, have been surgically verified as signifying contact and sometimes compression of the nerve, in a recent study by Attye et al.⁵⁹, with a high level of sensitivity. This would potentially assist the operating surgeon to anticipate difficulties relating to nerve dissection at the regions of contact with or compression of the facial nerve tract by the parotid tumour.

Apart from helping plan for and counsel patients as to the surgery to remove parotid pathology, diffusion tractography has some other important clinical uses when it comes to the extra-cranial course of the facial nerve. Other interventions that pose risk to the facial nerve include extra oral mandibular surgery. The mandibular condyle, when surgically exposed in both the traumatic and elective setting, is fraught with risk to the facial nerve.² No agreement in the literature has been reached as to most appropriate approach to the

mandibular condyle, with each approach posing a risk to the facial nerve or one of its branches.² Pre operative mapping of the facial nerve could help the operating surgeon, plan an approach that is able to avoid some of the main facial nerve branches at risk, a considerable possibility especially because mandibular condyle / ramus access surgery provide only a limited view of the structures involved through 1-2cm incisions, and hence more likelihood of damage, as opposed to the wide front (Lazy S) views provided with clear dissection of the facial nerve in parotid dissections.¹³

Diagnostically it is important to identify the relationship of the facial nerve to parotid tumours. However, it is also of crucial importance to be able to identify the nature of the parotid tumour to inform management. Currently, the gold standard for this is by ultrasound guided aspiration cytology or core biopsy.⁶¹ MRI assessment remains important in the diagnostic process. Morphological MRI characteristics of the parotid lesion in addition to gadolinium contrast-enhanced MR imaging, are efficient methods to assess and differentiate tumour type.⁶⁶ With the advent of diffusion weighted imaging, which relies on the concept of the apparent diffusion coefficient (ADC), the measurement of the ADC has been shown to be a possible differentiating variable among parotid tumours.^{66, 67} It has been shown that ADC can improve the accuracy of diagnosing parotid tumours with higher ADC values favouring a diagnosis of pleomorphic adenomas and lower ADC values favouring malignant masses.^{66, 67} While currently, diffusion imaging would greatly support the assessment of parotid tumours in addition to enhanced MRI techniques, the potential, in the future, for contrast free diffusion weighted magnetic resonance imaging of parotid lesions is available as shown by this study.

3.1.3 Diffusion Imaging

DWI relies on the concept of diffusion. Diffusion is the random spread of molecules in a medium such as water due to Brownian motion. In biological tissues, diffusion can be affected by the presence of other cellular structures and spatial constraints.⁶⁸ This spatial hindrance is usually not spatially symmetrical (i.e. not spherically symmetrical). For example, in an axon, diffusion would be hindered much more across the diameter of the axon, when compared to the longitudinal direction of the axon. This asymmetrical spatial constraint is termed anisotropy, whereas the condition of spherically symmetric spatial constraints is called isotropy.

Diffusion and anisotropy can be probed by MRI. First described by Stejskal and Tanner⁶⁹ in 1965, in the context of nuclear magnetic resonance, diffusion weighted imaging's (DWI) first application, in clinical imaging, was performed by Le Bihan in 1986.^{70, 71} DWI relies on the playing of a pair of diffusion gradients in a particular spatial direction on either side of a 180° pulse that serves to dephase and rephase the spins present in the tissue.⁶⁸ In an ideal but unrealistic situation without diffusion and motion, the spins would rephase perfectly, resulting in maximal signal recovery, subject to T2 relaxation. However, the presence of diffusion results in incomplete rephasing, thus a sub-optimal signal is recovered, resulting in signal loss. The principle of DWI is based on the anisotropy of the tissues or material – DWI probes the amount of signal loss in various directions and thus probes the microscopic asymmetry of the tissue.⁷⁰ Signal loss is fundamental to diffusion imaging in MRI and the amount of signal loss can reveal much about the structure, type, and orientation of the tissue imaged.

In DWI, several values are important. The b-value is a measure of the strength, duration, and spatial distance between the diffusion gradients. A high b-value can indicate high diffusion gradient amplitude, long spatial distance between the gradients, and/or long diffusion gradients. The b-value is decided by the user (e.g. radiologist) and together with

the diffusion coefficient of the tissue - a measure of diffusion in the tissue, it affects the degree of signal loss.⁶⁸ As diffusion coefficient estimations can be affected by experimental errors and artefacts, calculated diffusion coefficients are often referred to as apparent diffusion coefficients (ADCs).

Diffusion tensor imaging (DTI) is a specific but common diffusion imaging technique that measures the anisotropy of a material, requiring at least two b-values and six (often many more) independent diffusion gradient directions.⁶⁸

The principles of diffusion imaging can extend to tractography - the imaging of fiber tracts.^{72, 73} In general, the general algorithm involved in tractography involves seeding, tracking, and termination. Seeding is the placement of the starting voxel to allow the tractography algorithm to start its tracking; tracking is the construction of the fiber based on the seed; and termination is the decision to end tracking (i.e. end of fiber).⁷⁴ The algorithm would also take into consideration constraints such as the requirement for a tract to pass through a certain area, avoid certain areas, and the spatial bounds (i.e. within skull).⁷⁵ A major limitation of tractography revolves around the difficulty of identifying fibers and resolving fiber crossings and is reflected in the diffusion model used, the seed placement, and the tracking algorithm used.⁷⁶

So far, the vast majority of DTI and tractography has been used to image intracranial neuronal fiber tracts. The literature with regards to nerves outside the brain include the sciatic nerve and median and ulnar nerves in the wrist.^{77, 78} Extra-central nervous system cranial nerve diffusion tractography has only recently began to focus on the imaging of the facial nerve to identify its course through the parotid and contact with parotid tumours with surgical validation.^{59, 60}

While there are several technical challenges, diffusion imaging has benefited the clinical setting in the form of diagnosing, surgical planning and disease monitoring.⁷⁵ DTI has been used to correlate brain microstructure with brain function and related neurodegenerative diseases.^{74, 79} Surgical validation has shown that it is also reliable in the precise estimation of nerve location/course and may be used to prevent surgical injury to nerves.⁸⁰ Improvements are currently being made to areas such as tractography algorithms and diffusion models.^{81, 82}

3.1.4 Aims and Objectives

In this arm of the Doctorate project we hypothesise that DWI tractography of the extra-cranial course of healthy facial nerve (in disease free parotid glands) will enable the identification in three dimensions the facial nerve trunk and the point of bifurcation with varying lengths of the cervicofacial and temporofacial divisions.

Our aims are as follows

1. DWI tractography of the facial nerve main trunk, point of bifurcation and varying lengths of the cervicofacial and temporofacial divisions in three dimensions against an anatomical, high resolution T1 or T2 overlay, thereby eliminating the need for surgical landmarks as the exact location of the main trunk will be known by pre operative image analysis.
2. Metric validation of our findings by the use of fractional anisotropy measurements.
3. Surgically validation of our findings by the use of three cadaveric specimens who will undergo detailed facial nerve dissection post imaging.
4. Derive a reproducible imaging protocol post cadaveric imaging and analysis that can be applied to live subjects. Two live subjects will undergo imaging to test the imaging protocol derived and show clinical applicability.

3.2 Materials and Methods

3.2.1 Cadaveric scan & dissection

Collaboration was created between the Anatomy Department of Trinity College Dublin and the Neuroscience Institute's REDEEM trial of Trinity College Dublin. Two cadaveric subjects, donated to the Anatomy Department for teaching and research purposes were acquired for scanning at the Neuroscience Institute and subsequently returned to the Anatomy Department for detailed dissection and comparison to the image results. Two donors were scanned using DWI and subsequently dissected to allow for comparison and anatomic validation of the imaging results.

Subsequent to the cadaveric scans, once adequate results were obtained and validated by dissection and scanning parameters were outlined, two live subject scans were carried out to assess whether similar results were achievable in live scans without changing the scanning parameters used. All live subjects were 25-32 years of age, healthy with no history of head or neck pathology or previous surgery.

The first cadaveric subject was a 91 year old Irish Caucasian female, who at the time of death had not had any head or neck pathology or previous surgery. The second cadaveric subject was a 79 year old Irish Caucasian male, who at the time of death had not had any head or neck pathology or previous surgery. Both donors were embalmed using the new 'Dodge' embalming technique adopted by the anatomy department. Consent had been obtained from both subjects on making their decision to donate for purposes of medical study, research and teaching within Trinity College Dublin. Ethical and procedure approval was obtained from the management of both the Anatomy Department and the Neuroscience Institute of Trinity College Dublin.

Collaboration with the Professor of Radiology and Head of Neuroradiology at the Adelaide and Meath University Teaching Hospital (Trinity College Dublin affiliated) and the Professor / Chair of Oral & Maxillofacial Surgery Department of the Dublin Dental University Hospital, Trinity College Dublin was sought throughout this trial.

3.2.2 Donor embalming technique

In the context of increasing interest in cadaveric imaging, we describe a relatively novel technique of embalming that may have better tissue preservation properties than conventional methods of embalming. This may be of benefit, not only in enabling better dissection results, but also in image related functions such as acquisition, processing and analysis. Both cadaveric donors involved in the imaging arm of this Doctorate were embalmed by the department of Anatomy technical staff, using the ‘Dodge’ embalming technique within twenty four hours of death, as designed and marketed by the Dodge company limited, Units 11/14-15, Ardglan Industrial Estate, Whitechurch, Hampshire, RG28 7BB. The advertised advantage of Dodge is that it produces excellent long term results and provides a highly mobile cadaver, with good definition of all structures with reduced exposure to fumes and harmful chemicals. Tissues are softer and easier to dissect and the embalming formula can be altered for softer fixing of the tissues to enable the practice of surgical techniques.

The following protocol was applied to the cadaveric donors for embalming using Dodge:

- 1) The cadavers were shaved and washed using Dodge Disinfectant Concentrate. This stage generally allows for manipulation of the joints to relieve rigor mortis.
- 2) The cadavers were positioned on the embalming table and raised above the surface of the table using Dodge body rests or other suitable blocks. This step helps with distribution of chemicals to the posterior of the cadaver.

- 3) The cadavers were subsequently sprayed with Dodge Dis-Spray (appendix 2) over the entire surface of the body. This allows a coating to build up that will retard mould formation.
- 4) Both the right common carotid artery and the right internal jugular vein were used for injection in the two cadaveric subjects, as these are the manufacturer recommended sites for best results. The vessels were raised inferiorly in the neck, not interfering with the parotid tail in the superior neck.
- 5) The right internal jugular vein was ligated first and as large a diameter drain tube as possible was inserted to ensure effective removal of clotted blood. After preparation of the vein, the artery was then ligated and an injection tube inserted.
- 6) The pre-injection solution was prepared and injected into both cadaveric donors. The pre-injection is designed to breakdown blood clots and remove blood products from vascular system prior to injection of the preservative. This step should allow for better diffusion of preservative chemicals and reduce the need for hypodermic treatment of certain areas after arterial embalming. The suggested pre-injection mix is 100mls each of Dodge Metaflow (appendix 3) and Rectifiant (appendix 4) per litre of water.
- 7) The main embalming procedure was subsequently undertaken. The following solution was used. Into a ten litre pressure tank or embalming machine, the following constituents were mixed:

Dodge Metaflow

Dodge Rectifiant

Dodge Introfiant (appendix 5)

Dodge Dis-Spray

Dodge Restorative (appendix 6)

This solution was injected into the cadavers using the injection equipment available. Volumes of mixes were as generous as required to completely saturate the tissues of the cadaver.

- 8) Any areas of the body not receiving an adequate amount of solution were treated using hypodermic injection and the same arterial solution.
- 9) Once the arterial embalming and hypodermic treatments were carried out, treatment of the internal organs was subsequently performed. Using a hypodermic syringe and a medium course hypodermic needle low fuming Dodge Syn Cav was injected into the abdominal cavity to complete the process.
- 10) Both cadavers were re sprayed a final time with Dodge Dis-Spray and left to dry before being placed into the body bags for storage in the fridge. The body bags were also sprayed with Dis-Spray.
- 11) Once dissection started, both cadavers were periodically sprayed with Dis-Spray to overcome any airborne spores, which can lead to mould and desiccation.

3.2.3 Dissection technique

Both cadaveric subjects had a retrograde dissection of the facial nerve bilaterally to ascertain anatomic comparison to the diffusion imaging results. Dissection was carried out in the Anatomy department of Trinity College Dublin, under theatre lighting conditions, after the imaging process had been undertaken. High quality images captured using a Nikon D50 Digital SLR camera.

An extended pre-auricular approach was carried out and the entire parotid gland visualised. Skin and subcutaneous tissue was lifted and a plane developed subcutaneously, superior to the superior masseteric aponeurosis system (SMAS) layer. A large peripheral division of

the facial nerve was identified and followed in a retrograde fashion to the main trunk, removing the superficial lobe of the parotid gland in the process. The buccal branch was the large division most often identified and traced proximally. The main trunk was subsequently exposed and the temporofacial and cervicofacial divisions were followed until the five peripheral (temporal, zygomatic, buccal, marginal mandibular and cervical) nerve bundles were exposed with the superficial lobe of the parotid gland removed.

Great care was taken not to manipulate the nerve branches from their locations in the three dimensions – hence the deeper lobe of the parotid gland was left *in situ*, so as to allow accurate comparison to the diffusion tractography images.

3.2.4 Imaging protocol used and post-processing analyses

Image acquisition was carried out by the resident Radiographer at the Neuroscience Institute of Trinity College Dublin in liaison with the chief image analyst of the REDEEM trial. The REDEEM trial personnel performed post acquisition processing of the raw data to enable tractography analysis. Data analysis and the comparative calculations with the anatomic dissections were carried out by the studentship of this Doctorate project.

3.2.4.1 Anatomical (T1) imaging

180 axial high-resolution T1-weighted anatomic SPGR images (TE = 3.8 ms, TR = 1698.4 ms, FOV 230 mm, 0.898 x 0.898 mm² in-plane resolution, slice thickness 0.9 mm, 170 flip angle $\alpha = 80^\circ$) were obtained with an approximate acquisition time of 6.5 minutes.

3.2.4.2 Diffusion Weighted Imaging (DWI)

Whole brain plus head and neck, High Angular Resolution Diffusion Imaging (HARDI) 36,37 data was acquired for each participant (cadaveric and live subject participants) on a

Philips Intera Achieva 3.0 Tesla MR system (Best, Netherlands) equipped with a 32-channel head or head and neck coil. Diffusion weighted images were 175 acquired using a spin-echo echo-planar imaging (SE EPI) pulse sequence (TE = 52 ms, TR = 11.260 ms, flip angle $\alpha = 90^\circ$), FOV 224 mm, 60 axial slices $1.75 \times 1.75 \text{ mm}^2$ in-plane resolution, slice thickness 0.5 - 2 mm, b-value = 400 - 1500 s mm^{-2} in 61 non collinear gradient directions. The start of each series of directions was preceded by non-diffusion-weighted volume (comprised of four averages of the b = 0 image) so as to allow image registration and motion correction. Approximate acquisition time = 15 minutes. All scanning was conducted on the same scanner in Trinity College Institute of Neuroscience, Dublin.

3.2.4.3 DTI data pre-processing

Pre-processing and analysis was performed using 'ExploreDTI' (<http://www.exploredti.com/>), an academic research software suite (Figure 13) that permits the functionality of pre-processing, modeling and computation of diffusion data. Pre-processing was undertaken to a) allow for the conversion of the diffusion data into the appropriate format and b) correct for known and predicted systematic problems inherent in diffusion data. The pre-processing procedure consisted of File Standardisation, Signal Drift Correction, Gibbs Ringing Correction, Generation of *.mat file, Checking orientation of images, Correcting for eddy currents and head motion and Correcting for EPI deformations. These are described in detail in appendix 7.

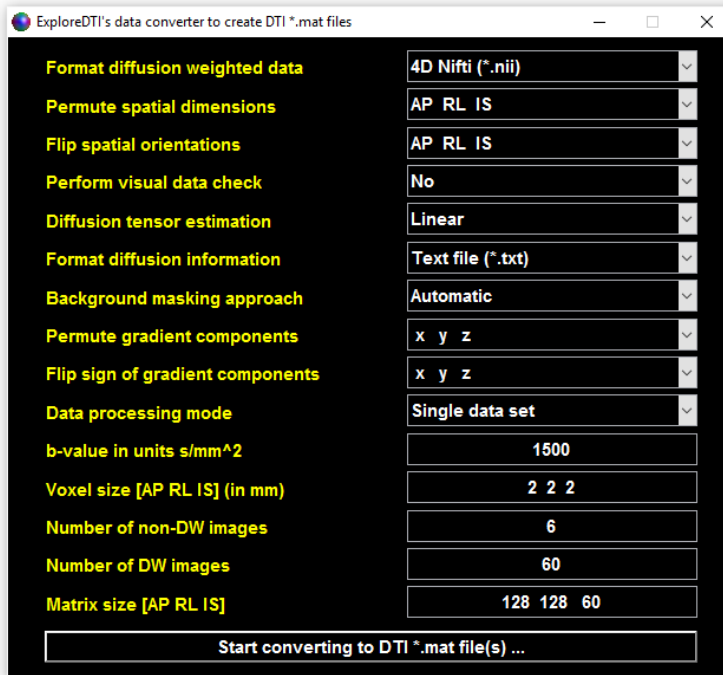


Figure 13 ExploreDTI data conversion tool

3.2.4.4 Post-processing Head and Neck tractography

‘ExploreDTI’ software allows for deterministic plus probabilistic fiber tractography, allows for clustering of fiber tracts and has an array of data quality assessment tools. Crucially, it permits Constrained Spherical Deconvolution (CSD)-based tractography which enables a more precise reconstruction of local fiber orientation in crossing fiber regions as compared to the classic tensor based or probabilistic methods⁸³. Inherent to ExploreDTI is its recursive calibration of the response function as the principle method of CSD calculation. The tractography that was performed, throughout the entire head and neck region in all our scanned subjects, modeled all potential deterministic streamlines according to the following parameters; seed point resolution was set at 2 x 2 x 2 mm, step size of 0.5, 1 and 2mm, the FOD (Fibre Orientation Distribution) threshold set to 0.1, with a maximum angle threshold set to 89 degrees.

3.3 Results

3.3.1 Cadaveric scan 1 right facial nerve

3.3.1.1 Dissection

The first cadaveric subject to undergo diffusion weighted imaging of the head and neck and subsequently dissection of both parotid glands to expose the extra cranial course of the facial nerve was a 91 year old Irish Caucasian female, with no history of head and neck pathology or surgery. Fig. 14 (a-d) describes the stages of dissection of the right facial nerve.

An extended pre-auricular incision was made (Fig. 14a) to expose the entirety of the parotid gland. Skin and subcutaneous tissue were raised and a plane developed superficial to the SMAS and the parotid capsule (Fig. 14b). A retrograde approach was planned and carried out. The large buccal terminal branch bundle was followed proximally to the main trunk, removing the superficial lobe of the parotid gland over the nerve while taking care not to manipulate the position of the nerve branch in the three dimensions (Fig. 14b).

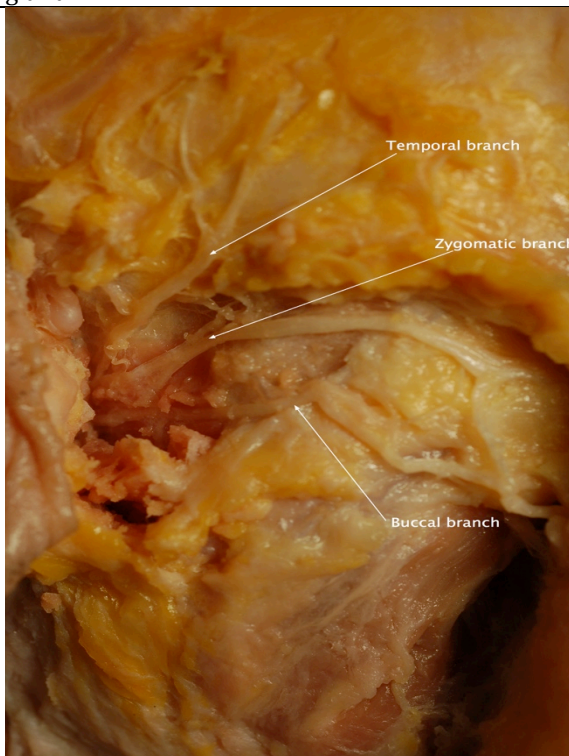
Once the main trunk was identified, the temporofacial division was followed distally, exposing the temporal and zygomatic branches in the same way the buccal branch was exposed (Fig. 14c). The deep lobe of the parotid gland was left in situ with only the superficial parotid lobe removed in order to preserve the nerve branch locations so as to allow correct comparison to imaging results done pre dissection. Once the temporofacial division was exposed, the cervicofacial division of the facial nerve was followed distally to expose the marginal mandibular and cervical branch bundles in addition to preserving the anastomotic branches between the cervicofacial and temporofacial divisions involving the buccal (temporofacial) and marginal mandibular (cervicofacial) branches (Fig. 14d).



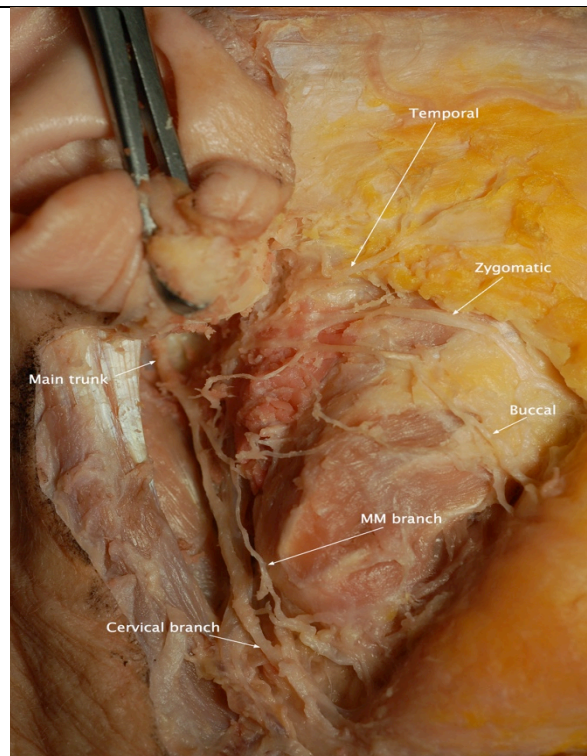
14a. Extended pre auricular approach to parotid gland.



14b. Skin & subcutaneous tissue was lifted and plane developed subcutaneously. Identification of the buccal division of the facial nerve



14c. TF division of facial nerve exposed showing zygomatic and temporal branches.



14d. Entire facial nerve with five terminal divisions.

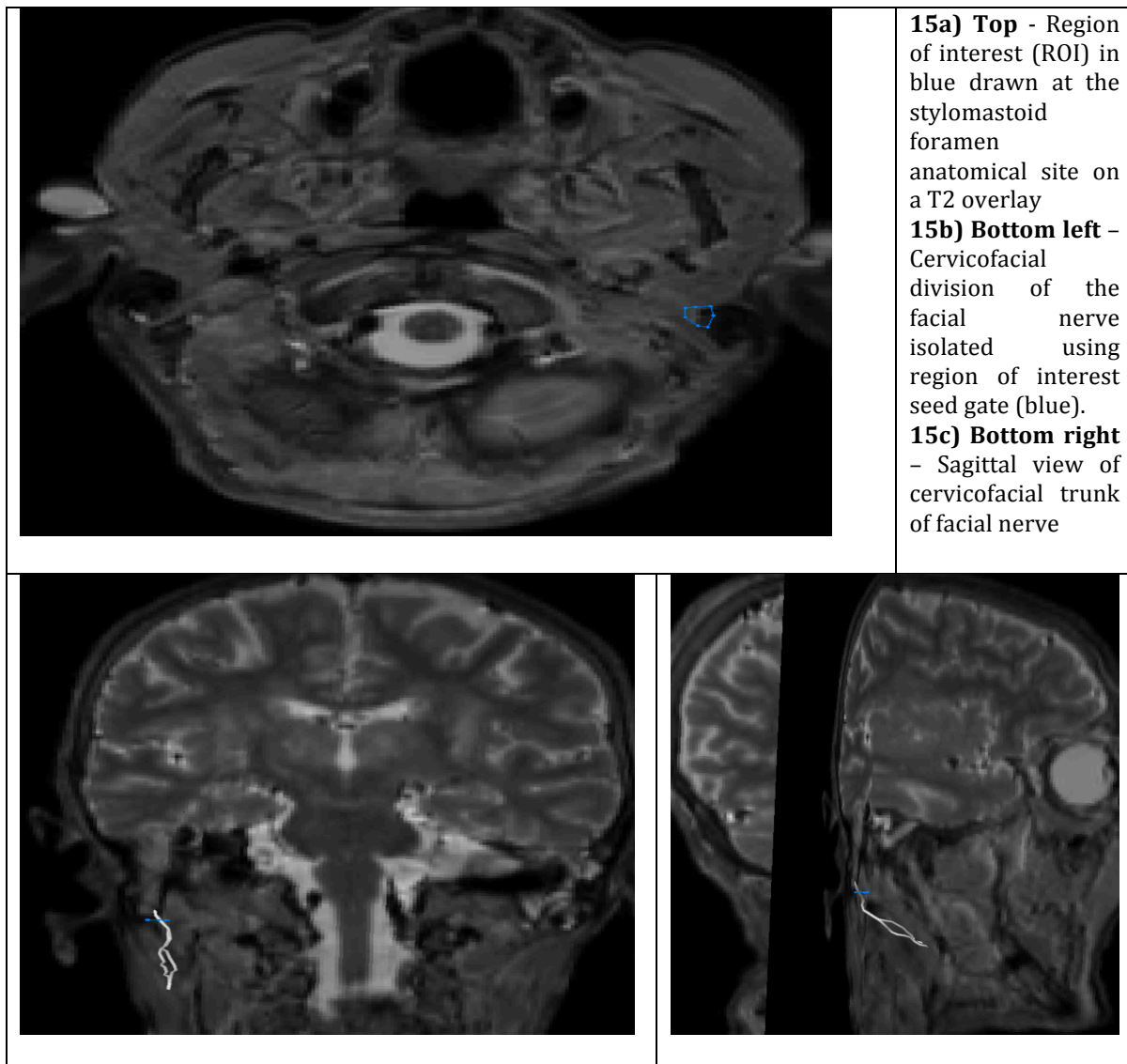
3.3.1.2 Diffusion tractography

Post-processing analysis took place in the Neuroscience Institute of Trinity College Dublin. Optimal results were obtained on scan parameters at a b value of 400, voxel size of 2mm^3 , 89 degrees at 1mm step size.

A three dimensional animation is available at this link;

<https://drive.google.com/file/d/1qnd2PksWb4orVO-n2jxYTA83TbchtDxh/view?usp=sharing>

A manually drawn region of interest (ROI) gate on an axial diffusion slice was drawn at the region of the stylomastoid foramen (Fig. 15a) using the calibrated anatomical sequence overlay of the baseline T2 MRI obtained at the beginning of the scanning process.



Figs. 15b & 15c show the lower division tract identified once tractology analysis was performed after isolating the stylomastoid foramen using a ROI gate. The cervicofacial trunk identified on imaging shows a tract that divides and re-joins at a caudal position.

This was identified as a stable segment (red – Figs. 16a & 16b) that could be compared to the cervicofacial trunk of the facial nerve dissection of the same subject (Fig. 14d).



Figure 16a. Comparable segment (red) of cervicofacial trunk used to compare diffusion tract to anatomic dissection

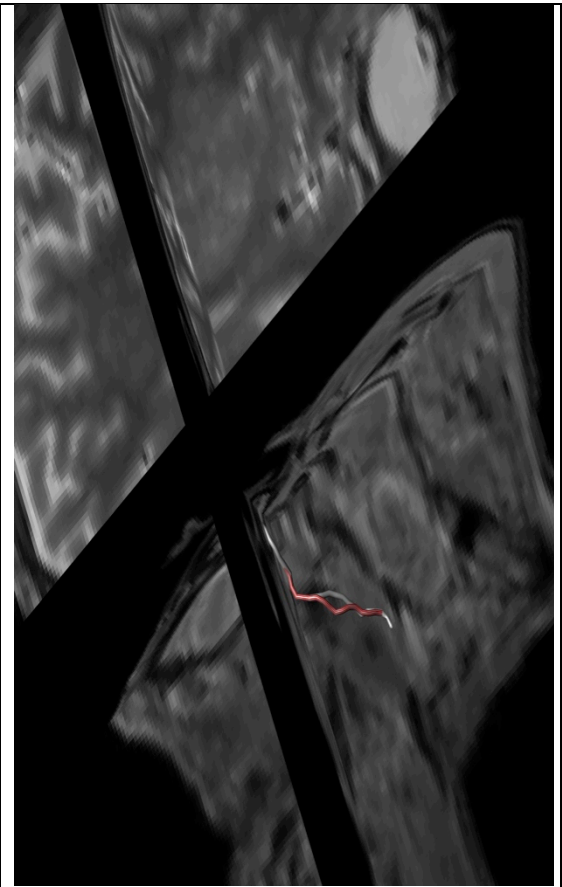
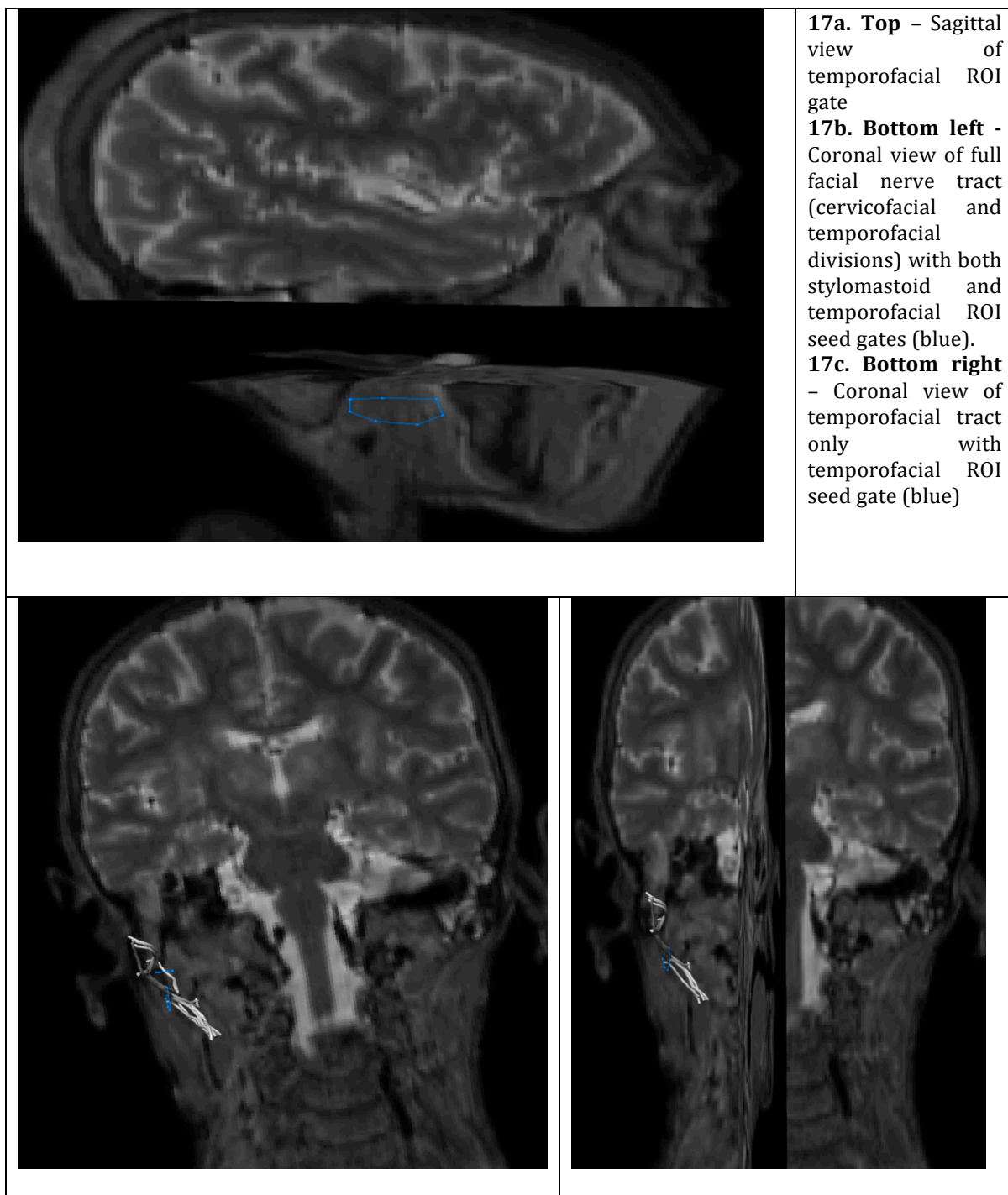


Figure 16b. Sagittal view of cervicofacial trunk with comparable segment (red) to anatomic dissection

An additional region of interest seed gate was required to enable adequate tracking of the temporofacial division. The ROI was placed laterally along the parotid gland substance on the T2 overlay (Fig. 17a).



Tractography analysis through the temporofacial ROI gate produced a tract of broadly two elements. One element seems to correlate with the direction and angulation of the cervicofacial trunk identified previously through the stylomastoid ROI gate. The other element is the temporofacial element that is angulated in both a lateral and superior aspect to the cervicofacial trunk (Figs. 17 b, c & 18).

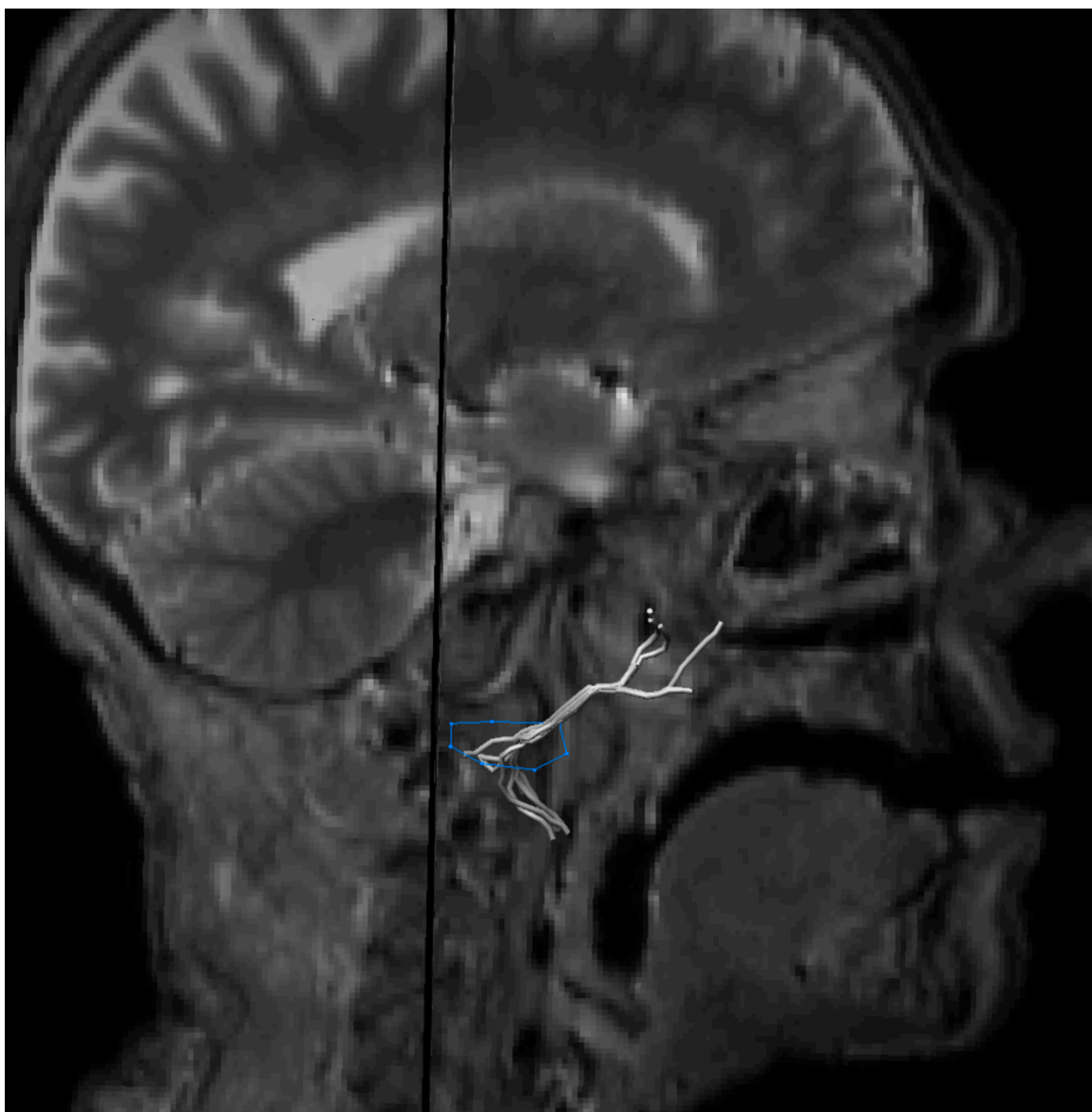


Figure 18. Sagittal view of temporofacial ROI gate with tract showing evidence of both cervicofacial and temporofacial trunks of facial nerve

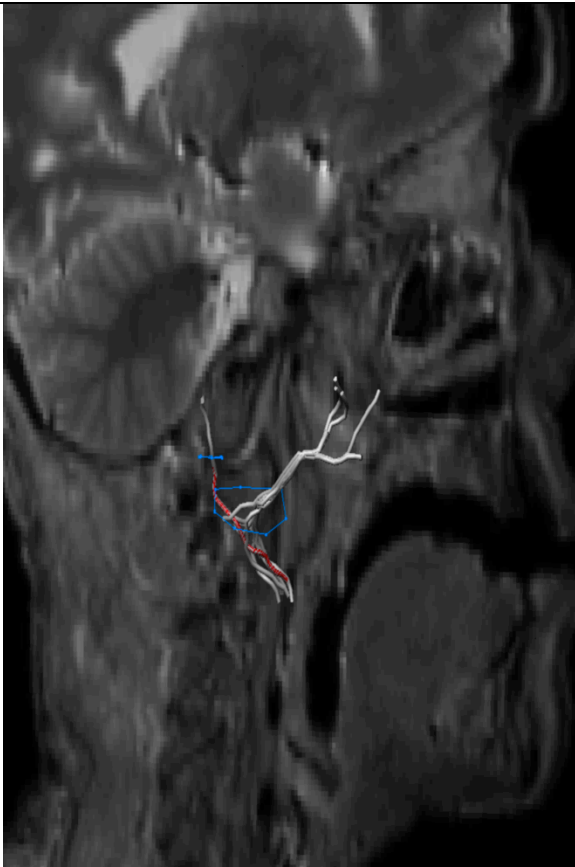


Figure 19a. Temporofacial tract as analysed through the temporofacial ROI (inferior blue) superimposed on cervicofacial tract as identified through the stylomastoid ROI gate (superior blue) with anatomically correlated segment (red).

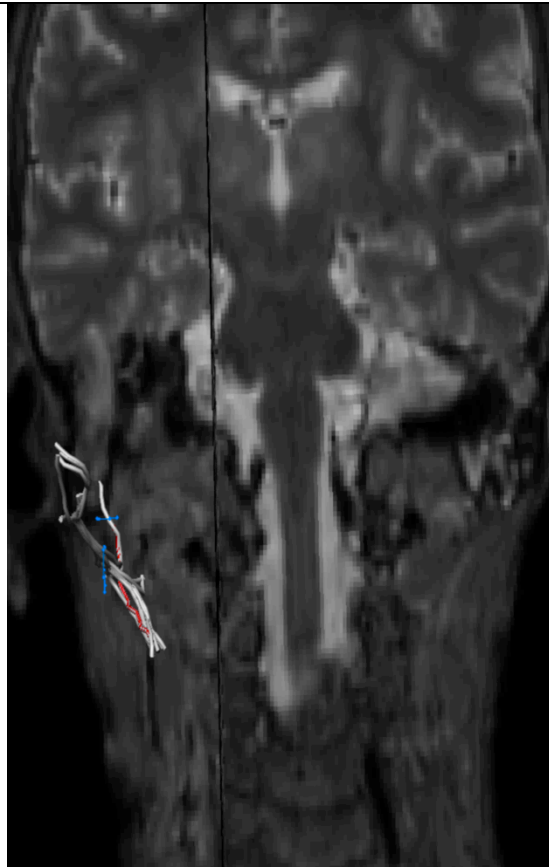


Figure 19b. Coronal aspect of superimposed tracts with both ROI gates (blue) and anatomically correlated segment (red) of cervicofacial division

Figs. 19 a & b show both tracts as analysed through both ROI gates superimposed. In addition, the anatomically correlated segment of the cervicofacial trunk (in red in both images) is highlighted. Fig. 19a is a sagittal view of the superimposed tracts and Fig. 19b is a coronal view, each providing a perpendicular view to the other of the entirety of the facial nerve. The anatomically correlated segment of the cervicofacial division is depicted in red and will act as point of reference from which to validate the temporofacial tract to the cervicofacial and also to validate the tracts to the detailed anatomic dissection of the same cadaveric subject in our discussion, to follow.

3.3.2 Cadaveric scan 2 – Right facial nerve tractography

3.3.2.1 Dissection

The second cadaveric subject to undergo diffusion weighted imaging of the head and neck and subsequently dissection of both parotid glands to expose the extra cranial course of the facial nerve was a 79 year old Irish Caucasian male, with no history of head and neck pathology or surgery. Fig 19. (a-d) describes the stages of dissection of the right facial nerve.

An extended pre-auricular incision was made (Fig. 20a) and a plane developed subcutaneously, superficial to the superior masseteric aponeurosis system (SMAS) to expose the parotid capsule. A terminal branch was identified as the buccal branch (Fig. 20b). The buccal branch was subsequently followed in a retrograde fashion to the main trunk of the facial nerve (Fig. 20c), removing the superficial lobe of the gland, leaving the deep lobe *in situ* so as preserve the location of the facial nerve. From the main trunk, the remainder of the facial nerve's two divisions – temporofacial and cervicofacial were exposed and the superficial parotidectomy completed (Fig. 20d).

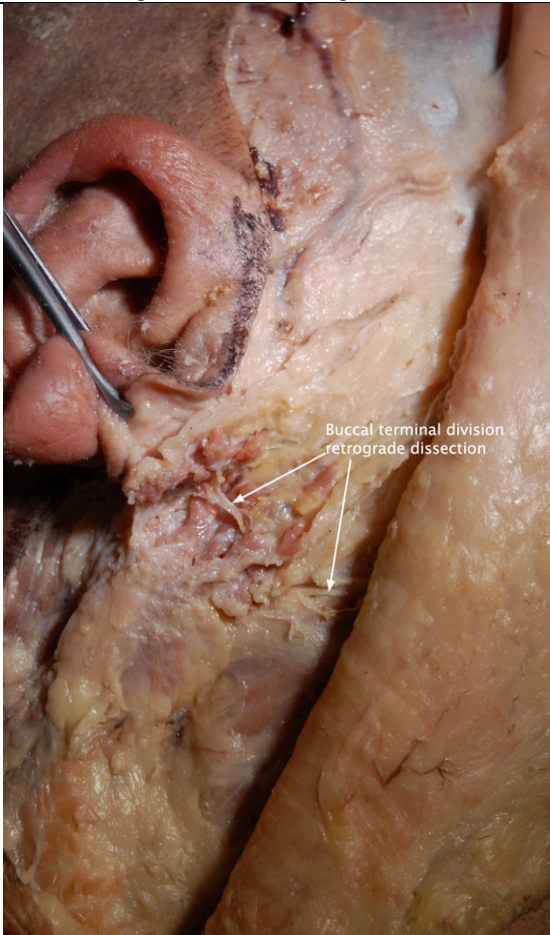
The completed dissection shows a single main trunk dividing into a temporofacial and cervicofacial divisions. The temporofacial division further subdivides into the temporal and zygomatic terminal nerve bundles. The cervicofacial division gives off the buccal, marginal mandibular and cervical nerve bundles (Fig. 21). There is no significant anastomosis between the two divisions.



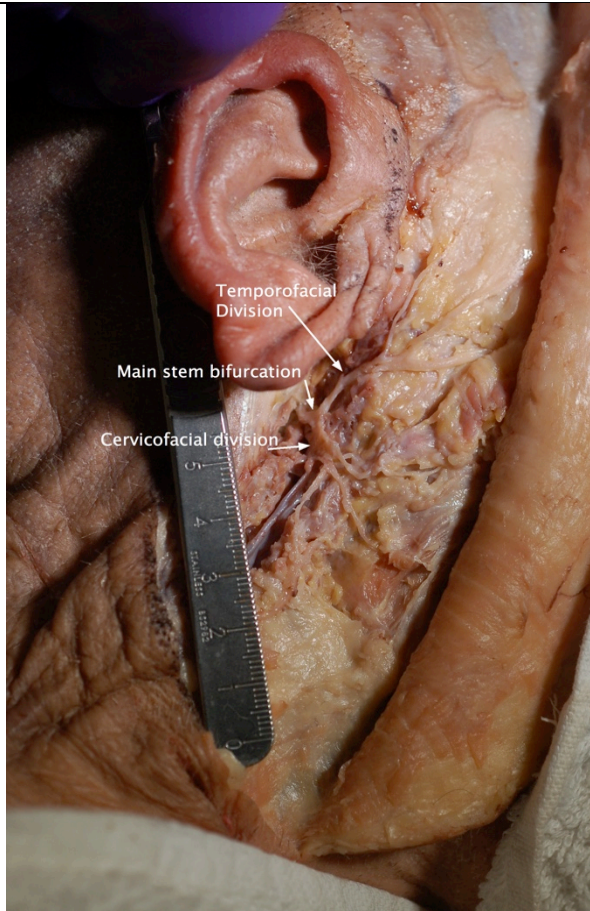
20a. Extended pre auricular incision pre marked



20b. Plane superficial to SMAS – terminal buccal branch identified



20c. Retrograde dissection of buccal terminal branch



20d. Completed dissection of facial nerve showing both divisions

Figure 20 (a-d). Stages of retrograde dissection (superficial parotidectomy) of facial nerve

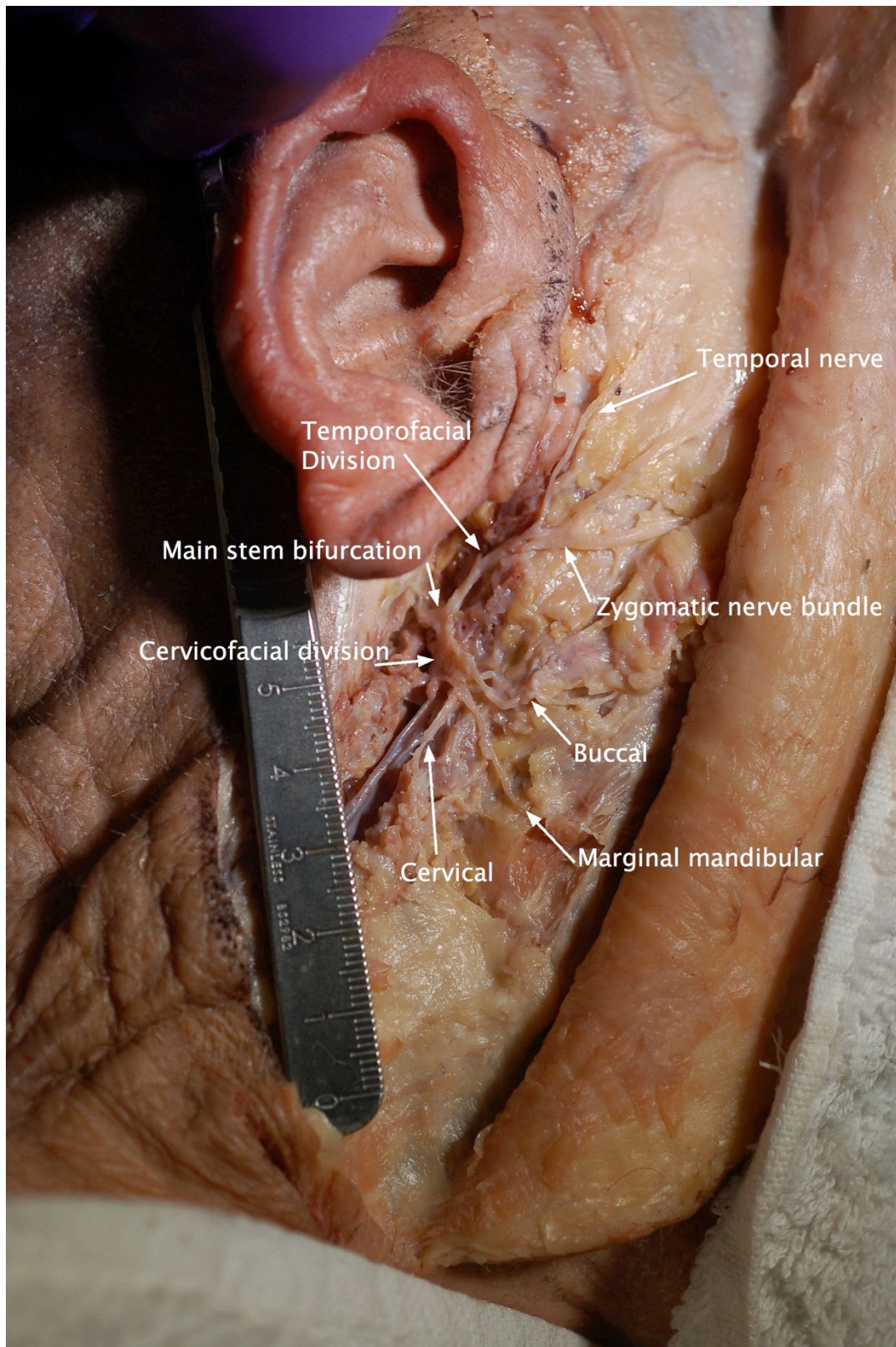


Figure 21. Fully labelled completed dissection of right facial nerve

3.3.2.2 Diffusion Tractography

Post-processing analysis took place in the Neuroscience Institute of Trinity College Dublin. Optimal results were obtained on scan parameters at a b value of 400, voxel size of 2mm^3 , 89 degrees at 0.5 mm step size.

A three dimensional animation is available at this link;

<https://drive.google.com/file/d/1qnd2PksWb4orVO-n2jxYTA83TbchtDxh/view?usp=sharing>

A manually drawn region of interest (ROI) gate on an axial diffusion slice was drawn at the region of the stylomastoid foramen (Fig. 22) using the calibrated anatomical sequence overlay of the baseline T2 MRI obtained at the beginning of the scanning process.

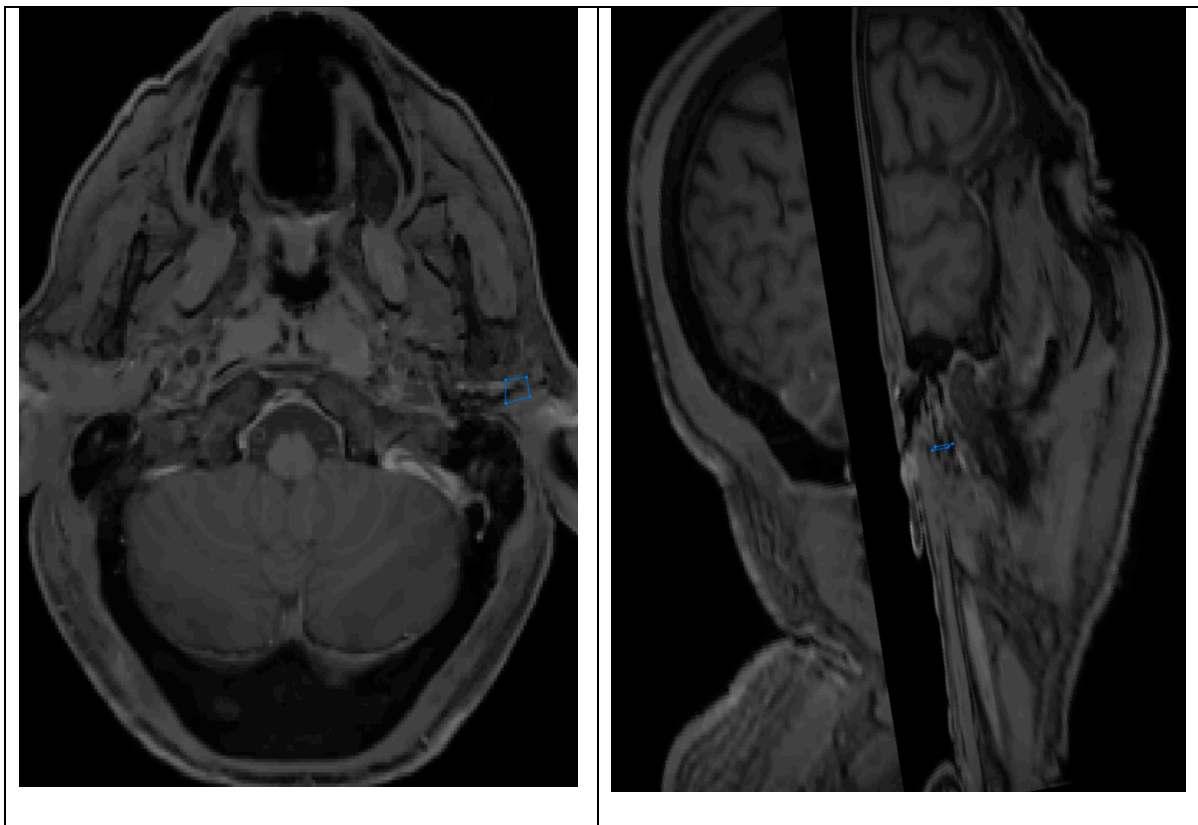


Figure 22. Axial (right) and sagittal (left) views of ROI gate (blue) placed at stylomastoid foramen

Tractography analysis through the region of interest seed gate as seen in Fig. 22, produced what appeared to be facial nerve cervicofacial division along with multiple artefactual tracts. The denser appearing, anatomically most relevant tracts which appeared to represent the cervicofacial division of the facial nerve were isolated with an ‘and’ gate so as to isolate tracts travelling through both the stylomastoid foramen ‘seed’ gate in blue and the ‘and’ gate in green (Fig. 23).

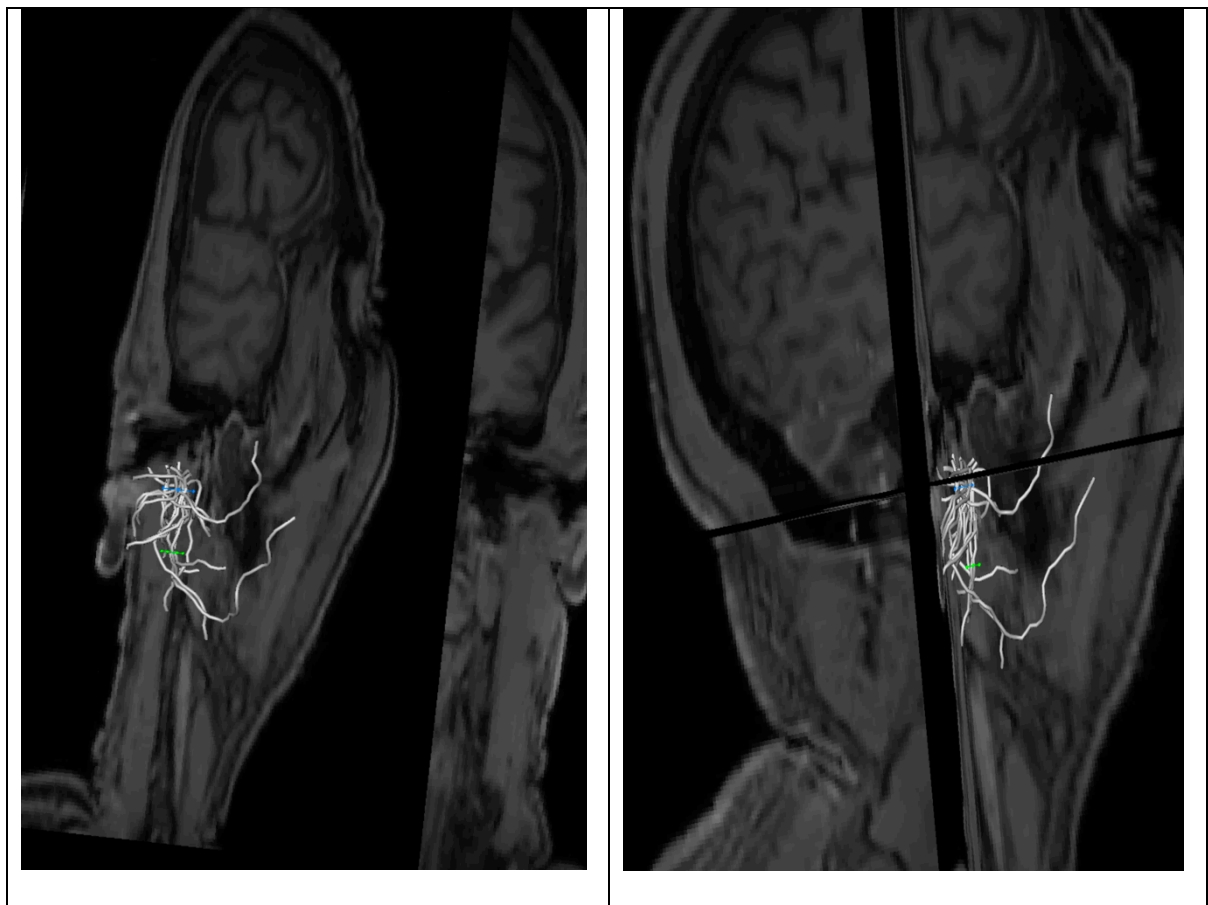


Figure 23. Coronal (right) and sagittal (left) views of tracts analysed through ‘seed’ ROI (blue) gate. ‘And’ ROI (green) gate placed to isolate most dense, anatomically relevant portion of tract

Analysis of the tracts proceeding through both the ‘seed’ ROI gate in addition to the ‘and’ ROI produced a tract that is anatomically relevant, coursing the retromandibular parotid region, likely representing the main stem, bifurcation and cervicofacial division (Fig. 24).

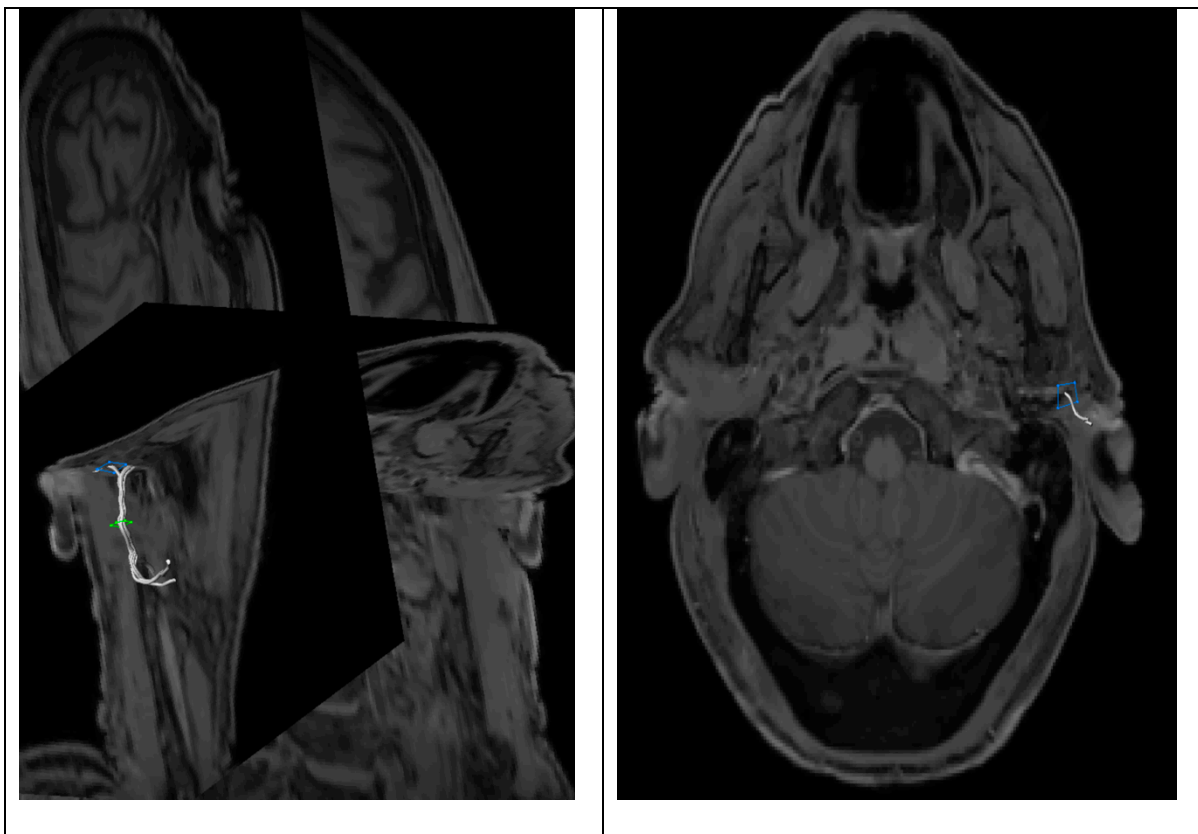


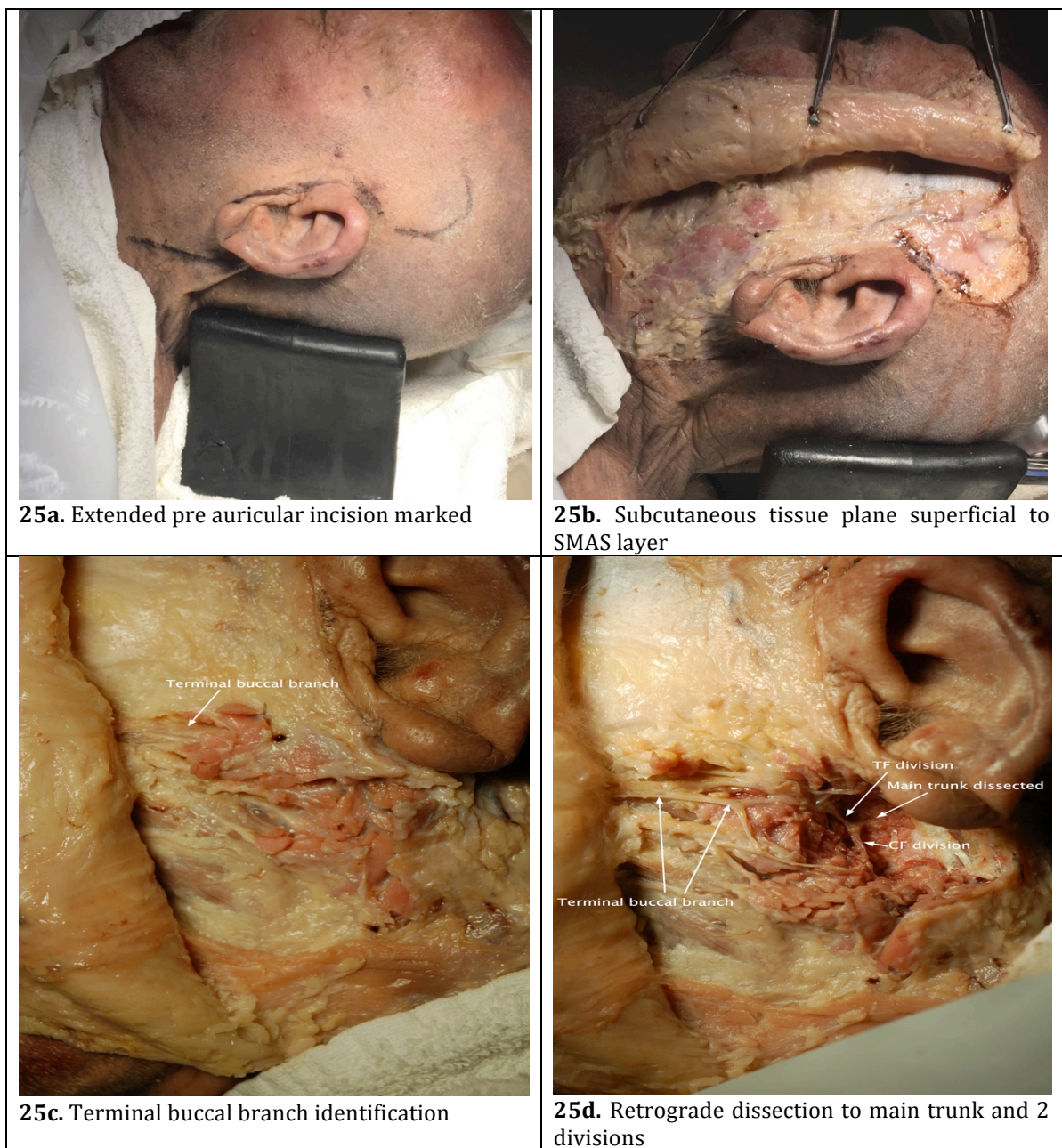
Figure 24. Coronosagittal view of isolated cervicofacial tract (left). Isolated tract passing through stylomastoid foramen (right) - axial view.

Metric analysis of the tract using explore dti software identified a tract density of six tracts, with a mean fractional anisometry value of 0.17 ± 0.06 standard deviation.

3.3.3 Cadaveric scan 2 – Left facial nerve tractography

3.3.3.1 Dissection

The left facial nerve of the same 79 year old, white Irish Caucasian, was dissected after the analysis of the right side was completed. Fig 25. (a-d) shows the stages of detailed, minimally traumatic or manipulating dissection.



The subject was placed supine and an extended pre-auricular incision was marked (Fig. 25a). The incision was made and a plane developed subcutaneously, superficial to the parotid capsule and the SMAS layer (Fig. 25b). A terminal buccal branch was identified

(Fig. 25c) which then allowed retrograde dissection of the branch to allow safe, minimally intrusive exposure of the facial nerve trunk and the two divisions (Fig. 25d) – temporofacial (TF) and cervicofacial (CF). Fig. 26 shows the fully dissected facial nerve with both divisions and all terminal branches clearly identified.

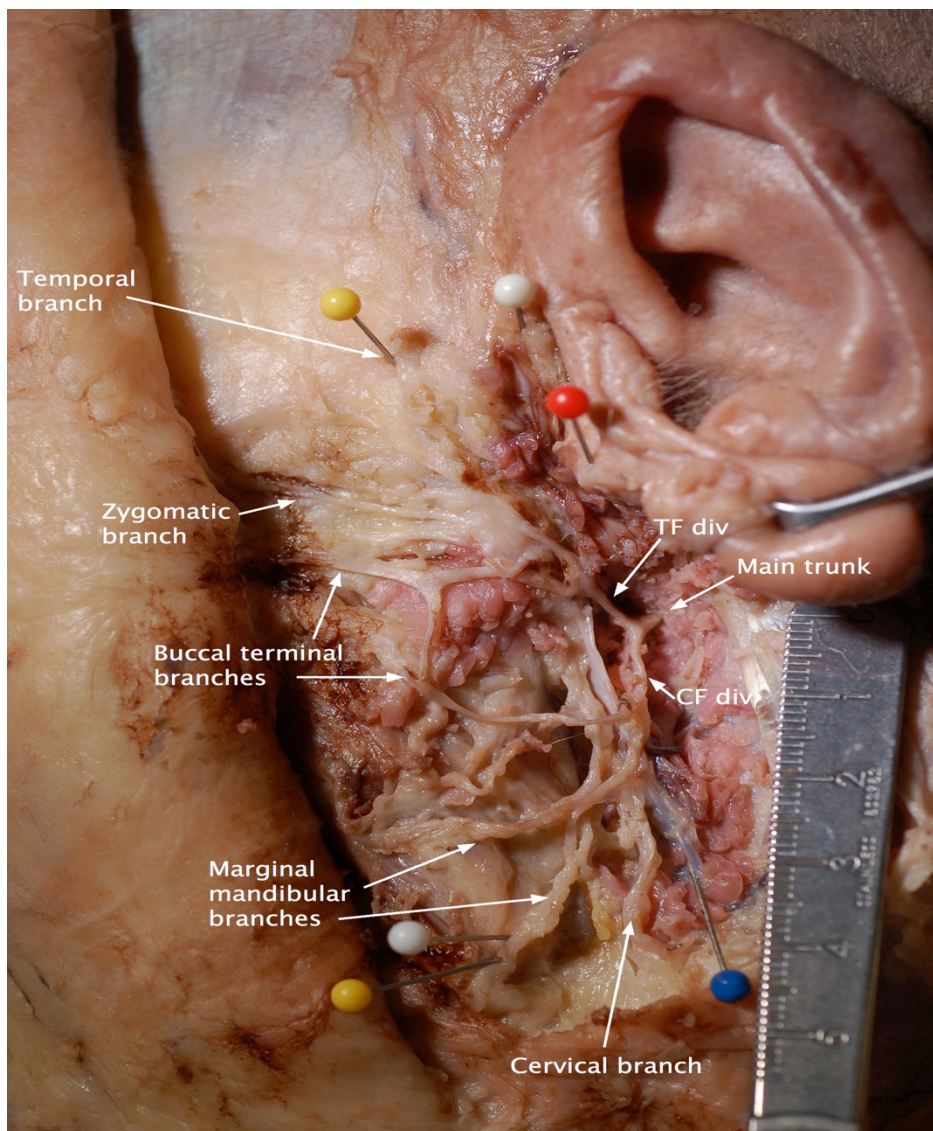


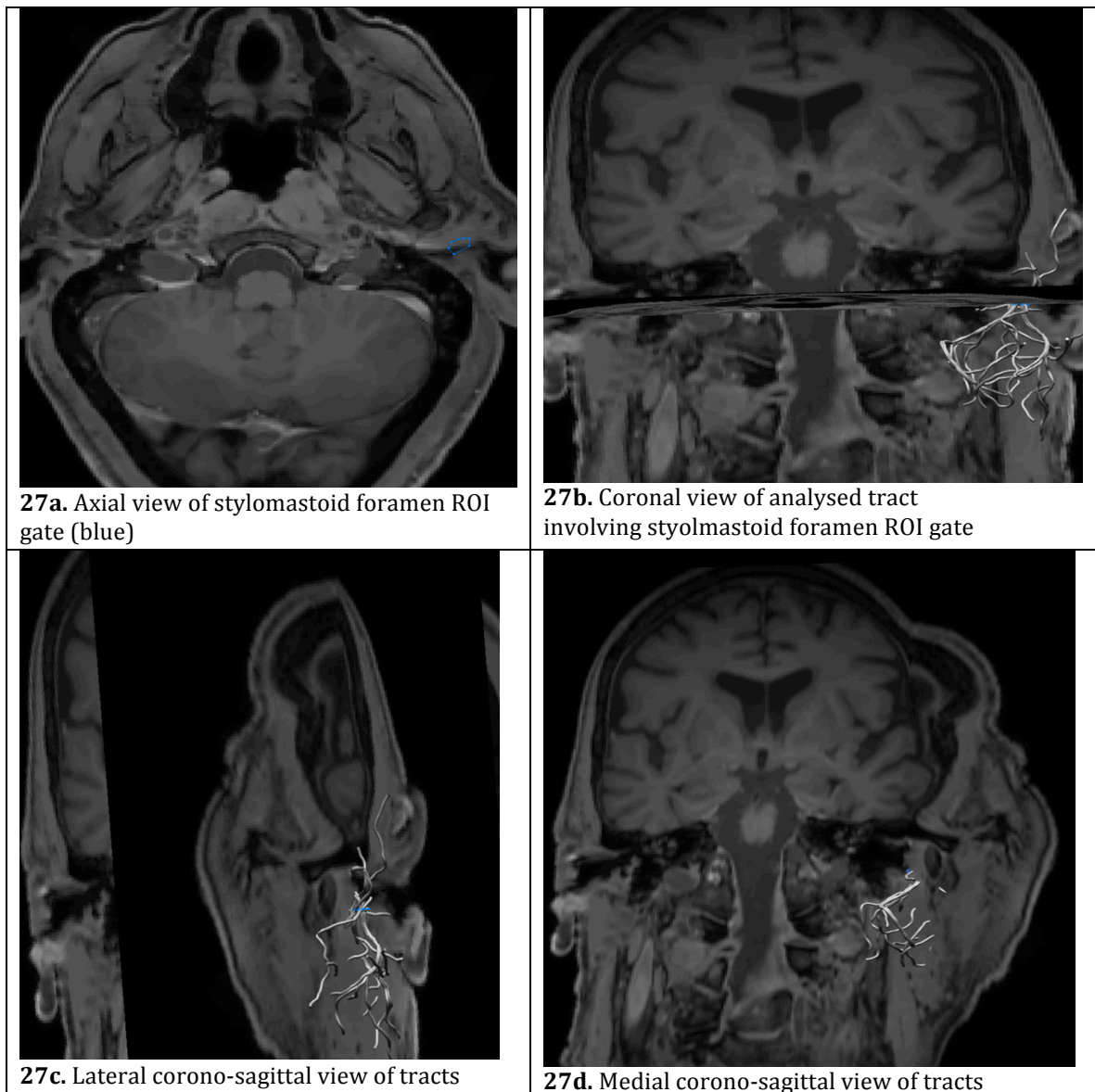
Figure 26. Completed dissection of left facial nerve. Main trunk shown with the two divisions (cervicofacial / CF & temporofacial / TF). Pins - White: bony landmarks - superior - outermost border of external acoustic meatus, inferior - angle of mandible. Yellow - superior - temporal branch as it crosses zygomatic arch, inferior - marginal mandibular as it crosses lower mandibular border. Red - Tragal pointer. Blue - Retromandibular vein

3.3.3.2 Diffusion Imaging

Post-processing tractography analysis took place in the Neuroscience Institute of Trinity College Dublin. Optimal results were obtained on scan parameters set at a b value of 400, voxel size of 2mm^3 , 45 degrees at 1 mm step size. A three dimensional animation is available at this link;

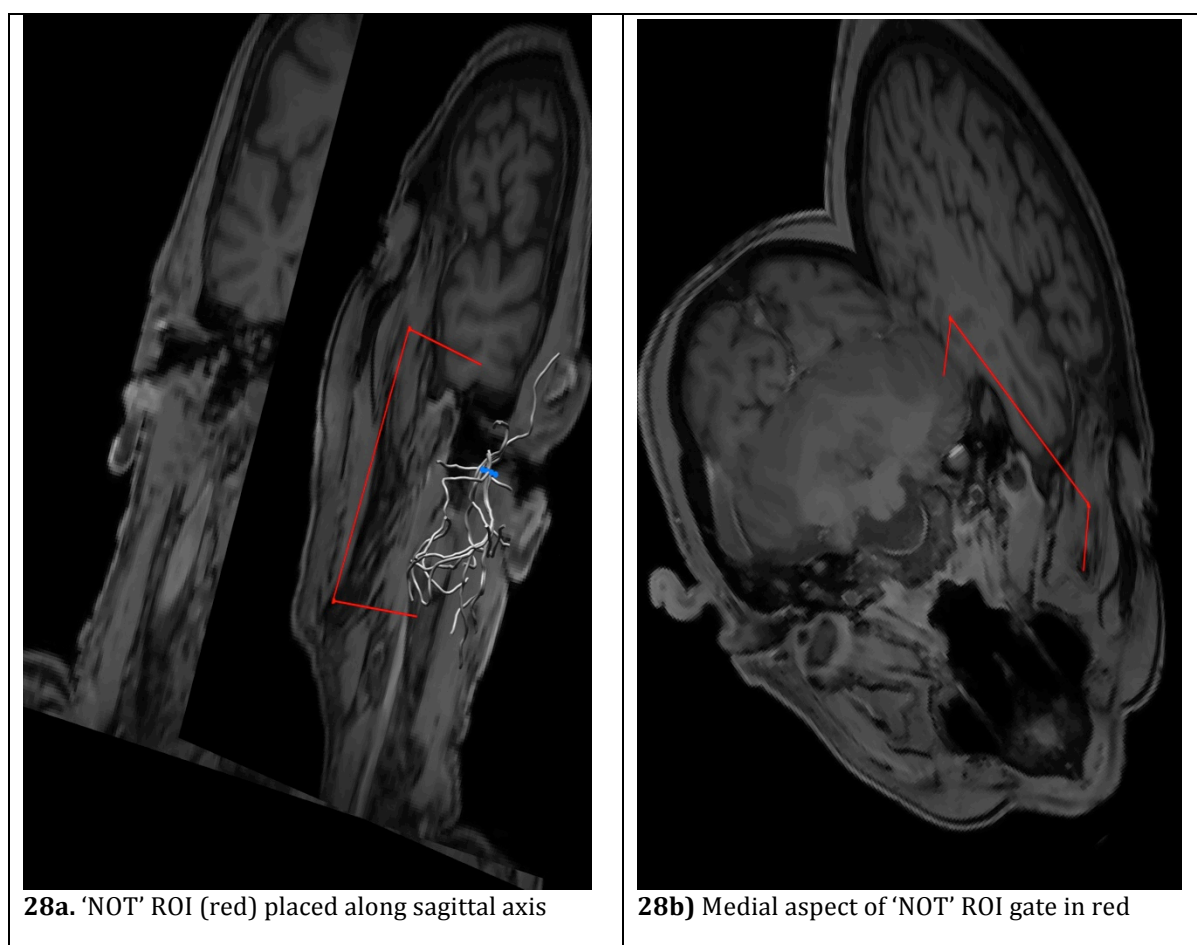
<https://drive.google.com/file/d/1qnd2PksWb4orVO-n2jxYTA83TbchtDxh/view?usp=sharing>

Initial tractography analysis involved drawing a broad region of interest gate at the stylomastoid foramen (Fig. 27a).



The tract produced using the broad region of interest gate is shown in Fig. 27b, displaying the tract from a coronal perspective – showing large and multiple tracts that extend from the parotid region laterally to medial extension posterior to the mandible. Fig. 27c shows a lateral view of a sagittal section where the tracts that remain lateral to the mandible, confined to the parotid region are highlighted with the medially extending tracts hidden medial to the sagittal section. Fig. 27d identifies the medial aspect of the sagittal section where the tracts medial to it are likely to be spurious and not contributory to facial nerve tracts.

In order to exclude the spurious tracts extending medially that anatomically do not correlate to facial nerve, a ‘NOT’ region of interest gate was placed medially along a strategically placed sagittal section lateral to the mandibular condyle (Fig. 28 a & b).



The ‘NOT’ gate acts as a region of interest through which tracts are not allowed to pass. Hence, any tract that would pass in part or in full, through the ‘NOT’ gate, will be omitted. Post ‘NOT’ analysis of the original tracts obtained using the general, broad stylomastoid region of interest gate (Fig. 27a), spurious tracts that extended medially that did not correlate with the facial nerve course were omitted (Fig. 29 a & b).

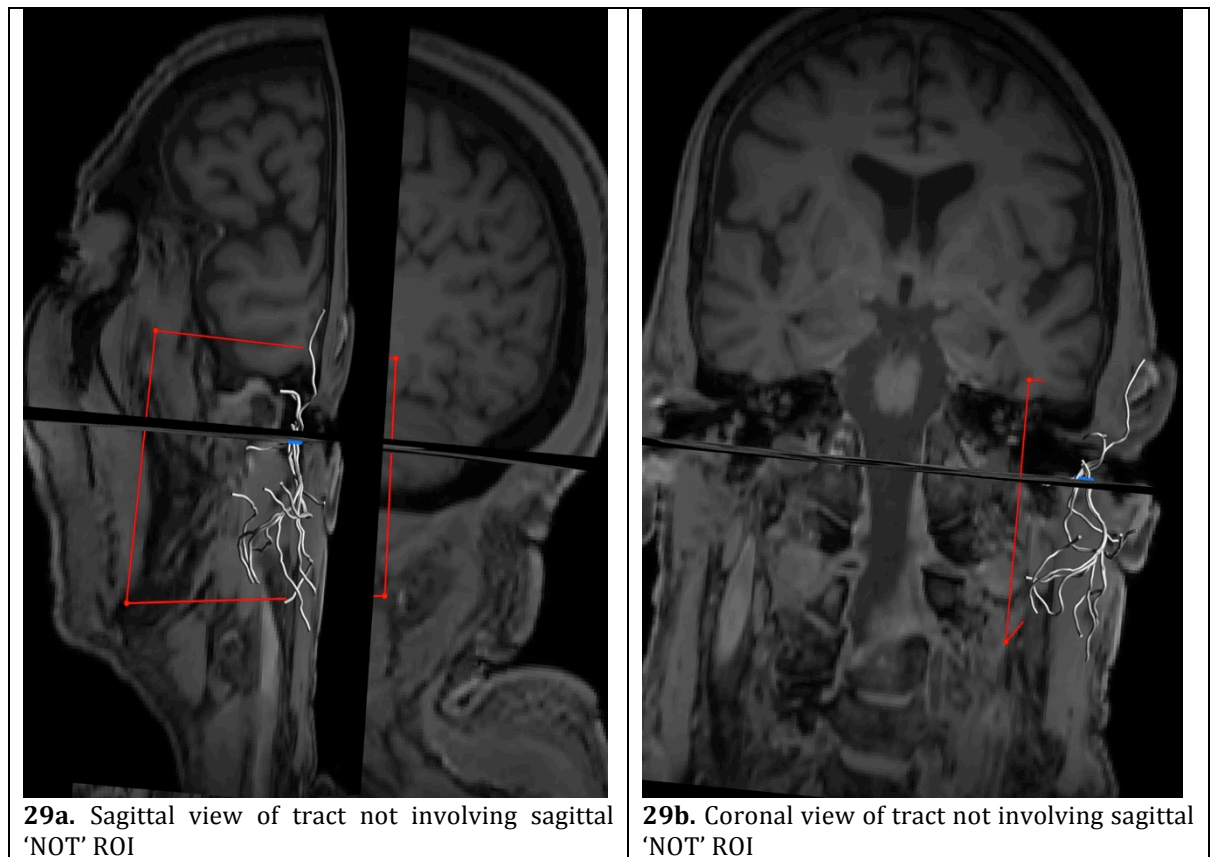


Fig. 29a shows a sagittal section of the resultant tract. The coronal view offered in Fig. 29b shows the lack of any tract segment extending medially beyond the ‘NOT’ gate, which would not correlate anatomically with the course of the facial nerve. In order to further isolate the facial nerve, the remaining tract was analysed for tangible segments that most likely represented neural tracts and not spurious artefacts. As such, the broad, general ‘SEED’ region of interest gate was consolidated into two smaller ‘SEED’ ROI gates that encircled the two main tract segments coming through the stylomastoid foramen (SMF) (Fig. 30).

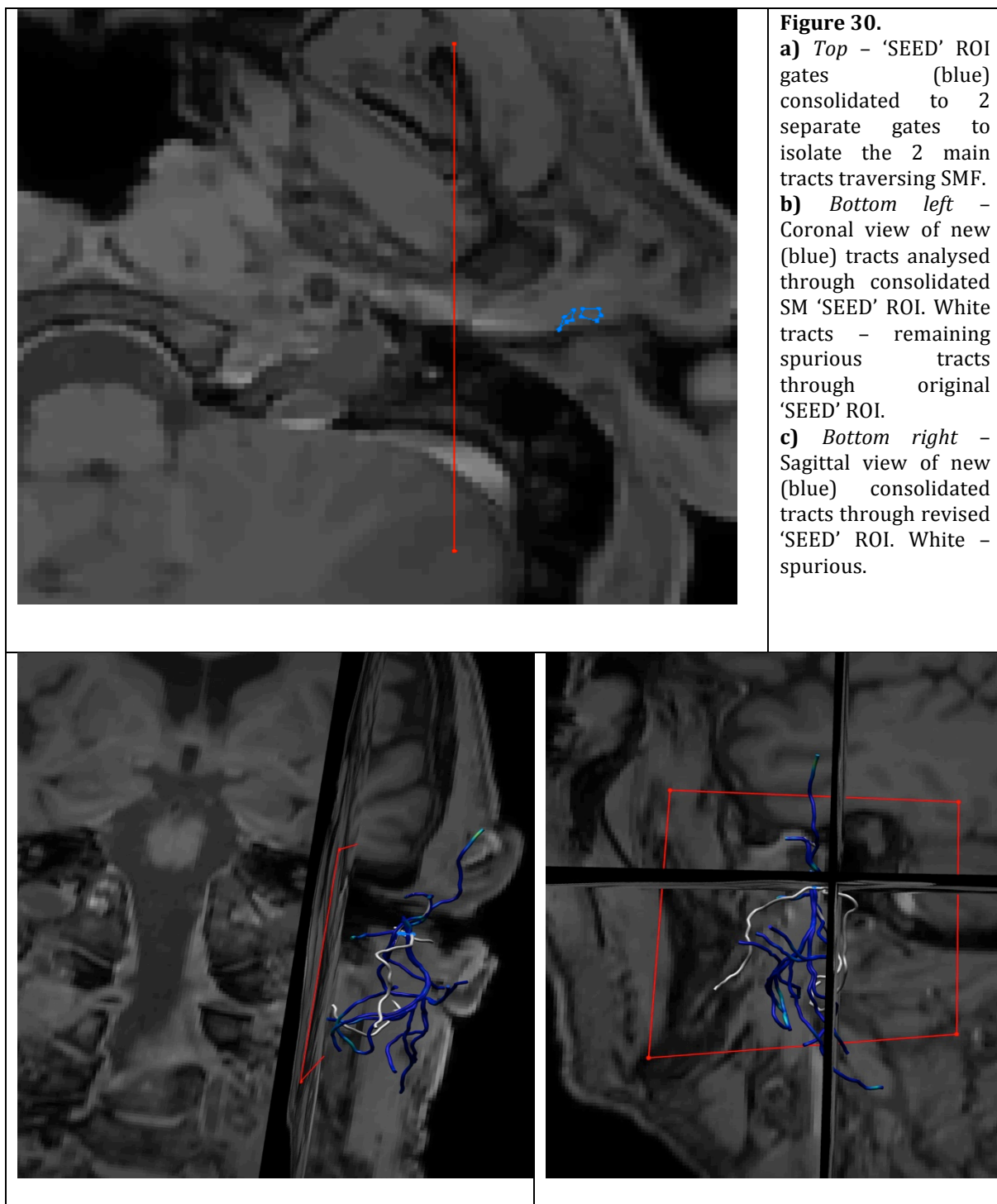


Fig. 30 b & c show the resultant tract (blue) on the background of the old tract (white). The resultant tract is felt to signify the facial nerve. Its varying components are highlighted in a close up image (Fig. 30). The spurious remaining white tracts are removed as have been excluded by the application of the revised stylomastoid foramen 'SEED' region of interest gates. Fig. 31 highlights the end result post processing of 'NOT' and revised 'SEED' region of interest gates to the facial diffusion weighted image of the left parotid region.



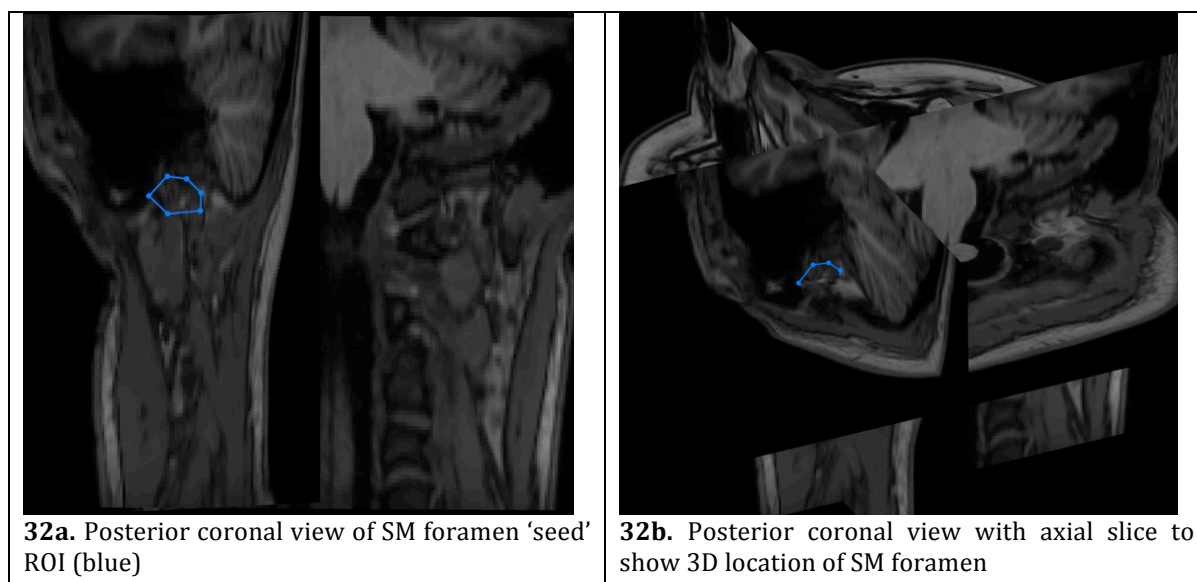
Figure 31. Facial nerve tract post processing of DWI image. Bifurcation highlighted with the two divisions – temporofacial and cervicofacial.

3.3.4 Live subject scan results

Using the scanning protocols derived from our cadaveric scans; two live subjects were imaged to assess the transferability of the scanning methods already established in cadaveric subjects to live subject scans.

3.3.4.1 Live subject A

The first live subject to undergo diffusion tractography was a thirty-two year old, white Irish Caucasian female who was medically fit and well with no previous history of parotid, neck pathology or surgery. Scanning parameters were set at a b value of 400 and a voxel size of 2mm^3 , using a 32 channel head and neck coil. Post-processing of the diffusion weighted imaging was undertaken at 75 degrees with a 1mm step size analysis. The diffusion weighted image was superimposed on a baseline T1 magnetic resonance image, obtained at the beginning of the scanning process. The initial diffusion weighted tractography study involved placing a broad region of interest ‘seed’ gate at the region of the stylomastoid foramen. This was deemed best placed on a coronal slice as shown in Fig 32. (a & b).



The tract produced through the ‘seed’ region of interest gate shown in Fig. 32 produced a wide yielding array of tracts that seemed to incorporate the facial nerve trunk and its

bifurcation. Additionally however, it also incorporated tracts that do not represent where the facial nerve would course. The tracts are shown in Fig. 33.

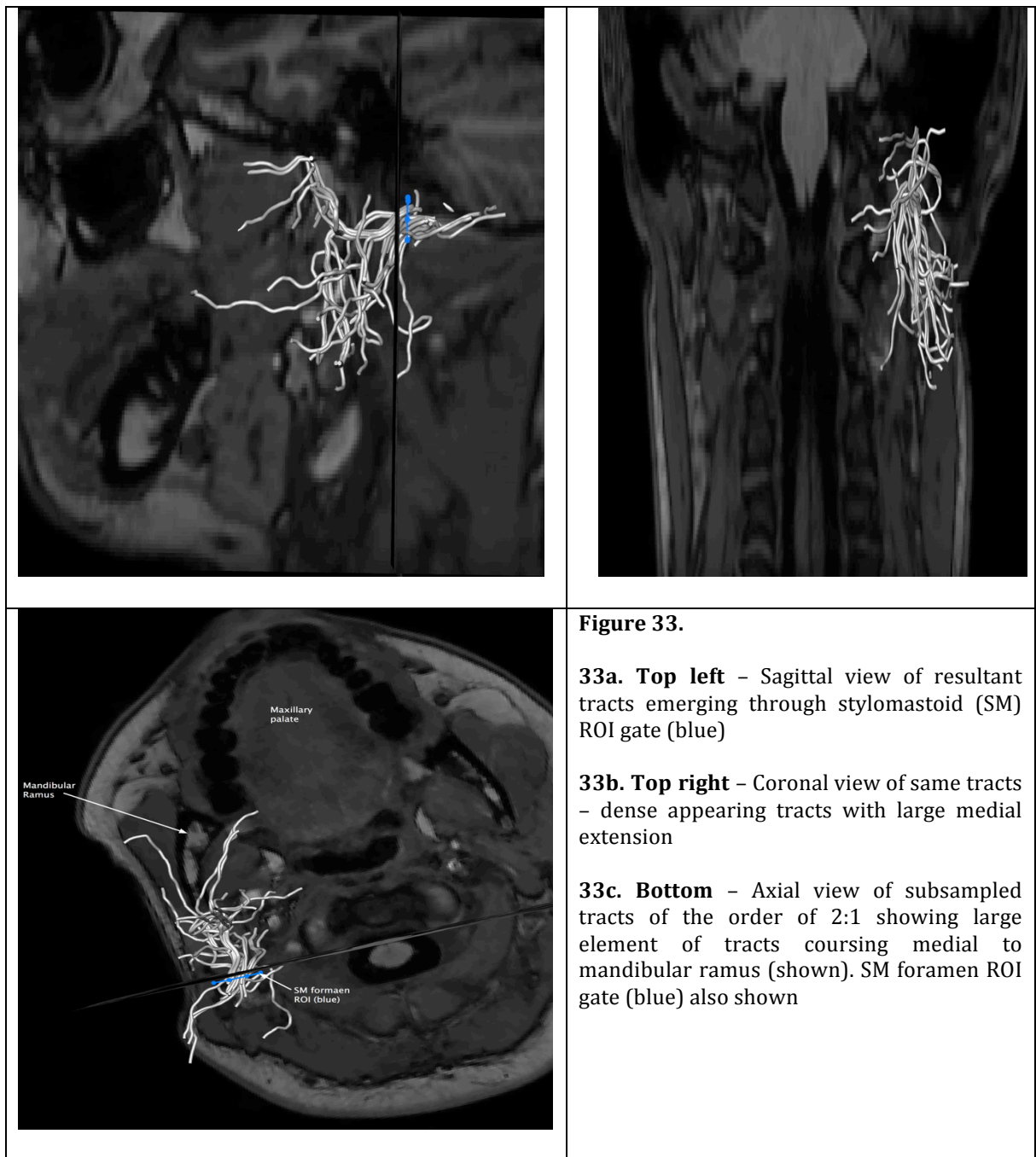


Fig. 33a shows a sagittal section of the resultant tract. The tract shows a dense main stem traversing the ROI gate which seems to definitively divide into an upper and a lower segment of tracts, which then course anteriorly as different individual tracts. The course seems to correlate to the anatomical course of the facial nerve as it divides from the main stem into temporofacial and cervicofacial trunks, which further subdivide into terminal

branches. Within the entirety of the tract segment, there are many spurious tracts evident that do not anatomically represent the facial nerve. Fig. 33b shows a coronal view of the entirety of the tracts. There is large medial extension to the tracts. The density of the tracts makes it difficult to appreciate the direction of the individual tracts. In order to further analyse, an axial section was analysed (Fig. 33c) with the tracts filtered down to a sub-sample ratio of the order of 2:1 so as to assess the main direction of the main tract segments and eliminate single, irrelevant tracts. From the axial cross section of the superimposed T1 image, it is evident that a significant portion of the tract extends medial to the mandibular ramus, which does not correlate with the anatomical course of the facial nerve, which remains lateral to the mandible, as it courses anteriorly through the parotid gland. In order to eliminate these non-contributory segments of the tracts, 'NOT' region of interest gate was inserted as shown in Fig. 34.

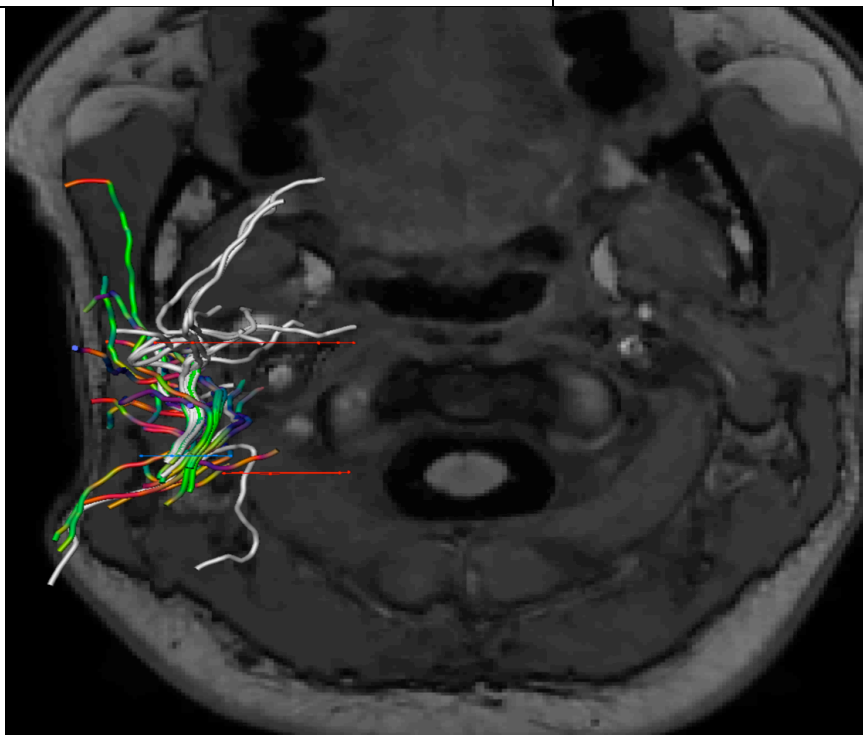
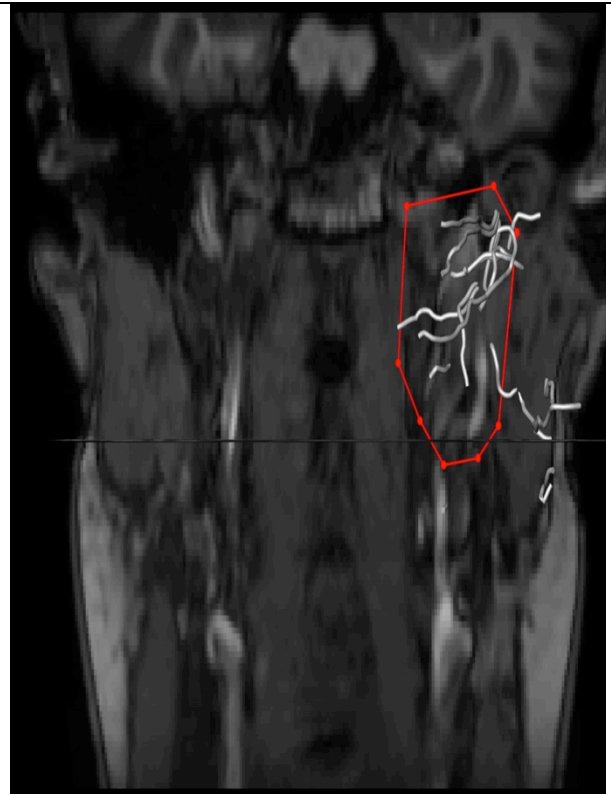
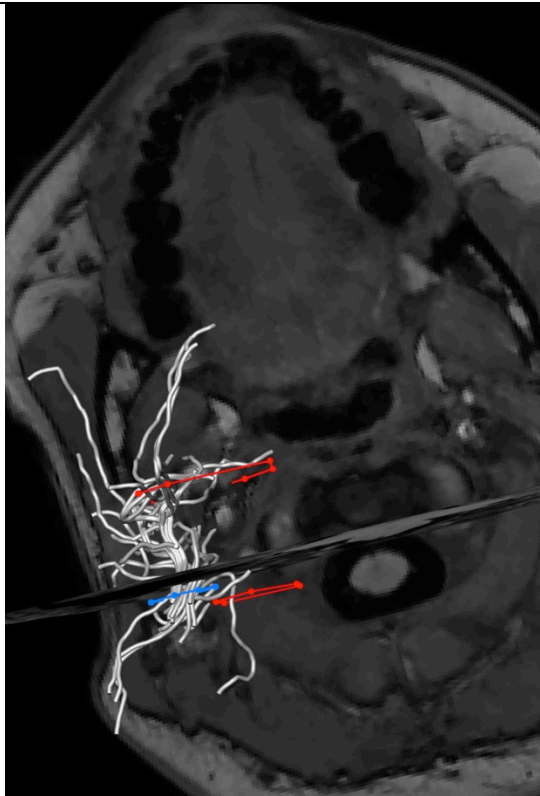


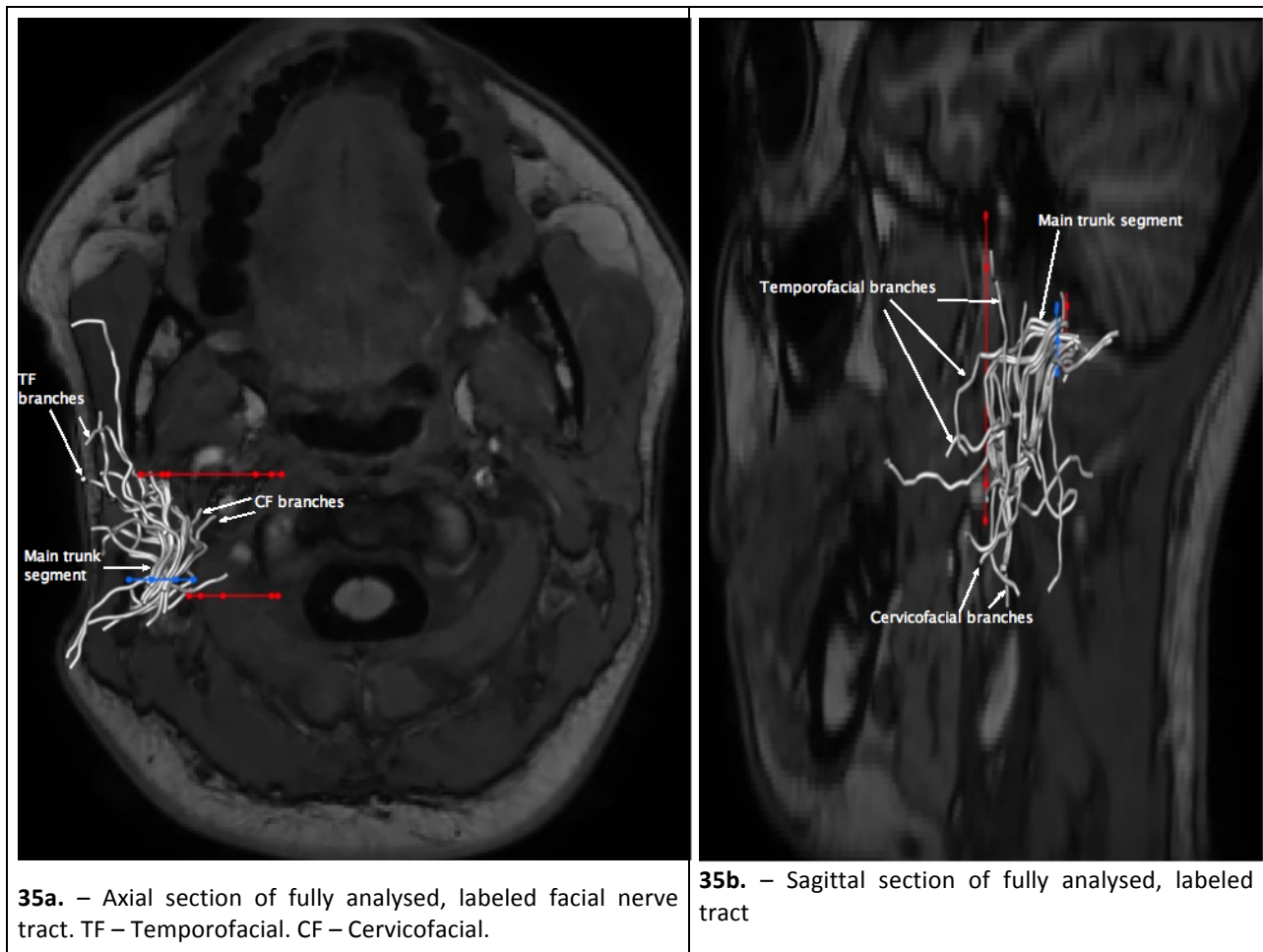
Figure 34.

34a) Top left – Axial view of tract with 'seed' ROI (blue) and two 'not' ROI gates (red) – one anteriorly to exclude tract segment coursing medial to mandible and one posteriorly to exclude non contributory tracts to main trunk segment

34b) Top right – Coronal view of anterior 'not' ROI gate to exclude tracts coursing medial to mandible

34c) Bottom – Axial view of new tract (coloured) superimposed on old white tract. Non contributory tracts excluded

Fig. 34c shows an axial cross section of the resultant tract. The coloured tract is the tract that traverses the ‘seed’ ROI gate but not the ‘not’ ROI gates placed anteriorly and posteriorly. This tract is superimposed on the background of the white tract that passes through the ‘seed’ ROI gate alone. The remaining white tracts are thought to be spurious, non-contributory to the facial nerve tract.

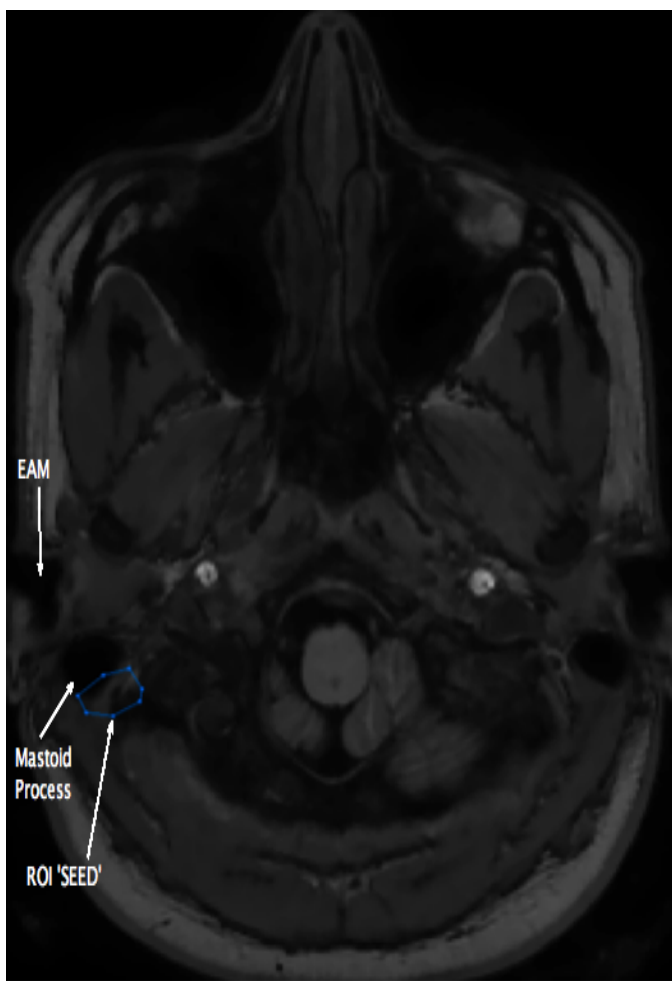


Figs. 35 a & b show the fully analysed tracts, traversing the stylomastoid ‘seed’ ROI gate (blue) but not the two ‘not’ ROI gates (red). Mean FA values for the tract were 0.22 ± 0.12 standard deviation.

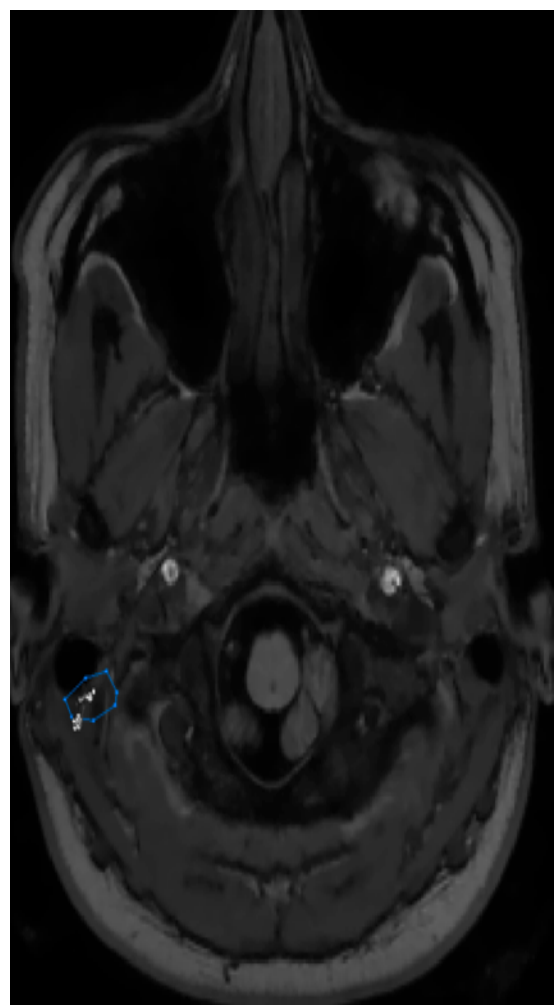
3.3.4.2 Live subject B

The second live subject to undergo diffusion weighted imaging of the head and neck was a 31 year old, white, Irish, Caucasian female, who was medically fit and well with no history of pathology affecting the parotid or neck and no history of surgery in the area of interest.

Scanning parameters were set at a b value of 400 and a voxel size of 2mm^3 , using a 32 channel head and neck coil. Post-processing of the diffusion weighted imaging was undertaken at 75 degrees with a 1mm step size analysis. The diffusion weighted image was superimposed on a baseline T1 magnetic resonance image obtained at the beginning of the scanning process. Initial analysis of the diffusion weighted image, similarly to the all the other imaging analyses undertaken, involved placing a broad 'seed' region of interest gate at the stylomastoid foramen. The only tangible, resultant tracts that mimicked the course of the facial nerve are shown in Fig. 36 (a & b), and appear to exit on a more medial and posterior aspect to the mastoid process rather than anterior.



36a. Axial view of stylomastoid foramen seed ROI (blue). EAM – External acoustic meatus. Mastoid process – shown.



36b. Axial view of ROI with tracts in situ

The tract produced is a dense tract traversing the ‘seed’ ROI before dividing into several branches. The tract appears to correspond anatomically, in three-dimensional MRI analysis to the course of the main stem and the cervicofacial division with some evidence of where the bifurcation takes place. The temporofacial division is not captured fully (Fig. 37).

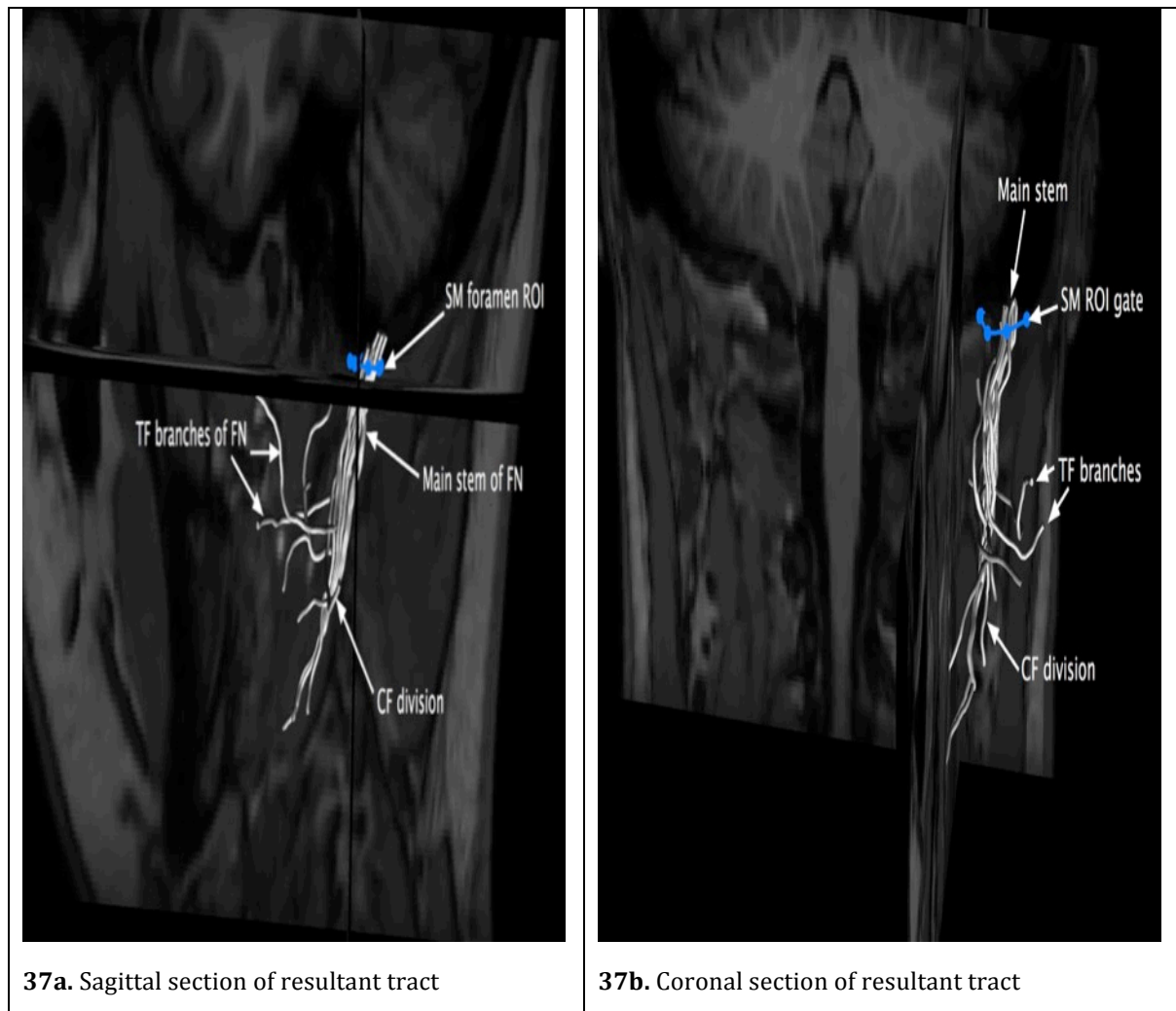


Fig. 37 a & b show the left sided facial nerve tract. The stem and cervicofacial (CF) divisions are clearly delineated as dense stable segments. The temporofacial division appears as several smaller branches which indicate where the bifurcation occurs, but cannot be followed as distally as the cervicofacial division. The FA value for the resultant tract measured at a mean of 0.37 ± 0.12 .

3.4 Discussion

3.4.1 Cadaveric scan 1 – right facial nerve

For the purposes of this study, investigating whether the extra-cranial course of the facial nerve can be reproduced using diffusion tractography, we initially investigated what we knew to be facial nerve and subsequently drew our comparisons.

Figs. 14d & 38, represents an *in situ*, fully dissected extra cranial facial nerve with the superficial lobe of the parotid gland removed. A closer inspection of the facial nerve reveals that the cervicofacial division of the facial nerve divides (point A, Fig. 38), shortly after the main trunk splits into the temporofacial and cervicofacial trunks. The cervicofacial division continues caudally as two trunks, before rejoining to become one trunk at a more caudal position in the neck (point B, Fig. 38). This division and subsequent reunification of the cervicofacial branches is depicted in Fig. 38 by a freely drawn white line along the more substantial posterior trunk of the cervicofacial division and by a point to point straight line drawn from point A to point B.

Calibrated measurement of this point-to-point measurement using Image J produced the results tabulated in Table 6 – showing a length of 33-35 millimetres in length.

	Area	Mean	Min	Max	Angle	Length
Freehand	2.097	111.134	88	141.891	0	35.761
Straight	1.729	207.696	147.614	255	-77.065	33.336

Table 6. Point A – point B measurement (mm - red) along the cervicofacial (CF) division of the anatomical dissection of the facial nerve depicted in Fig 37.

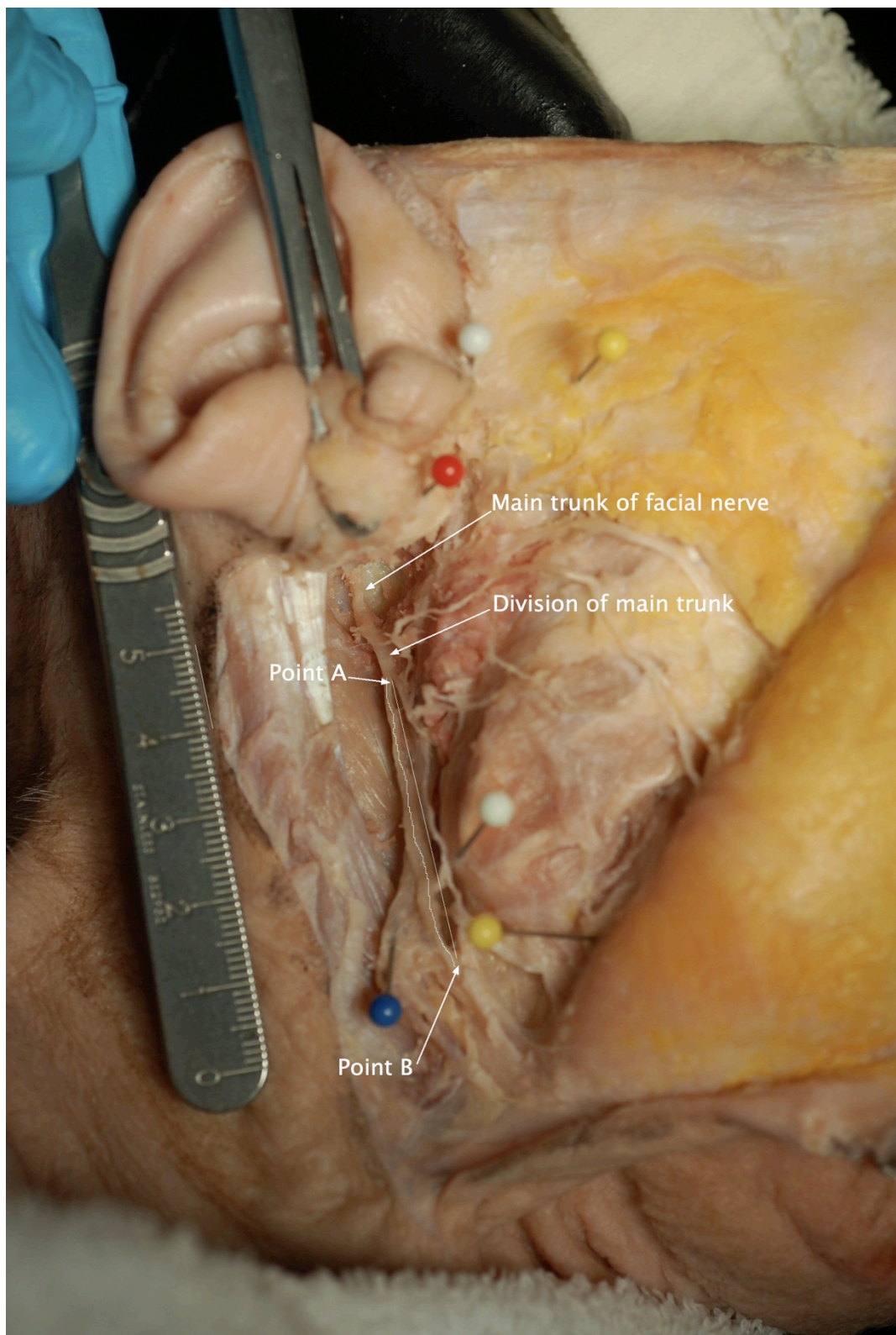


Figure 38. Point to point calibrated measurement of CF trunk division to reunification

Using this reproducible landmark along the cervicofacial trunk of the facial nerve where the trunk definitively undergoes a division followed by a subsequent reunification, a

similar pattern was investigated on the diffusion tractography imaging of the same facial nerve.

Fig. 16 (a & b) show coronal and sagittal views of the cervicofacial trunk tract that resulted from tractography analysis post placing a ROI seed gate at the stylomastoid foramen using the anatomical T2 image overlay. Analysis of this tract segment shows that it is confined to the parotid gland in the retromandibular region in three dimensions along the course of the tract. In addition, the tract does undergo division and subsequent reunification at a caudal position – point A to point B as shown in Fig. 39. Further tract analysis of the posterior tract segment (depicted in red in Figs. 16 a,b & 39) showed a tract length of 32 millimetres (Table 7).

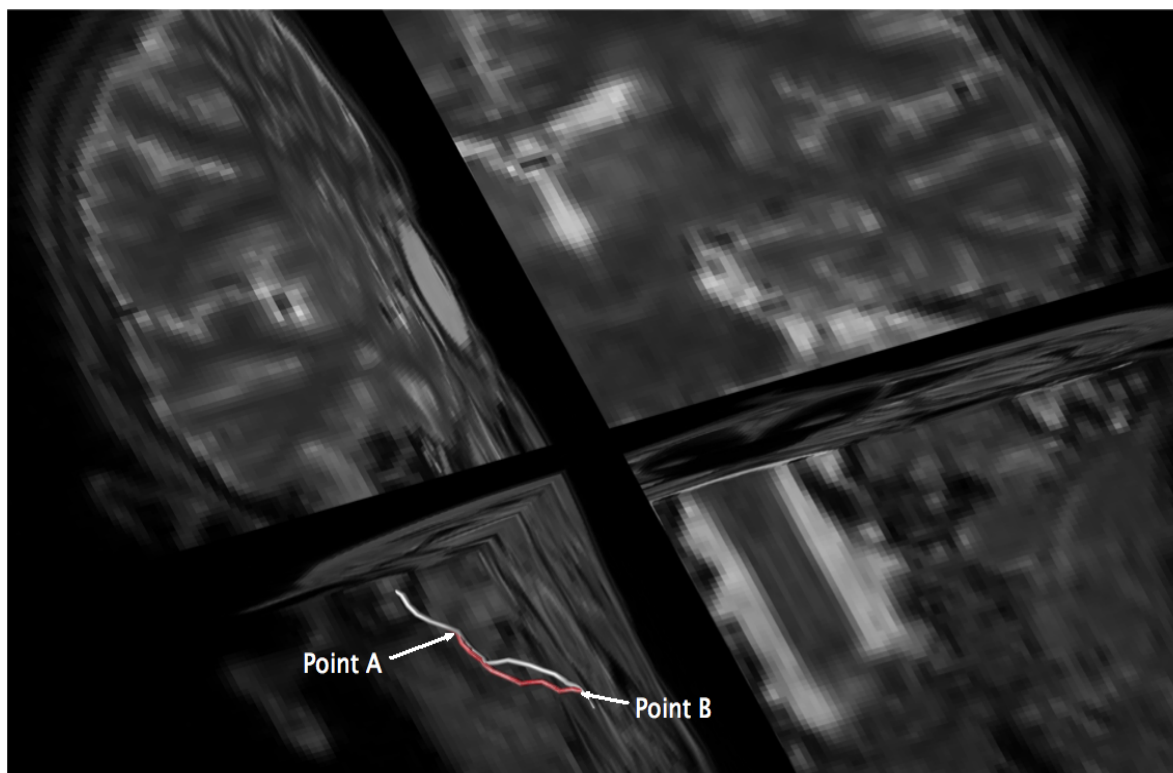


Figure 39. Coronal aspect of CF trunk showing division (point A) and reunification (point B) with a distance of the posterior of the divided tract segment shown in red.

Number of tracts	Number of points (from all tracts)	Mean tract length (in mm)	SD tract length (in mm)	Median tract length (in mm)	IQR_L tract length (in mm)	IQR_H tract length (in mm)	Approximate tract volume (in mm ³)	Mean FA	SD FA
1	17	32	0	32	32	32	12.325966	0.162808	0.0747

Table 7 – Tract metric analysis of comparable (red) segment of CF trunk as on images 8, 9 & 17. Boxes highlighted in red are related to tract length (32.00000381 mm) and FA value of tract (0.16 with standard deviation (SD) of 0.075).

A tract length of 32mm from point A to point B, as shown on Fig. 38 is a very close comparison to the anatomic dissection distance of 33 – 35 mm. The comparable distance in addition to the similar anatomical course of the tract and the dissected cervicofacial trunk would indicate that both are a direct match. It is felt the 1-3 mm divergence between the dissection and imaging tract lengths are predominantly attributed to the mild unavoidable manipulation of the tissues during dissection in addition to the difficulty in establishing a hundred per cent accuracy in calibration of the anatomic dissection measurement. Whereas, the tractography measurement is a digital calculation that is extremely accurate, using Explore DTI software.

In addition to the correlating distances, the Fractional Anisometry (FA) value (0.16 +/- 0.075) of the tract segment analysed (table 7) correlates to the value that would be expected for a facial nerve in the parotid gland with high sensitivity.⁵⁹

Fractional Anisometry (FA) is a scalar value between zero and one that describes the anisotropy of a tissue undergoing a diffusion imaging process. Zero would mean that diffusion is isotropic – unrestricted in all directions. One would mean that diffusion occurs in only one axis and is restricted in all other directions. FA is a value used in diffusion imaging that is dependent on and reflective of fiber density, axonal diameter and myelination in a white matter tract. In the parotid gland, the correct FA value of neuronal tissue representing the facial nerve is thought to range from 0.1 – 0.4, with values of 0.1 –

0.2 showing a hundred per cent sensitivity to detecting the facial nerve trunk, the cervicofacial or temporofacial branches.⁵⁹

Using the cervicofacial division as a reference, we subsequently analysed the feasibility of establishing the temporofacial tract. A region of interest seed gate was placed laterally in the substance of the parotid gland (Fig. 17a). This location was chosen as a detailed analysis of the anatomic dissection of the same facial nerve shows the temporofacial division making a significant lateral turn after coming off the bifurcation of the facial nerve. Subsequently, the nerve division courses anteriorly through the parotid gland as the temporal, zygomatic and buccal terminal branches (Fig. 40). Placing a seed ROI gate laterally in the sagittal plane, within the substance of the parotid gland would ideally capture the temporofacial division as it makes the sharp lateral turn after coming off the bifurcation of the main facial nerve stem (Fig 17. b & c).

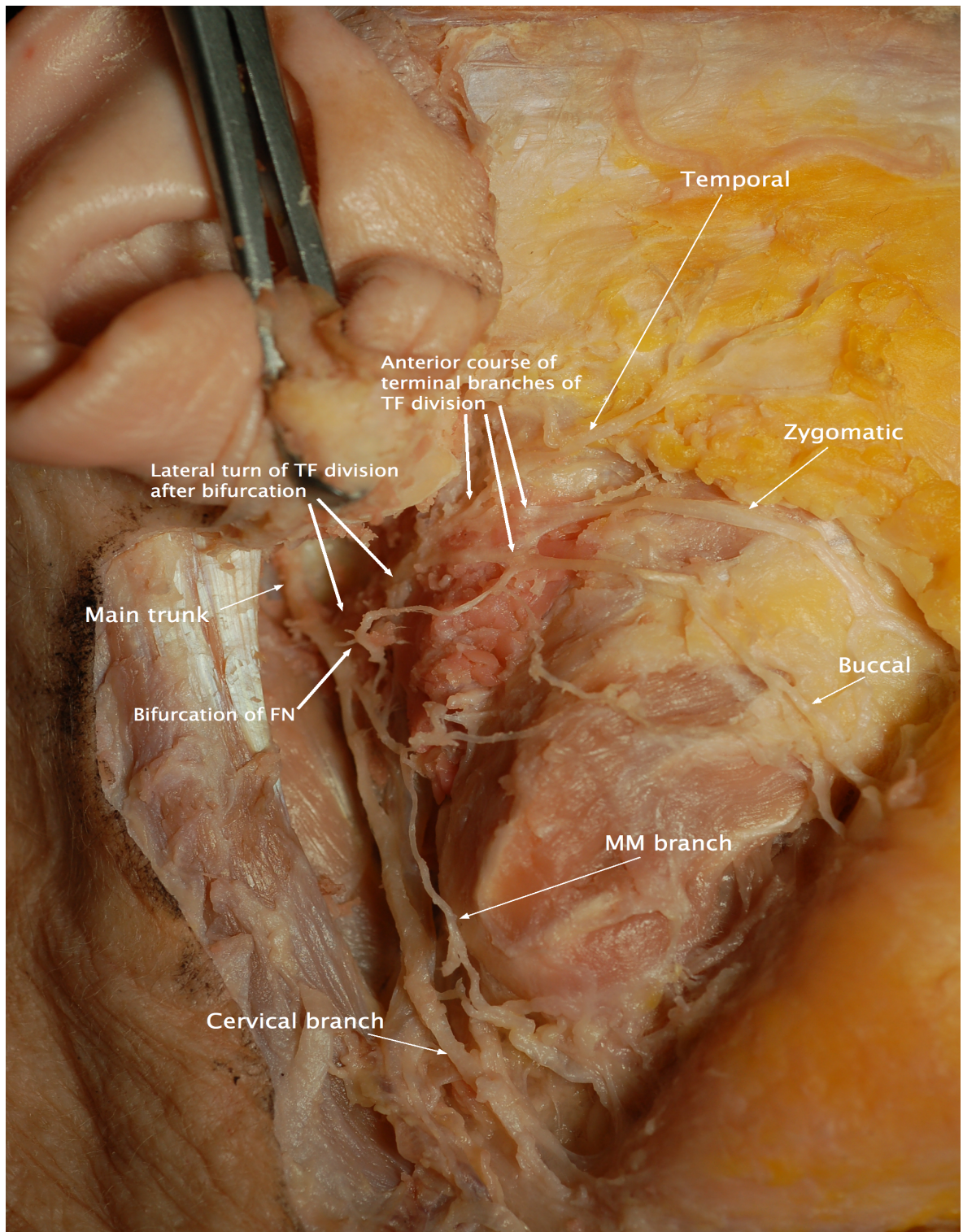


Figure 40. Lateral and subsequent anterior course of temporofacial (TF) of facial nerve (FN)

The tract produced is one that is made of broadly two elements (Fig. 40). A cervicofacial element that courses in the same direction and is within the same anatomical retromandibular region as the cervicofacial trunk isolated through the stylomastoid foramen region of interest gate. In addition, a temporofacial element

that has a significant lateral curvature before coursing anteriorly as terminal branch tracts. This lateral curvature is best depicted on a coronal image of the tract against the T2 anatomical image overlay (Fig. 41).

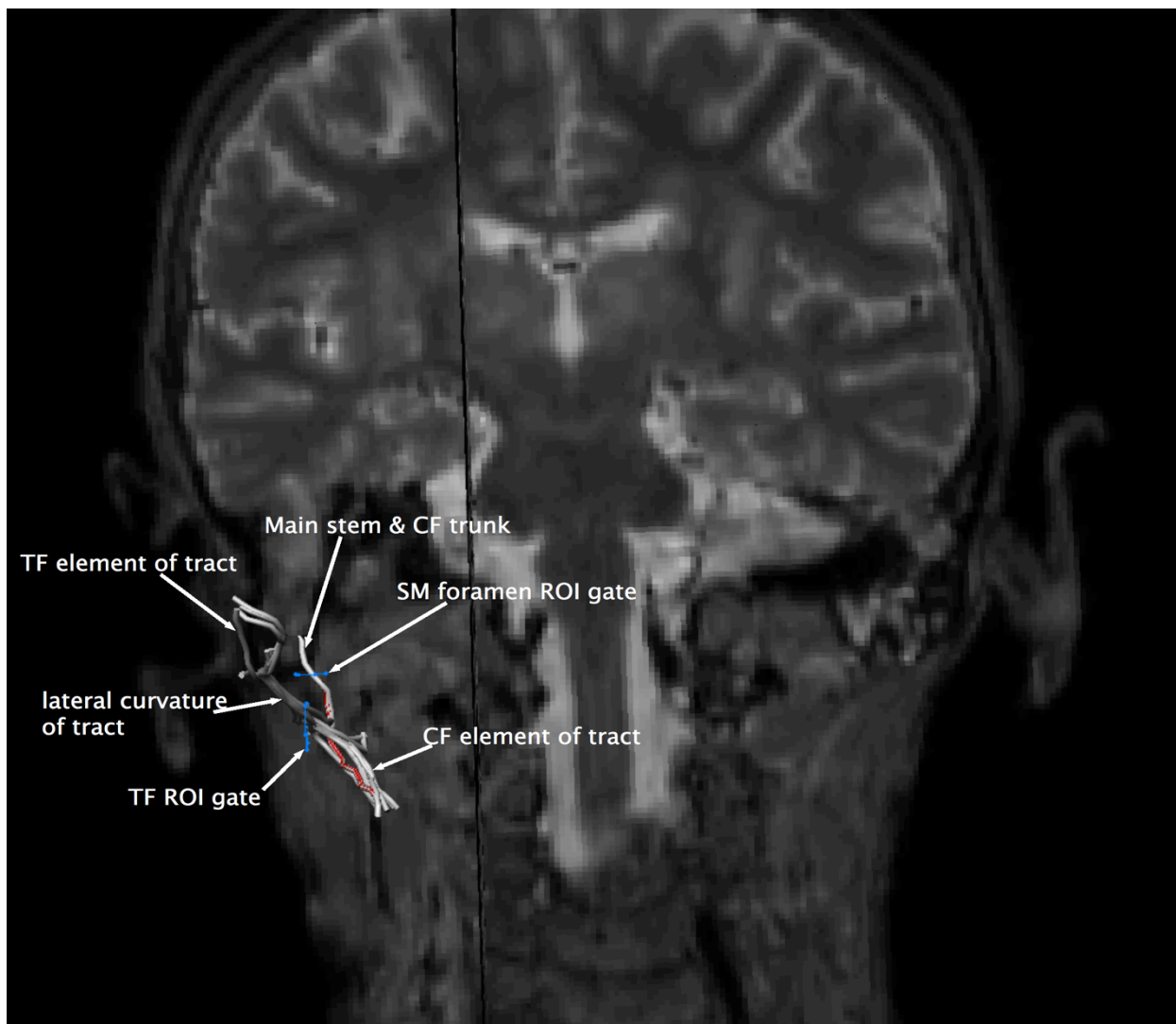


Figure 41. Coronal image of both tracts with anatomically correlated segment of CF tract highlighted in red. Temporofacial (TF) and cervicofacial (CF) elements of new tract shown

Fig. 42 depicts the new tract from a sagittal perspective. Both the temporofacial and the cervicofacial element of the tracts are shown along with the anterior course of the temporofacial terminal branches, as described in the analysis of the anatomic dissection. Overall, it is felt that the new ROI gate placed laterally within the substance of the parotid gland did allow for effective tracking of the temporofacial division of the facial nerve on two counts. Firstly, the cervicofacial element of the new tract coincides significantly with the anatomically correlated cervicofacial trunk already tracked using the stylomastoid

foramen ROI gate. In addition, both Figs. 41 & 42 show that, much like the anatomical dissection of the same facial nerve, the temporofacial nerve tract undergoes a lateral curve prior to taking an anterior course through the parotid.

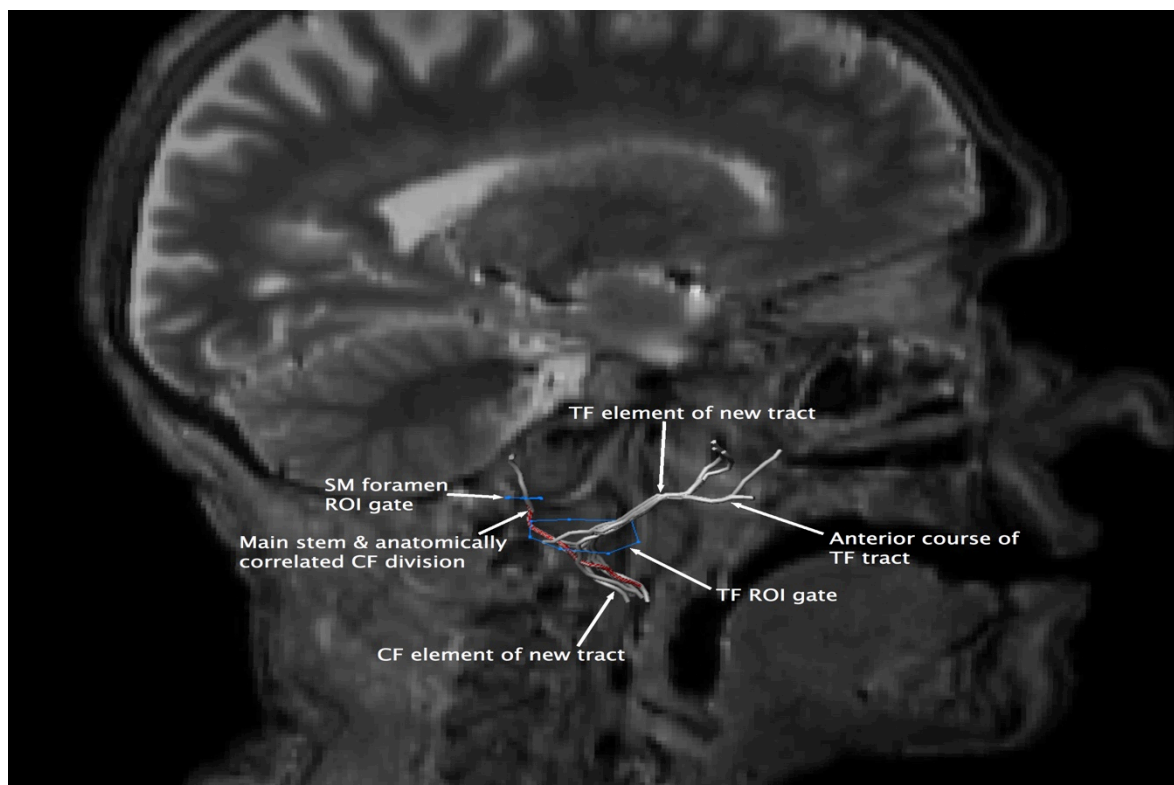


Figure 42. Sagittal view of new tract superimposed on anatomically correlated CF tract depicting anterior course of the TF element of the tract. The CF element also depicted.

Tract	Mean FA	SD FA	Median FA
Anatomically correlated tract CF div	0.163	0.075	0.153
Temporofacial tract via TF ROI gate	0.237	0.106	0.22

Table 8 – Tract analysis using DTI explore software comparing Fractional Anisometry (FA) values between anatomically correlated (red) segment of cervicofacial (CF) trunk and tract isolated through temporofacial (TF) ROI seed gate.

Table 8 tabulates the FA values of the two tracts identified through the two ROI seed gates applied to the diffusion image. We know that the FA value for the anatomically correlated cervicofacial tract is 0.16. On account of this value being within the range of FA values that represent 100% sensitivity to being the facial nerve within the substance of the parotid gland ⁵⁹, and due to the anatomical correlation between tract and dissection, it is

established that the cervicofacial tract is an accurate representation of the facial nerve. The new superimposed temporofacial tract that was established using the new ROI gate placed laterally within the parotid gland has a mean FA value of 0.23. This is within the range of 0.1 – 0.2 where Attye et al.⁵⁹ deemed the sensitivity of the tract within the parotid gland to be highly representative of the facial nerve. Perhaps the reason the value is higher than that of the cervicofacial division is due to the higher density of the tract as compared to the single tract of the cervicofacial division (marked red in Figs. 39, 41 & 42) that was singularly analysed to compare to the anatomic dissection.

In addition to the FA value, we are able to anatomically infer that this is the temporofacial division due to the nature of the lateral curvature followed by the anterior coursing of the terminal branches of the facial nerve on both the dissection and the image. Therefore, we feel that both tracts superimposed, do indeed represent both divisions of the facial nerve trunk.

3.4.2 Cadaveric scan 2 – right facial nerve

Detailed comparison was made between the anatomic dissection and the diffusion tractography results so as to assess the feasibility of identifying the facial nerve trunk, bifurcation and an element of either division (temporofacial or cervicofacial). Initial analysis focused on what we knew to be facial nerve on the anatomic dissection. It became evident that the bifurcation of the facial nerve would be an important landmark from which to compare the tracts to the dissection as both divisions are separate and make definitively opposing angles from which they bifurcate.

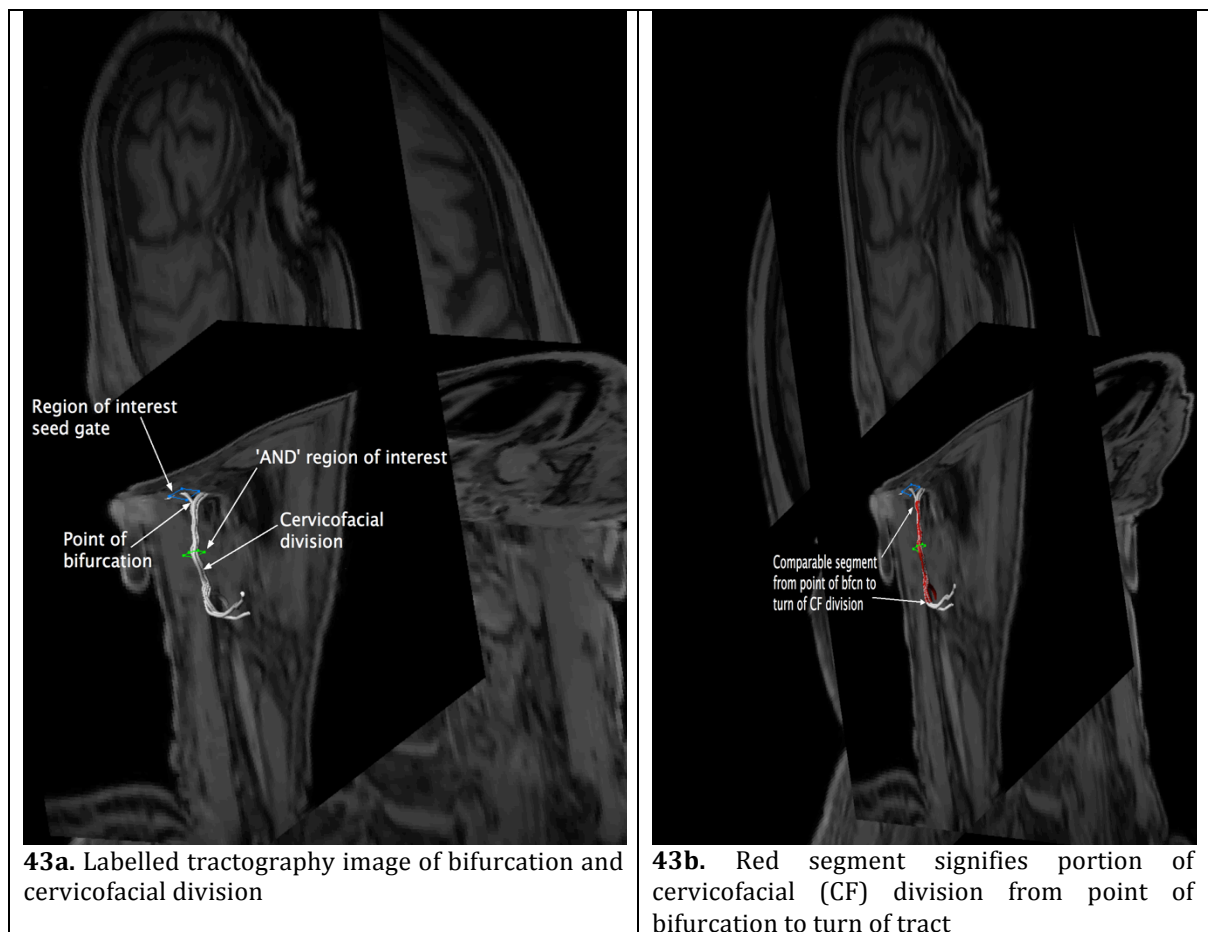


Fig. 43a shows the tract produced as analysed through the ‘seed’ plus ‘and’ region of interest gates. The bifurcation is marked along with the clear cervicofacial division. The cervicofacial division tract travels within the retromandibular parotid in the three dimensions throughout the distance of the tract. At the caudal end of the tract, a relatively sharp anterior turn is taken where the tract seems to subdivide into several branches.

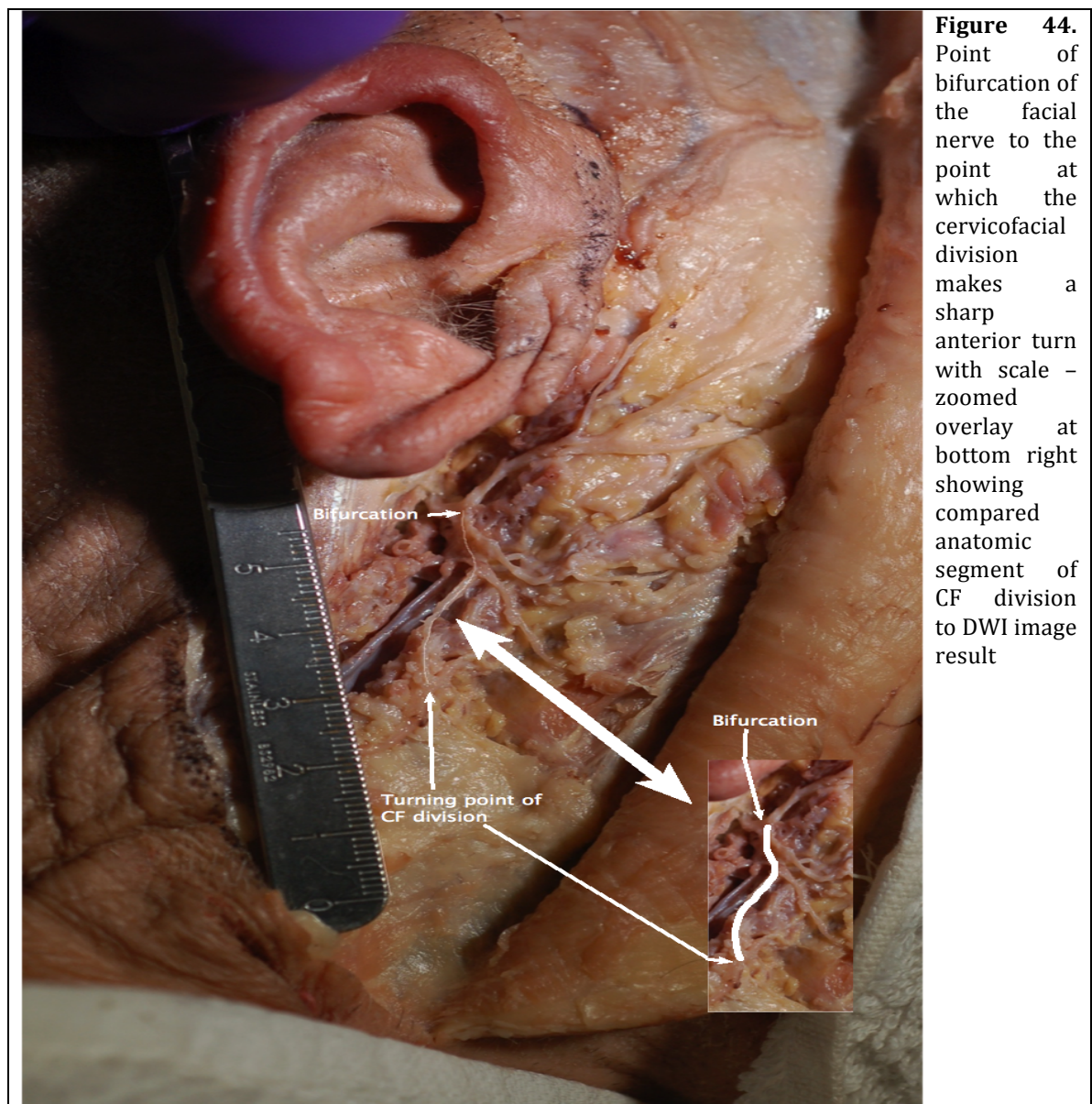
Fig. 43b, marks in red the distance the tract makes from the point of bifurcation of the tract, to the point the tract makes its anterior turn at the caudal limit of the tract. This segment of tract was analysed in detail in order to allow for comparison to the cervicofacial division of the anatomic dissection.

Number of tracts	Number of points (from all tracts)	Mean tract length (in mm)	SD tract length (in mm)	Median tract length (in mm)	Mean FA	SD FA	Median FA
6	189	30.50000191	2.34521055	29.00000763	0.16865985	0.06514262	0.16293016

Table 9 – Metric analysis of the ‘red’ segment of cervicofacial tract.

The mean length of the comparable segment of the cervicofacial tract was 30.5mm (+/-) 2.35mm standard deviation (Table 9). The FA value of the tract was within the 0.1 – 0.2 limit for being a hundred per cent sensitive to the tract being the facial nerve.

A similar portion of the cervicofacial division was subsequently analysed in the anatomic dissection. A line was drawn caudally from the point of bifurcation, along the caudal length of the division to where the division made an anterior turn. This is shown in Fig. 44 in faint white along the course of the cervicofacial division, to where the division does make an anterior turn to give off the cervical branch of the facial nerve.

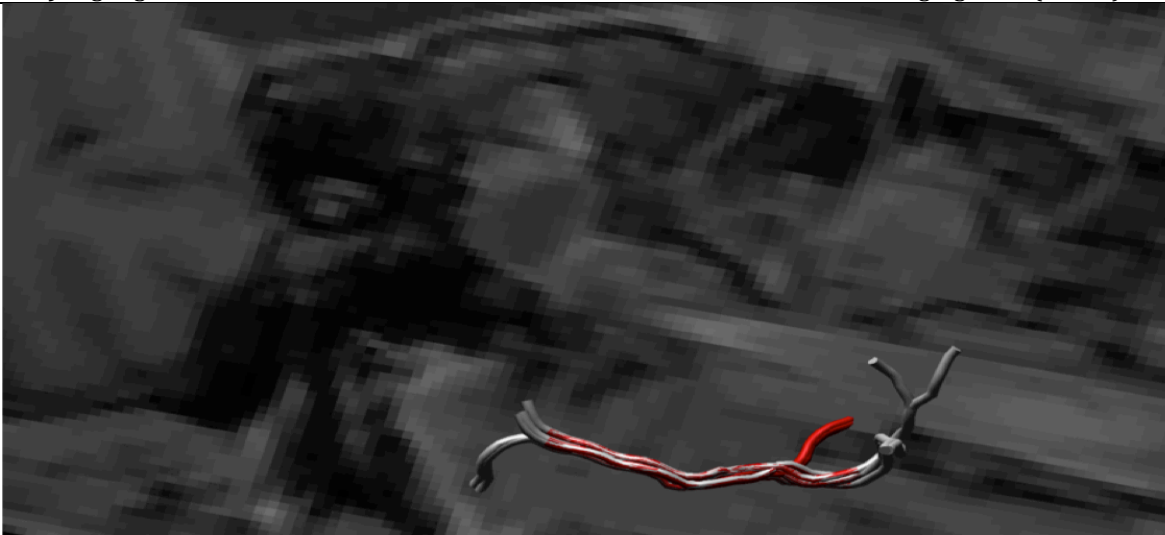


Calibrated measurement of this anatomic distance was performed using Image J software. The length of distance between the point of bifurcation to the where the most caudal branch of the cervicofacial division begins to make the anterior turn was 29.08 mm, on the anatomic dissection. This measurement corresponds closely with the metric analysis of the same tract on diffusion imaging (30.5mm (+/-) 2.35mm). Even though the dissection measurement falls within the standard deviations of lengths of the measured tracts on imaging, it is felt that the mild discrepancy between the two absolute values can be attributed to mild manipulation of the tissues during dissection and the difficulty in getting the scale to hundred per cent accuracy. Nonetheless, what the two measurements prove is

that the tract identified does correspond to the cervicofacial division as highlighted in Fig. 45.



45a) Highlighted anatomic dissection of CF division with scale, correlated to imaging tract (below).



45b) Corresponding diffusion imaging tract highlighted in red

3.4.3 Cadaveric scan 2 – left facial nerve

Detailed analysis of the diffusion tractography image obtained, identifies the cervicofacial division yet again, to be a stable segment, which can be compared to the anatomic dissection. Similarly as for the previous analyses, the point of bifurcation was used as a landmark from which, detailed calibrated measurements can be made and compared to the anatomic dissection.



Two different measurements were made on the cervicofacial division of the facial nerve tract. The first distance measured was the distance from the point of bifurcation of the facial nerve to the point of first branch (marginal mandibular division) along the tract – marked red in Figs 46. b & c. From this branching point of the marginal mandibular division, the distance was measured to the point of first division of the marginal mandibular branch itself – marked purple in fig 46. b & c. These measurements were made using precise metric analysis of the individual tract segments in question using explore dti. The results are tabulated in Table 10.

Tract	No. of tracts	Number of points (from all tracts)	Mean tract length (in mm)	SD tract length (in mm)	Approximate tract volume (in mm ³)	Mean FA	SD FA	Median FA
RED	6	108	17.0000019	0.0000065	28.9547978	0.0993887	0.0348919	0.0846792
PURPLE	4	34	7.49999523	0.5773456	11.5819191	0.1268749	0.0395580	0.1207284

Table 10 – Metric analysis of both tract segments of facial nerve – red and purple.

The red tract, measuring the distance from the point of bifurcation to the point of branching of the marginal mandibular branch from the cervicofacial trunk had a mean length of 17mm. The mean FA value was approximately 0.1 – meaning that there is a high likelihood that this is a neuronal structure with 100% sensitivity.

The purple tract segment measures the distance from the branching of the marginal mandibular branch off the cervicofacial trunk, to its first point of division. This measured 7.5mm with a mean FA value of 0.12, meaning that once again, this tract segment likely represents a neuronal structure within the parotid gland with a high level of sensitivity.

Comparison of these measurements with the anatomic dissection is shown in Fig. 47. The two comparable tract segments are highlighted on the dissection in white.

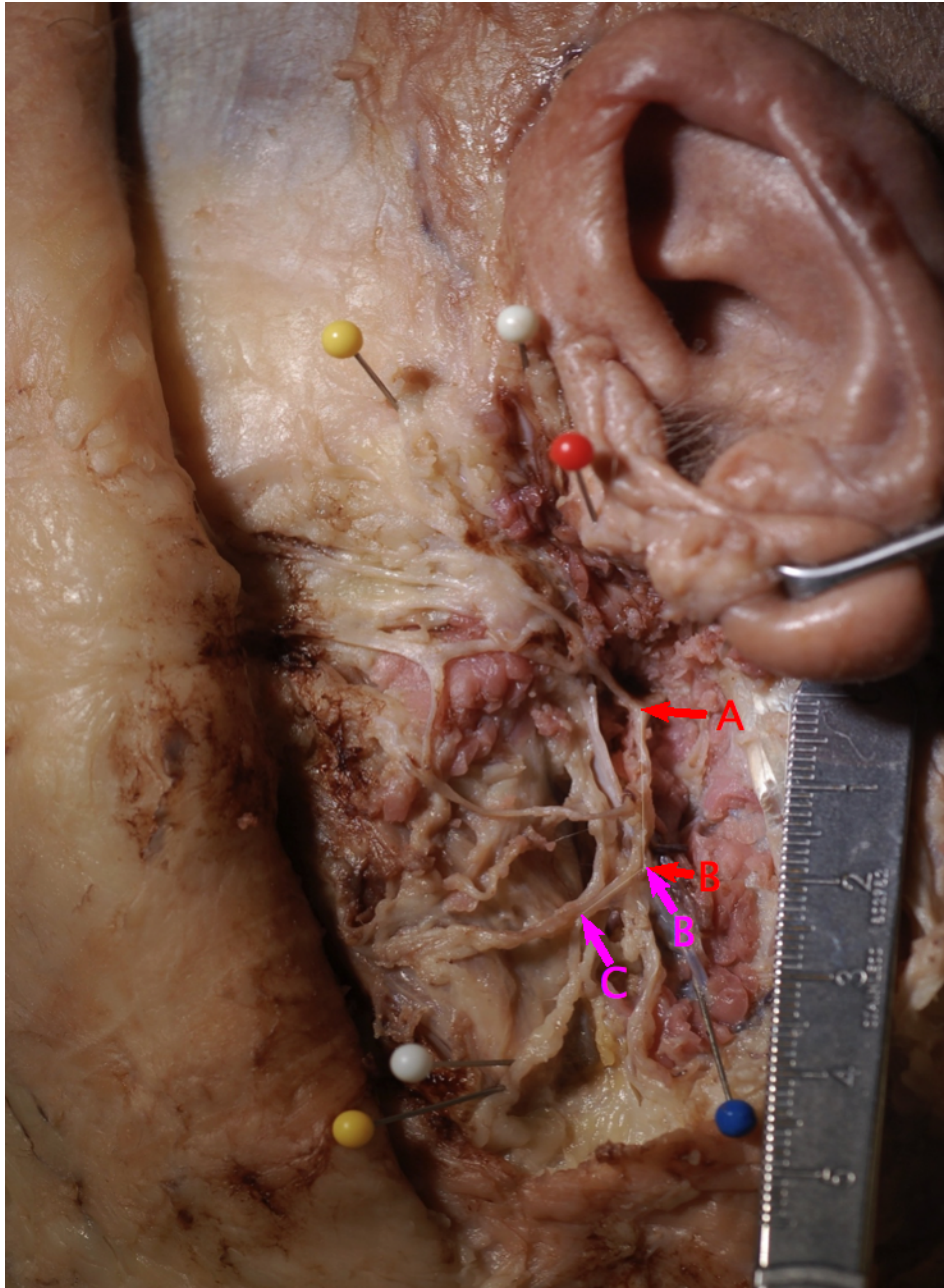


Figure 47. Left facial nerve dissection with both tract segments highlighted in a white lines. The 'red' tract on imaging compares to the white line along the cervicofacial trunk from the point of bifurcation to the branching of the marginal mandibular branch (red 'A' to red 'B'). The 'purple' tract on imaging compares to the white line drawn along the marginal mandibular branch from the cervicofacial trunk to its first point of division (purple 'B' to purple 'C').

The lengths of the measured anatomic segments are shown in table 11 as follows.

	Area	Mean	Min	Max	Angle	Length
Red - main stem	0.771	132.436	89.103	204.872	-89.071	16.872
Pueple -1st br	0.341	207.627	174.114	255	-140.464	7.449

Table 11 – Calibrated clinical measurements of the respective segments of the facial nerve.

Calibrated clinical measurement, using Image J software, of the segment of the facial nerve cervicofacial trunk, from the point of bifurcation to the point where the marginal mandibular branches, measured 16.8mm. This corresponds to the 'RED' tract segment analysed to be 17mm in length on the tractography image. The clinical measurement of the marginal mandibular branch of the facial nerve – from the point where it comes off the cervicofacial division to the point where it first divides measured 7.4mm in length. This corresponds to the 'PURPLE' tract segment analysed on the diffusion image, which measured a length of 7.499mm. Both the measurements in comparison between the diffusion image and the clinical dissection measurements are almost an exact match. Therefore, it would be feasible to conclude that the cervicofacial tract identified on imaging corresponds exactly to the cervicofacial division clinically identified on careful dissection. Furthermore, from this correlation, it would be possible to assume that the bifurcation point and hence the temporofacial division on the tractography image does indeed branch at the same point as the clinical facial nerve dissection. By deduction, we have therefore proven that the bifurcation and the cervicofacial division identified on the diffusion weighted image is a true representation of the left facial nerve in this subject.

3.4.4 Clinical applicability to live subject scans

The aim of our live subject study was to assess the transferability of the derived protocol from our cadaveric scan analyses, which we know represent the facial nerve, to live subjects. In order to fully verify our findings on the live subjects, surgical dissection of the facial nerve post-imaging would be the gold standard. However, short of this, the next best validation technique was to assess for the anatomical course of the tracts identified radiologically and ensure they correspond to what we know to be the general course the facial nerve takes as it courses through the parotid gland. In addition, the FA values were

also analysed to assess whether these tracts fell within the range of values the extra cranial facial nerves usually represent.⁵⁹

There are obvious differences between cadaveric and live tissue magnetic resonance imaging. Some of the technical challenges faced when scanning post-mortem tissue with diffusion weighted imaging specifically include the post-mortem interval (PMI), which represents the time between death and commencement of tissue fixation⁸⁴⁻⁸⁶ and the scan interval (SI), a measure of the duration the sample remains in fixative.⁸⁷ Increased duration of the PMI has reportedly shown decreased apparent diffusion coefficient (ADC) and fractional anisotropy when it comes to post-mortem analysis of neuronal structures within brain tissue.⁸⁴ In addition, tissues stored in fixative for lengthy durations (increased SI), have shown decreased apparent diffusion coefficient values, decreased proton density and reduced T_2 vs T_2^* relaxation when compared to in vivo diffusion weighted imaging of brain tissue.^{84, 88-90} Both cadaveric subjects included in this study were fixated within a twenty-four hour period of death. Cadaveric donor 1 and cadaveric donor 2 had respective SI times of 26 and 11 months. However, the above technical difficulties relate to post-mortem brain tissue diffusion weighted imaging. Post-mortem diffusion weighted imaging of the dense, tightly packed, glandular parotid tissue that encase the neuronal structures we were aiming to scan has not been studied before. Our results show that we were able to accurately reproduce the facial nerve main stem and bifurcation with varying lengths of the cervicofacial division, with healthy FA values - similar to those reported in the limited literature available on diffusion weighted imaging of the extra cranial facial nerve in live subjects who underwent surgical dissection of the nerve post-imaging.⁵⁹⁻⁶¹ In addition, by using cadaveric subjects to test the varying scan parameters, we were in an advantageous position to be able to scan for hours, without any movement artefact or claustrophobia fears, that have been a constant limitation for live subject diffusion weighted imaging

analyses throughout the literature.^{91, 92} To arrive at the protocol used for our live subject scans, which allowed for 15 minute average scan time, an average of 4-5 hours were spent on each cadaveric subject, testing b values from 400 – 1500 and voxel sizes of 1.2mm³ and 2mm³.

The results of both our live subject diffusion weighted imaging scans identify tracts that broadly correspond to the anatomical course of the facial nerve. As was performed in the cadaveric scan studies, the post processing, tractography analysis is initiated by placing a broad ‘seed’ region of interest gate at the stylomastoid foramen site. This initial step was sufficient to produce the facial nerve tract for live subject 2 (Figs. 37 a & b). What these images show is a dense main stem passing through the stylomastoid foramen seed gate and continues without too much deviation into becoming the cervicofacial trunk, which ultimately begins dividing at the caudal end. The temporofacial branches are seen branching off the main stem, indicating that the bifurcation occurs at that particular point. In essence, it would seem that we have been able to reproduce the main trunk of the facial nerve and the bifurcation, with more of the cervicofacial division than the temporofacial division. These results correlate very much with the results of the three validated facial nerve tracts that we established through our cadaveric imaging study.

The results of the diffusion weighted imaging for live subject 1 were largely similar but required more refining to filter the resultant tract. The initial placement of the broad stylomastoid ‘seed’ region of interest gate produced very dense tracts including a large segment of spurious tracts that passed medial to the mandibular ramus and body, which is not in keeping with facial nerve anatomy principles (Fig. 33 a-c). By being able to radiologically read the superimposed T1 magnetic resonance image, we were able to deduce where inhibitory ‘not’ region of interest gates were required – on the medial aspect

of the mandibular condyle and ramus anteriorly and the medial aspect of the mastoid process posteriorly, in order to omit spurious, non contributory tracts (Fig. 34 a-c). The resultant tracts (Fig. 35 a & b) show a definite main trunk segment, with a predominantly caudal extension likely representing the cervicofacial division, but with more evidence of temporofacial branching than live subject 2 image results. Once again, these results largely correlate with our previous findings both for cadaveric and live subject 2 results, that the main trunk and bifurcation are highlighted, with a larger proportion of the cervicofacial division evident as compared to the temporofacial division.

The analysis process is largely similar for all our scans, always initiated by isolating the stylomastoid foramen and subsequently filtering the tracts, by strategic use of inhibitory 'not' ROI gates or inclusive 'and' ROI gates to further define the most significant tract segment that anatomically most represents the facial nerve. The only literature assessing diffusion tractography of the facial nerve in the parotid by Attye et al., 2016 ⁵⁹, showed similar, if not slightly reduced yield in the ability to track the extra-cranial facial nerve course. In twenty-six patients with parotid tumours, requiring surgery, Attye et al, carried out diffusion weighted imaging pre operatively and compared his tractography results to intra operative findings of the location and direction of the facial nerve as the gold standard. In all twenty six, the main trunk and the bifurcation into temporofacial and cervicofacial divisions were identified on tractography, which matched intra operative findings. Beyond the bifurcation into the two divisions, there were limited tractography results. The decreasing density and the high variability in the branching patterns are cited as reasons as to why the diffusion weighted imaging is unable to track the more distal branches of the facial nerve.

Despite having a smaller sample size – three cadaveric scan results that could be compared to detailed dissection followed by two live subject scan results that could not be verified surgically, our study has some advantages over that of Attye et al. Firstly, all our subjects were disease free parotid specimens that did not have the disadvantage of a parotid tumour that could potentially alter the position of the facial nerve by compression or worse, alter the integrity of the nerve by neurovascular invasion. Secondly, cadaveric scanning allowed us to test a wide range of b values and voxel sizes without the concern of time spent within the scanner. We found that a lower b value of 400 was sufficiently adequate to produce the results we were aiming to achieve. The higher the b value, the more signal is lost and the signal to noise ratio is reduced.^{59, 93} If a higher b value is used, to counteract the effect on signal to noise, it is recommended that a higher number of directions be used in image acquisition.^{93, 94} In fact, it has been recommended that the number of directions should be more than a minimum of 45 DW directions for high order tractography studies.⁹⁴ We used 61 directional acquisitions as compared to the 32 directions acquired by Attye et al. With the combination of the lower b value and the higher directions, we are confident that our signal to noise ratio is kept to a high level – a parameter that is particularly relevant to cadaveric diffusion imaging to counteract the effects of background noise post mortem decomposition can have.

Perhaps, the reason we have been able to produce a slightly higher yield in our tracts as compared to Attye et al, was as outlined above, due to the higher directional acquisition and the lower b value. It was a recurring trend across all our scan results (cadaveric and live) that we were able to produce the main stem, bifurcation and varying lengths of the cervicofacial division. The temporofacial division seemed to evade accurate tracking as it courses distally. We believe we were able to track a large segment of it in the results achieved in cadaver 1 right (Figs. 41 & 42). This was achieved by placing a new ‘seed’

ROI gate laterally within the substance of the parotid gland, in addition to the ‘seed’ ROI placed at the stylomastoid foramen site (Figs. 17 & 18). This technique did not work when tried in our other diffusion images.

The reasons behind the evasiveness of the temporofacial division in allowing some distal tracking of its course probably lie in its, often very large angulation to the main trunk in addition to the ‘fiber crossing problem’ in voxels with more than one white matter fascicle – an issue with diffusion tensor imaging explored previously in the literature.⁹⁵ It is important to note that the upper and lower motor divisions of the facial nerve derive from different parts of the facial nerve motor nucleus within the pons, and hence could constitute two or more different white matter tracts travelling together as more than one white matter fascicle. Further research would be required to assess how improvements to the diffusion tensor image acquisition or its post processing techniques could capture such deviant angles and multiple neuronal tracts within essentially the same nerve.

Chapter 4. Conclusion

Facial nerve landmarks

We have studied the commonly used soft tissue landmark - the tragal pointer, as well as the uncommonly used osseous landmark – the angle of the mandible, in their effectiveness as landmarks to enable simple identification of the facial nerve trunk and thereby avoid inadvertent surgical damage.

In our series, the point of bifurcation of the facial nerve to the tragal pointer mean distance measured $16.89\text{mm} \pm 5.12\text{mm}$, inferior and deep. This result coincides with the most commonly used distances where it is widely known that the facial nerve trunk lies 1-2cm inferior and deep to the tragal pointer. However, not all studies in the literature coincide. The discrepancy in results could relate to the soft tissue characteristics of the tragal pointer - the variability in its size and shape and the direction in which the landmark 'points'. In addition, cadaveric studies may not represent life like representation of the tragal pointer. The post-mortem effects in anatomic lab based studies, such as this one, has the effect of influencing absolute distances by shortening them while the effects of port-mortem embalming can lead to fixation artefacts – cartilaginous structures are softer and the fixed position of the landmark may not reflect the true position in real life. An additional inter study variability is the reproducibility of the reference point along the facial trunk to which the distance to the tragal pointer is measured. While we used the point of bifurcation, other studies have used the shortest distance to the facial nerve trunk. Ultimately, the tragal pointer is a landmark that is easy to palpate, reproducible, does not require extensive dissection to reach but must not be taken as the sole determinant in parotid surgery to identify the facial nerve.

An uncommonly used and studied osseous landmark is the angle of the mandible. Our measurements from the angle of the mandible to the point of bifurcation were $28.26\text{mm} \pm 9.75\text{ mm}$. While these measurements vary from the limited measurements available of this landmark in the literature by an order of at least 10mm, it is evident that the distance of the angle of the mandible would probably be too large to use as closely related landmark to help identify the facial nerve trunk.

The angle of mandible is an easily palpable, osseous landmark not amenable to the same decomposition effects as soft tissue landmarks. However, the mandible's varying sizes between males and females, its mobility and the differing effects of edentulousness are all variables that make the angle of mandible an unreliable landmark with which to estimate the position of the facial nerve trunk intra-operatively.

'Safe zone' pre-auricular line to temporal branch of facial nerve

Our study of twenty-six facial halves showed that the most posterior ramus of the temporal nerve ranged from 6.18mm to 23.45mm anterior to the reference point on the external acoustic meatus, with a resultant 'safe zone' as per our dissections of less than 6.18mm. Less than 6mm implies a smaller safe zone than that advocated by Al Kayat & Bramley in 1979 and Gosain et al. in 1997.

Comparing our study to those studying the same distance, it is clear that it is not about the absolute distance, but rather, by remaining as close as possible to the reference point on the external acoustic meatus when creating a pre-auricular incision, one is unlikely to encounter the posterior most ramus of the temporal branch of the facial nerve.

Intra parotid venous variation to facial nerve – retromandibular vein

Of our twenty-six dissections, 31% (8/26) showed variation of the intra-parotid venous structures to the facial nerve. Three of these eight variants were variations of the retromandibular vein to the facial nerve. In two of these three variants, the retromandibular vein was superficial to the cervicofacial division of the facial nerve. In the third variant, the retromandibular vein was found to pass through a neural ring of facial nerve trunk, whereby the facial nerve trunk was found to be both superficial and deep to the retromandibular vein, before rejoining to subsequently bifurcate into the temporofacial division and cervicofacial divisions.

The retromandibular vein is an important landmark in both pre-operative imaging of the parotid gland in order to help identify the location of the facial nerve to parotid pathology and in intra-operative surgical approaches to help locate and hopefully protect the facial nerve. In both these contexts, the vein is assumed to be in its normal location, deep to the facial nerve, which is considered to be the most superficial of all intra parotid structures. Published reports have widely described retromandibular vein variation to the facial nerve. Variation of the vein to the cervicofacial division has been described in detail before and corresponds to type 4 variant according to Toure and Vacher's classification.²³ However, the finding of the retromandibular vein encircled by a neural ring of the facial nerve trunk is a variant that has not been described in the literature. Venous rings surrounding the nerve have been described, but not the converse.

The implications of not recognising the potential variation of the vein to the nerve in surgical approaches such as the retromandibular transparotid approach to the condyle, where the emphasis is to stay deep to the vein so as to avoid the facial nerve, would be devastating. Surgical text and descriptions that rely on the position of the retromandibular

vein to the facial nerve are at present inadequate for the most part to deal with variations where the vein is superficial to the nerve. Our series has shown the potential is there to iatrogenically damage, particularly the main or cervicofacial trunk where it was found that the RMV can more often than not, be superficial to these important parts of the proximal extra-cranial facial nerve – a finding also reported by the percentage variations found across the literature in addition to our series. The consequences of damage in these locations are much more serious than iatrogenic damage at a more distal level of the nerve.

Intra-parotid venous variation to facial nerve – superficial temporal vein

Five of the eight venous variants we found were not of the retromandibular vein, but rather, the superficial temporal vein. This vein is commonly found at the superior portion of the parotid, where it joins the maxillary vein, to form the retromandibular vein.

Variations of the superficial temporal vein to the facial nerve are not widely described in the literature. One of the five variants we found was of the temporal branch of the facial nerve, coursing deep to the superficial temporal vein. The other four were variants of entire facial nerve trunk and the two main divisions to the superficial temporal vein. In these variants, the facial nerve appeared forked between the superficial temporal vein and the maxillary vein, before they joined to form the retromandibular vein much more inferior than is expected within the parotid gland.

The implication of this kind of variation is that the superficial temporal can be confused for the retromandibular vein. Relying on the retromandibular vein as a surgical guide in this case could have devastating consequences, as it may not be realised that it is the superficial temporal vein that is first encountered within the substance of the parotid gland, deep to which is the facial nerve and the large maxillary vein complex.

The results of our study show that when considering intra-parotid surgery, reference to the retromandibular vein alone, as in most surgical texts can be misleading. The superficial temporal / maxillary vein complex and the resultant retromandibular vein should be seen as an intra-parotid venous complex that is likely to be as varied in each of its components as much as the facial nerve is likely to vary in each of its components. This conclusion was accepted for peer-reviewed publication as part of the work undertaken in this Doctorate.¹³

Potential for extra-cranial facial nerve imaging

We set out to assess the novel possibility of being able to reproduce the extra-cranial facial nerve tract by diffusion weighted magnetic resonance imaging, a relatively new and promising technique for the imaging of non CNS white matter tracts. Being able to visualize the extra-cranial facial nerve would have diagnostic, staging and crucially surgical planning and interventional advantages. It would go a long way to help avoiding iatrogenic facial nerve injury, especially when it comes to mandibular access surgeries where the a trans-parotid route maybe required, and the advantages of wide front views are not available due to use of small 1-2 cm incisions to ensure minimal facial scarring and deformity.

A total of three cadaveric scans were compared to detailed, atraumatic facial nerve dissections in the department of Anatomy dissection theatre. Several hours of scanning at a variety of parameters, negating the disadvantages of time limitation and movement artifacts, produced the ideal parameters with which we could produce validated facial nerve tracts that were successfully used in subsequent live subject scans.

A low b value of 400 at a voxel size of 2 mm³ with 61 directional acquisition in a 3 tesla MRI scanner with post processing using ExploreDTI suite software at 1-2 mm step sizes of

diffusion at angles of up to 89 degrees were the derived parameters that gave most convincing results of facial nerve tracts. The analysis process was largely similar for all our scans, always initiated by isolating the stylomastoid foramen and subsequently filtering the tracts, by strategic use of inhibitory ‘not’ ROI gates or inclusive ‘and’ ROI gates to further define the most significant tract segment that anatomically most represents the facial nerve.

In our three cadaveric and two live, all parotid healthy, scans, we were able to successfully produce the facial nerve main stem, bifurcation and varying lengths of the cervicofacial trunk. We successfully traced the temporofacial trunk in one of our cadaveric scans, however due to difficulty with large angulation with the main stem and the well known ‘fiber crossing’ phenomenon, the temporofacial division seemed to evade successful tracking beyond the bifurcation, for the most part. The cadaveric scans were anatomically validated using calibrated measurement of comparable segments of the tracts with the dissection results of the same facial nerves. In addition, all FA values (cadaveric and live subject) were within the range of values that represent the facial nerve within the parotid gland with a high level of sensitivity. Finally, all our results were presented to the Professor of Radiology in a University affiliated Radiology department in addition to the Head of Neuroradiology in the same department and full corroboration of our results was achieved.

Overall, despite the small sample size of this study, we are the first to have successfully recreated the facial nerve extra-cranial tract using non-invasive diffusion weighted magnetic resonance imaging in parotid healthy subjects. The parameters used and acquisition time and process are ones that can easily be reproduced in local Radiology departments in major and minor hospitals and institutions.

While surgical acumen and awareness of the high potential for variability of the facial nerve in relation to studied landmarks or the retromandibular or even the superficial temporal vein, an ultimate game changer would be the ability to visualize the three dimensional course the facial nerve takes within the parotid gland pre-operatively. This could allow for appropriate planning of surgical access and technique to limit the risk as much as is possible, especially when it comes to revision surgeries and also focused counseling to the patient about to undergo surgery as to the realistic likelihood of damage to a particular segment of the facial nerve and the likely deformity that may ensue. In addition, from a diagnostic and staging point of view, as shown in the limited literature on the topic, DWI of the extra-cranial facial nerve would allow for the diagnosis of parotid tumours and the likelihood of compression or neurovascular invasion of the facial nerve, by use of the FA values.

While much promise has been shown and advocated by our study, further larger scale trials would need to be conducted to assess the actual incidence of facial nerve injury post-operatively where pre-operative DWI was undertaken and used for pre-operative surgical planning. Ultimately, with regards iatrogenic facial nerve injury, prevention far outweighs the costs and surgical efforts currently present to cure such injury, with often-limited success. Diffusion weighted imaging with resultant tractography of the facial nerve, is an advanced, non-invasive, speedy investigative process that can be applied to most MRI scanners available in our health institutions, that shows potential to further tip the scale towards prevention of facial nerve injury and may be a safer method to plan surgical access than arbitrary surgical landmarks and guides which are often prone to variation and to which there is no consensus amongst the surgical community who operate in this region.

References

1. Hohman MH, Bhama PK, Hadlock TA. Epidemiology of iatrogenic facial nerve injury: a decade of experience. *Laryngoscope*. 2014;124:260-5.
2. Weiss JP, Sawhney R. Update on mandibular condylar fracture management. *Curr Opin Otolaryngol Head Neck Surg*. 2016;24:273-8.
3. Eisele DW, Wang SJ, Orloff LA. Electrophysiologic facial nerve monitoring during parotidectomy. *Head Neck*. 2010;32:399-405.
4. Wilson L, Lin E, Lalwani A. Cost-effectiveness of intraoperative facial nerve monitoring in middle ear or mastoid surgery. *Laryngoscope*. 2003;113:1736-45.
5. Frijters E, Hofer SO, Mureau MA. Long-term subjective and objective outcome after primary repair of traumatic facial nerve injuries. *Ann Plast Surg*. 2008;61:181-7.
6. Hamra ST. The deep-plane rhytidectomy. *Plast Reconstr Surg*. 1990;86:53-61; discussion 2-3.
7. Coulson SE, O'Dwyer N J, Adams RD, Croxson GR. Expression of emotion and quality of life after facial nerve paralysis. *Otol Neurotol*. 2004;25:1014-9.
8. Danner CJ. Facial nerve paralysis. *Otolaryngol Clin North Am*. 2008;41:619-32, x.
9. Grant GA, Goodkin R, Kliot M. Evaluation and surgical management of peripheral nerve problems. *Neurosurgery*. 1999;44:825-39; discussion 39-40.
10. Harner SG, Daube JR, Ebersold MJ. Electrophysiologic monitoring of facial nerve during temporal bone surgery. *Laryngoscope*. 1986;96:65-9.
11. Weinberg S, Kryshchuk B. Facial nerve function following temporomandibular joint surgery using the preauricular approach. *J Oral Maxillofac Surg*. 1992;50:1048-51.
12. Politi M, Toro C, Cian R, Costa F, Robiony M. The deep subfascial approach to the temporomandibular joint. *J Oral Maxillofac Surg*. 2004;62:1097-102.
13. El Kininy W, Davy S, Stassen L, Barry DS. Novel variations in spatial relations between the facial nerve and superficial temporal and maxillary veins. *Folia Morphol (Warsz)*. 2018.
14. Piagkou M, Tzika M, Paraskevas G, Natsis K. Anatomic variability in the relation between the retromandibular vein and the facial nerve: a case report, literature review and classification. *Folia Morphol*. 2013;72:371-5.
15. Al-Moraissi EA, Ellis E, 3rd. Surgical treatment of adult mandibular condylar fractures provides better outcomes than closed treatment: a systematic review and meta-analysis. *J Oral Maxillofac Surg*. 2015;73:482-93.
16. Al-Moraissi EA, Louvrier A, Colletti G, Wolford LM, Biglioli F, Ragaey M, et al. Does the surgical approach for treating mandibular condylar fractures affect the rate of seventh cranial nerve injuries? A systematic review and meta-analysis based on a new classification for surgical approaches. *J Craniomaxillofac Surg*. 2018;46:398-412.
17. Neff A, Chossegros C, Blanc JL, Champsaur P, Cheynet F, Devauchelle B, et al. Position paper from the IBRA Symposium on Surgery of the Head--the 2nd International Symposium for Condylar Fracture Osteosynthesis, Marseille, France 2012. *J Craniomaxillofac Surg*. 2014;42:1234-49.
18. Ellis E, 3rd, Moos KF, el-Attar A. Ten years of mandibular fractures: an analysis of 2,137 cases. *Oral Surg Oral Med Oral Pathol*. 1985;59:120-9.
19. Haug RH, Prather J, Indresano AT. An epidemiologic survey of facial fractures and concomitant injuries. *J Oral Maxillofac Surg*. 1990;48:926-32.
20. Gupta S, Mends F, Hagiwara M, Fatterpekar G, Roehm PC. Imaging the facial nerve: a contemporary review. *Radiol Res Pract*. 2013;2013:248039.

21. Kim DI, Nam SH, Nam YS, Lee KS, Chung RH, Han SH. The marginal mandibular branch of the facial nerve in Koreans. *Clin Anat*. 2009;22:207-14.
22. Kopuz C, Ilgi S, Yavuz S, Onderoglu S. Morphology of the retromandibular vein in relation to the facial nerve in the parotid gland. *Acta Anat (Basel)*. 1995;152:66-8.
23. Toure G, Vacher C. Relations of the facial nerve with the retromandibular vein: anatomic study of 132 parotid glands. *Surg Radiol Anat*. 2010;32:957-61.
24. Choi KY, Yang JD, Chung HY, Cho BC. Current Concepts in the Mandibular Condyle Fracture Management Part II: Open Reduction Versus Closed Reduction. *Arch Plast Surg*. 2012;39:301-8.
25. Haug RH, Brandt MT. Closed reduction, open reduction, and endoscopic assistance: current thoughts on the management of mandibular condyle fractures. *Plast Reconstr Surg*. 2007;120:90S-102S.
26. Al-Kayat A, Bramley P. A modified pre-auricular approach to the temporomandibular joint and malar arch. *Br J Oral Surg*. 1979;17:91-103.
27. Bhattacharyya N, Varvares MA. Anomalous relationship of the facial nerve and the retromandibular vein: A case report. *J Oral Maxil Surg*. 1999;57:75-6.
28. Lim CY, Chang HS, Nam KH, Chung WY, Park CS. Preoperative prediction of the location of parotid gland tumors using anatomical landmarks. *World J Surg*. 2008;32:2200-3.
29. Muhleman MA, Wartmann CT, Hage R, Matusz P, Shoja MM, Tubbs RS, et al. A review of the tragal pointer: anatomy and its importance as a landmark in surgical procedures. *Folia Morphol (Warsz)*. 2012;71:59-64.
30. Ellis E, 3rd, Dean J. Rigid fixation of mandibular condyle fractures. *Oral Surg Oral Med Oral Pathol*. 1993;76:6-15.
31. Pather N, Osman M. Landmarks of the facial nerve: implications for parotidectomy. *Surg Radiol Anat*. 2006;28:170-5.
32. Rea PM, McGarry G, Shaw-Dunn J. The precision of four commonly used surgical landmarks for locating the facial nerve in anterograde parotidectomy in humans. *Ann Anat*. 2010;192:27-32.
33. Wetmore SJ. Surgical landmarks for the facial nerve. *Otolaryngol Clin North Am*. 1991;24:505-30.
34. Gosain AK, Sewall SR, Yousif NJ. The temporal branch of the facial nerve: how reliably can we predict its path? *Plast Reconstr Surg*. 1997;99:1224-33; discussion 34-6.
35. Conley J, Hamaker RC. Prognosis of malignant tumors of the parotid gland with facial paralysis. *Arch Otolaryngol*. 1975;101:39-41.
36. de Ru JA, Bleys RL, van Benthem PP, Hordijk GJ. Preoperative determination of the location of parotid gland tumors by analysis of the position of the facial nerve. *J Oral Maxillofac Surg*. 2001;59:525-8; discussion 9-30.
37. de Ru JA, van Benthem PP, Bleys RL, Lubsen H, Hordijk GJ. Landmarks for parotid gland surgery. *J Laryngol Otol*. 2001;115:122-5.
38. Conn IG, Wiesenfeld D, Ferguson MM. The anatomy of the facial nerve in relation to CT/sialography of the parotid gland. *Br J Radiol*. 1983;56:901-5.
39. Ariyoshi Y, Shimahara M. Determining whether a parotid tumor is in the superficial or deep lobe using magnetic resonance imaging. *J Oral Maxil Surg*. 1998;56:23-6.
40. El-Hakim H, Mountain R, Carter L, Nilssen EL, Wardrop P, Nimmo M. Anatomic landmarks for locating parotid lesions in relation to the facial nerve: cross-sectional radiologic study. *J Otolaryngol*. 2003;32:314-8.
41. Imaizumi A, Kuribayashi A, Okochi K, Ishii J, Sumi Y, Yoshino N, et al. Differentiation between Superficial and Deep Lobe Parotid Tumors by Magnetic

- Resonance Imaging: Usefulness of the Parotid Duct Criterion. *Acta Radiol.* 2009;50:806-11.
42. Howlett DC. High resolution ultrasound assessment of the parotid gland. *Br J Radiol.* 2003;76:271-7.
43. Babademez MA, Acar B, Gunbey E, Karabulut H, Karasen RM. Anomalous Relationship of the Retromandibular Vein to the Facial Nerve as a Potential Risk Factor for Facial Nerve Injury During Parotidectomy. *J Craniofac Surg.* 2010;21:801-2.
44. Kawakami S, Tsukada S, Taniguchi W. The Superficial Temporal and Retromandibular Veins as Guides to Expose the Facial-Nerve Branches. *Ann Plas Surg.* 1994;32:295-9.
45. Bhattacharyya N, Varvares MA. Anomalous relationship of the facial nerve and the retromandibular vein: a case report. *J Oral Maxillofac Surg.* 1999;57:75-6.
46. Dingman RO, Grabb WC. Surgical anatomy of the mandibular ramus of the facial nerve based on the dissection of 100 facial halves. *Plast Reconstr Surg Transplant Bull.* 1962;29:266-72.
47. JW L. Surgical anatomy of the temporal branch and marginal mandibular branch of the facial nerve based on the dissection of 54 facial halves [Doctoral dissertation]: Yonsei University, Seoul; 1987.
48. Laing MR, McKerrow WS. Intraparotid anatomy of the facial nerve and retromandibular vein. *Br J Surg.* 1988;75:310-2.
49. Savary V, Robert R, Rogez JM, Armstrong O, Leborgne J. The mandibular marginal ramus of the facial nerve: an anatomic and clinical study. *Surg Radiol Anat.* 1997;19:69-72.
50. Wang TM, Lin CL, Kuo KJ, Shih C. Surgical anatomy of the mandibular ramus of the facial nerve in Chinese adults. *Acta Anat (Basel).* 1991;142:126-31.
51. Piagkou M, Tzika M, Paraskevas G, Natsis K. Anatomic variability in the relation between the retromandibular vein and the facial nerve: a case report, literature review and classification. *Folia Morphol (Warsz).* 2013;72:371-5.
52. Ellis E, 3rd, McFadden D, Simon P, Throckmorton G. Surgical complications with open treatment of mandibular condylar process fractures. *J Oral Maxillofac Surg.* 2000;58:950-8.
53. Shi D, Patil PM, Gupta R. Facial nerve injuries associated with the retromandibular transparotid approach for reduction and fixation of mandibular condyle fractures. *J Craniomaxillofac Surg.* 2015;43:402-7.
54. Sawhney R, Brown R, Ducic Y. Condylar fractures. *Otolaryngol Clin North Am.* 2013;46:779-90.
55. Kochhar A, Larian B, Azizzadeh B. Facial Nerve and Parotid Gland Anatomy. *Otolaryngol Clin North Am.* 2016;49:273-84.
56. Al-Noury K, Lotfy A. Normal and pathological findings for the facial nerve on magnetic resonance imaging. *Clin Radiol.* 2011;66:701-7.
57. Li C, Li Y, Zhang D, Yang Z, Wu L. 3D-FIESTA MRI at 3 T demonstrating branches of the intraparotid facial nerve, parotid ducts and relation with benign parotid tumours. *Clin Radiol.* 2012;67:1078-82.
58. Qin Y, Zhang J, Li P, Wang Y. 3D double-echo steady-state with water excitation MR imaging of the intraparotid facial nerve at 1.5T: a pilot study. *AJNR Am J Neuroradiol.* 2011;32:1167-72.
59. Attyé A, Alexandre Karkas, Irène Troprès, Matthieu Roustit, Adrian Kastler, Georges Bettega, Laurent Lamalle, Félix Renard, et al. Parotid gland tumours: MR tractography to assess contact with the facial nerve. *European Radiology.* 2016;26:2233-41.

60. Attyé A, Karkas A, Tropres I, Lamalle L, Renard F, Bettega G, et al. Surgical validation of extracranial facial nerve magnetic resonance tractography. 23rd Annual Meeting of International Society for Magnetic Resonance in Medicine. Toronto 2015.
61. Attye A, Tropres I, Rouchy RC, Righini C, Espinoza S, Kastler A, et al. Diffusion MRI: literature review in salivary gland tumors. *Oral Dis.* 2017;23:572-5.
62. Chen DQ, Quan J, Guha A, Tymianski M, Mikulis D, Hodaie M. Three-dimensional in vivo modeling of vestibular schwannomas and surrounding cranial nerves with diffusion imaging tractography. *Neurosurgery.* 2011;68:1077-83.
63. Taoka T, Hirabayashi H, Nakagawa H, Sakamoto M, Myochin K, Hirohashi S, et al. Displacement of the facial nerve course by vestibular schwannoma: preoperative visualization using diffusion tensor tractography. *J Magn Reson Imaging.* 2006;24:1005-10.
64. Guntinas-Lichius O, Klusmann JP, Wittekindt C, Stennert E. Parotidectomy for benign parotid disease at a university teaching hospital: outcome of 963 operations. *Laryngoscope.* 2006;116:534-40.
65. Ho AL, Scott AM, Klassen AF, Cano SJ, Pusic AL, Van Laeken N. Measuring quality of life and patient satisfaction in facial paralysis patients: a systematic review of patient-reported outcome measures. *Plast Reconstr Surg.* 2012;130:91-9.
66. Yabuuchi H, Fukuya T, Tajima T, Hachitanda Y, Tomita K, Koga M. Salivary gland tumors: diagnostic value of gadolinium-enhanced dynamic MR imaging with histopathologic correlation. *Radiology.* 2003;226:345-54.
67. Yabuuchi H, Matsuo Y, Kamitani T, Setoguchi T, Okafuji T, Soeda H, et al. Parotid gland tumors: can addition of diffusion-weighted MR imaging to dynamic contrast-enhanced MR imaging improve diagnostic accuracy in characterization? *Radiology.* 2008;249:909-16.
68. Bernstein MA, King KF, Zhou XJ. *Handbook of MRI pulse sequences*: Elsevier; 2004.
69. Stejskal EO TJ. Spin diffusion measurements: Spin echoes in the presence of a time-dependent field gradient. *The Journal of Chemical Physics.* 1965;42:288 - 92.
70. Stejskal EO, Tanner JE. Spin diffusion measurements: spin echoes in the presence of a time - dependent field gradient. *Journal of Chemical Physics.* 1965;42:288-92.
71. Le Bihan D, Breton E, Lallemand D, Grenier P, Cabanis E, Laval-Jeantet M. MR imaging of intravoxel incoherent motions: application to diffusion and perfusion in neurologic disorders. *Radiology.* 1986;161:401-7.
72. Xue R, van Zijl P, Crain BJ, Solaiyappan M, Mori S. In vivo three - dimensional reconstruction of rat brain axonal projections by diffusion tensor imaging. *Magnetic Resonance in Medicine.* 1999;42:1123-7.
73. Basser PJ, Pajevic S, Pierpaoli C, Duda J, Aldroubi A. In vivo fiber tractography using DT-MRI data. *Magnetic Resonance in Medicine.* 2000;44:625-32.
74. Assaf Y, Pasternak O. Diffusion tensor imaging (DTI)-based white matter mapping in brain research: a review. *Journal of Molecular Neuroscience.* 2008;34:51-61.
75. Johansen-Berg H, Behrens TE. *Diffusion MRI: from quantitative measurement to in vivo neuroanatomy*: Academic Press; 2013.
76. Roebroek A, Galuske R, Formisano E, Chirry O, Bratzke H, Ronen I, et al. High-resolution diffusion tensor imaging and tractography of the human optic chiasm at 9.4 T. *Neuroimage.* 2008;39:157-68.
77. Skorpil M, Karlsson M, Nordell A. Peripheral nerve diffusion tensor imaging. *Magnetic Resonance Imaging.* 2004;22:743-5.
78. Hiltunen J, Suortti T, Arvela S, Seppä M, Joensuu R, Hari R. Diffusion tensor imaging and tractography of distal peripheral nerves at 3 T. *Clinical Neurophysiology.* 2005;116:2315-23.

79. Kennedy KM, Raz N. Aging white matter and cognition: differential effects of regional variations in diffusion properties on memory, executive functions, and speed. *Neuropsychologia*. 2009;47:916-27.
80. Ung N, Mathur M, Chung LK, Cremer N, Pelargos P, Frew A, et al. A Systematic Analysis of the Reliability of Diffusion Tensor Imaging Tractography for Facial Nerve Imaging in Patients with Vestibular Schwannoma. *Journal of Neurological Surgery Part B: Skull Base*. 2016;77:314-8.
81. Behrens TE, Berg HJ, Jbabdi S, Rushworth MF, Woolrich MW. Probabilistic diffusion tractography with multiple fibre orientations: What can we gain? . *Neuroimage*. 2007;34:144-55.
82. Clatworthy PL, Williams GB, Acosta-Cabronero J, Jones SP, Harding SG, Johansen-Berg H, et al. Probabilistic tractography of the optic radiations—an automated method and anatomical validation. *Neuroimage*. 2010;49:2001-12.
83. Jeurissen B, Leemans A, Jones DK, Tournier JD, Sijbers J. Probabilistic fiber tracking using the residual bootstrap with constrained spherical deconvolution. *Human brain mapping*. 2011;32:461-79.
84. D'Arceuil H, de Crespigny A. The effects of brain tissue decomposition on diffusion tensor imaging and tractography. *Neuroimage*. 2007;36:64-8.
85. Miller KL, Stagg CJ, Douaud G, Jbabdi S, Smith SM, Behrens TE, et al. Diffusion imaging of whole, post-mortem human brains on a clinical MRI scanner. *Neuroimage*. 2011;57:167-81.
86. Shepherd TM, Flint JJ, Thelwall PE, Stanisiz GJ, Mareci TH, Yachnis AT, et al. Postmortem interval alters the water relaxation and diffusion properties of rat nervous tissue--implications for MRI studies of human autopsy samples. *Neuroimage*. 2009;44:820-6.
87. Dawe RJ, Bennett DA, Schneider JA, Vasireddi SK, Arfanakis K. Postmortem MRI of human brain hemispheres: T2 relaxation times during formaldehyde fixation. *Magn Reson Med*. 2009;61:810-8.
88. Pfefferbaum A, Sullivan EV, Adalsteinsson E, Garrick T, Harper C. Postmortem MR imaging of formalin-fixed human brain. *Neuroimage*. 2004;21:1585-95.
89. Sun SW, Neil JJ, Liang HF, He YY, Schmidt RE, Hsu CY, et al. Formalin fixation alters water diffusion coefficient magnitude but not anisotropy in infarcted brain. *Magn Reson Med*. 2005;53:1447-51.
90. Sun SW, Neil JJ, Song SK. Relative indices of water diffusion anisotropy are equivalent in live and formalin-fixed mouse brains. *Magn Reson Med*. 2003;50:743-8.
91. Foxley S, Jbabdi S, Clare S, Lam W, Ansorge O, Douaud G, et al. Improving diffusion-weighted imaging of post-mortem human brains: SSFP at 7 T. *Neuroimage*. 2014;102 Pt 2:579-89.
92. Jiang Y, Johnson GA. Microscopic diffusion tensor imaging of the mouse brain. *Neuroimage*. 2010;50:465-71.
93. Jones DK. The effect of gradient sampling schemes on measures derived from diffusion tensor MRI: a Monte Carlo study. *Magn Reson Med*. 2004;51:807-15.
94. Tournier JD, Calamante F, Connelly A. Determination of the appropriate b value and number of gradient directions for high-angular-resolution diffusion-weighted imaging. *NMR Biomed*. 2013;26:1775-86.
95. Farquharson S, Tournier JD, Calamante F, Fabinyi G, Schneider-Kolsky M, Jackson GD, et al. White matter fiber tractography: why we need to move beyond DTI. *J Neurosurg*. 2013;118:1367-77.
96. Lim CY, Chang HS, Nam KH, Chung WY, Park CS. Preoperative prediction of the location of parotid gland tumors using anatomical landmarks. *World J Surg*. 2008;32:2200-3.

97. Kahn CE, Jr., Carrino JA, Flynn MJ, Peck DJ, Horii SC. DICOM and radiology: past, present, and future. *Journal of the American College of Radiology : JACR*. 2007;4:652-7.
98. Jones DK, Leemans A. Diffusion tensor imaging. *Methods in molecular biology* (Clifton, NJ). 2011;711:127-44.
99. Benner T, van der Kouwe AJ, Kirsch JE, Sorensen AG. Real-time RF pulse adjustment for B0 drift correction. *Magnetic resonance in medicine*. 2006;56:204-9.
100. Vos SB, Tax CM, Luijten PR, Ourselin S, Leemans A, Froeling M. The importance of correcting for signal drift in diffusion MRI. *Magnetic resonance in medicine*. 2017;77:285-99.
101. Kellner E, Dhital B, Kiselev VG, Reisert M. Gibbs-ringing artifact removal based on local subvoxel-shifts. *Magnetic resonance in medicine*. 2016;76:1574-81.
102. Perrone D, Aelterman J, Pizurica A, Jeurissen B, Philips W, Leemans A. The effect of Gibbs ringing artifacts on measures derived from diffusion MRI. *Neuroimage*. 2015;120:441-55.
103. Soares JM, Marques P, Alves V, Sousa N. A hitchhiker's guide to diffusion tensor imaging. *Frontiers in neuroscience*. 2013;7:31.
104. Rohde GK, Barnett AS, Basser PJ, Marengo S, Pierpaoli C. Comprehensive approach for correction of motion and distortion in diffusion-weighted MRI. *Magnetic resonance in medicine*. 2004;51:103-14.
105. Mohammadi S, Moller HE, Kugel H, Muller DK, Deppe M. Correcting eddy current and motion effects by affine whole-brain registrations: evaluation of three-dimensional distortions and comparison with slice-wise correction. *Magnetic resonance in medicine*. 2010;64:1047-56.
106. Tournier JD, Mori S, Leemans A. Diffusion tensor imaging and beyond. *Magnetic resonance in medicine*. 2011;65:1532-56.
107. Le Bihan D, Mangin JF, Poupon C, Clark CA, Pappata S, Molko N, et al. Diffusion tensor imaging: concepts and applications. *J Magn Reson Imaging*. 2001;13:534-46.
108. Irfanoglu MO, Walker L, Sarlls J, Marengo S, Pierpaoli C. Effects of image distortions originating from susceptibility variations and concomitant fields on diffusion MRI tractography results. *Neuroimage*. 2012;61:275-88.

Appendix 1: Peer reviewed publication

ONLINE FIRST

This is a provisional PDF only. Copyedited and fully formatted version will be made available soon.



ISSN: 0015-5659

e-ISSN: 1644-3284

Novel variations in spatial relations between the facial nerve and superficial temporal and maxillary veins

Authors: Walid El Kininy, Shane Davy, Leo Stassen, Denis Stephen Barry

DOI: 10.5603/FM.a2018.0019

Article type: CASE REPORTS

Submitted: 2018-01-19

Accepted: 2018-02-13

Published online: 2018-02-26

This article has been peer reviewed and published immediately upon acceptance.
It is an open access article, which means that it can be downloaded, printed, and distributed freely,
provided the work is properly cited.
Articles in "Folia Morphologica" are listed in PubMed.

Novel variations in spatial relations between the facial nerve and superficial temporal and maxillary veins

Running head: Facial nerve variation in the parotid gland

Walid El Kininy¹, Shane Davy¹, Leo Stassen¹, Denis Stephen Barry²

¹Department of Anatomy, Trinity Biomedical Sciences Institute, Trinity College, University of Dublin, Dublin, Ireland

²Department of Oral/Maxillofacial Surgery, Dublin Dental University Hospital, Trinity College Dublin, Dublin, Ireland

Address for correspondence:

Dr. Denis Barry, BSc, PhD, Department of Anatomy, Trinity College Dublin, University of Dublin, Dublin 2, Ireland, e-mail; debarry@tcd.ie

Dr. Walid El Kininy, B.Dent.Sc, MFDS RCSI, MB, BCh, BAO, MRCS RCSI
Department of Anatomy, Trinity College Dublin, University of Dublin, Dublin 2, Ireland,
e-mail; elkininw@tcd.ie

Abstract

Variations in the relationship of the retromandibular vein to the facial nerve have been widely reported due to their relevance for surgical approaches in parotid, osteotomy and mandibular condyle surgery. In the context of the retromandibular retroparotid approach, remaining deep to the retromandibular vein is advised to decrease the likelihood of encountering the facial nerve during mandibular condyle surgery.

In the present report, an unusual variant of the superficial temporal vein lying superficial to the facial nerve is described. This represents a variation of the venous branching pattern within the parotid gland, whereby the superficial temporal vein joins the maxillary vein inferior to its usual communication. These findings are discussed in the context of commonly used surgical approaches to the mandible for condylar trauma or osteotomy surgery.

Key words: facial nerve variation, retromandibular vein, superficial temporal vein, mandibular condyle surgery, parotidectomy

1. Introduction

The retromandibular vein generally lies medial to the facial nerve ^{14, 23, 43}. It is formed by the merging of the superficial temporal vein and the maxillary vein within the superior aspect of the parotid gland, at the level of the neck of the mandible. The vein then courses through the parotid gland between the external carotid artery medially and the facial nerve laterally, which gives an important anatomical landmark in parotid and mandibular surgery ¹⁴. The major risk in these surgeries is injury to the facial nerve due to compression, damage or transection on approach, which has significant morbidity for the patient ³⁶. If damage of the nerve is identified, surgical nerve repair impacts the duration of the operation ³⁶.

The retromandibular vein is used as a landmark during pre-operative magnetic resonance imaging (MRI) ³⁹⁻⁴¹, computed tomography (CT) ^{40, 96} and sonography ⁴² to identify the most likely location of the facial nerve within the parotid gland. In addition, the retromandibular vein is used intra-operatively as an important landmark to reveal the facial nerve branches inside the parotid substance as the vein may be traced superiorly into the gland after its identification. The facial nerve is usually found superficial to the vein ^{23, 43}. Likewise, the superficial temporal vein has been shown to be a useful indicator during dissection of the upper parotid gland. Its usual superficial and superior location within the parotid gland serves as a guide to the beginning of the retromandibular vein ^{43, 44}. Variations in the relationships between the intra-parotid venous structures and the facial nerve are widely described ^{21, 22, 43, 44}. While a universally recognised classification system does not exist, Toure and Vacher (2010) classified six facial nerve and retromandibular vein variants ²³ (Table 1).

In the present case-report, we encountered a previously unreported variant of the facial nerve in relation to the superficial temporal and maxillary veins of a cadaveric female. We discuss the importance of this variant in the context of parotid and condylar surgery.

2. Case report

As part of our cadaveric study of facial nerve variations with respect to extra oral approaches to the mandibular condyle, a standard dissection of both parotid glands was performed in a 58 year old Caucasian Irish formalin embalmed female cadaver.

A pre-auricular incision was made with extensions to the mastoid process posteriorly and to the neck inferiorly (Lazy S incision). Skin and subcutaneous tissue was lifted and a plane developed subcutaneously, superior to the superficial masseteric aponeurosis system (SMAS) layer.

The dissection through the SMAS was performed onto the parotid gland from the tragus inferiorly. This was followed by blunt dissection into the parotid to identify the main trunk of the facial nerve. The trunk of the facial nerve was followed anteriorly, to identify the branching pattern of the facial nerve. A note was made of the anatomic relationships of venous structures to the facial nerve. Images were captured using a Nikon D50 Digital SLR camera.

The right and left parotid glands were dissected to show potential variations between the facial nerve and venous systems. The left facial nerve showed considerable variation in relation to the venous structures in the parotid substance. The main trunk of the facial nerve exited the stylomastoid foramen and appeared within the parotid between the superficial temporal vein and maxillary vein superior to their junction (Fig. 1A - E). As such, the main trunk of the facial nerve lay deep to the superficial temporal vein prior to turning to course superficial to the maxillary vein (Fig. 1C, D).

After appearing between the two veins, the main trunk divided into upper and lower divisions. The upper division divided into temporal, zygomatic and buccal branches, while the lower division showed another variation (Fig. 1A – D). The lower division did not divide immediately. It travelled for 1.5 cm in an anterior to inferior direction before

dividing into another buccal branch. This anastomosed with the buccal branch emerging from the upper division, a marginal mandibular branch and a cervical branch. The cervical branch passed inferiorly to dive deep to a communicating vein and subsequently move inferiorly towards the neck.

The right facial nerve of the same cadaver did not show the same variation (Fig. 2A, C). The retromandibular vein was deep to all facial nerve branches. The main trunk of the facial nerve divided as expected into upper and lower trunks. The upper trunk divided into temporal, zygomatic branches, and buccal branches. This buccal branch anastomosed with another buccal branch from the lower division. The lower division continued inferiorly after giving the buccal branch before dividing into the marginal mandibular and cervical branches.

3. Discussion

The classification system identified by Toure and Vacher 2010 ²³, based on an anatomical study of 132 parotid glands demonstrated that the retromandibular vein was found to be situated medial to the facial nerve in the majority of the cases (Type 1, 65.2%, 86/132) and lateral to it in 28% (Type 2, 37/132). Types 3 to 6 constituted subtypes of Type 2 (Table 1).

The present case-report shows a facial nerve variation that is different and cannot be placed in this classification system. The main trunk lay medial to the superficial temporal vein before becoming superficial to the maxillary vein. Piagkou et al, 2013 ¹⁴ described a similar variant, in which the superficial temporal vein was encountered lying over both the facial nerve divisions while the upper division crossed superior to the vein.

It should be noted that this study and the present case-report may also represent a variation in the formation of the retromandibular vein. This is due to the superficial temporal vein joining the maxillary vein in the parotid substance inferior to the tragal point, which is much more inferior than is generally recognised ⁴⁴. Considering the aberrant location of the superficial temporal vein, lying lateral to the facial nerve trunk in this case, and not the expected retromandibular vein the potential for injury to the facial nerve is significant. This is especially relevant in the context of parotid and condylar surgeries for clinicians who use the retromandibular vein as a landmark deep to which the facial nerve is not expected to be encountered ¹⁴. In particular, the present report demonstrates that the superficial temporal vein may be the first venous landmark encountered during a retromandibular - retroparotid surgical approach to the condyle.

Descriptions of both the transparotid and retroparotid approaches to the mandibular condyles stress the importance of remaining superficial to the retromandibular vein ¹⁴. Both surgical approaches rely on conventional knowledge of normal anatomy of the facial nerve

and its relationship to the retromandibular vein. In particular, the retroparotid approach relies heavily on the knowledge that the facial nerve lies superficial to the retromandibular vein¹⁴.

We present a case where the arrangement of the intra-parotid venous structures is such that the superficial temporal vein would not likely be confused with the retromandibular vein. The anatomical variant would not be appreciated through a small 1 - 2 cm incision during mandibular condyle surgery. As such, the facial nerve, which lies deep to the superficial temporal vein, is at great risk and the level of damage likely in our case, would be damage to the main trunk, resulting in hemifacial weakness.

Potential variations of the facial nerve and its relationship to the venous structures within the parotid gland should be considered during surgery. Mandibular condyle access surgeries provide limited views of the structures involved. Hence, there is more likelihood of damage, as opposed to the wide front (Lazy S) views provided by parotid dissections, especially if variations exist.

In the present report, the main trunk of the facial nerve lies medial to the superficial temporal vein, yet lateral to the maxillary vein. In addition, the maxillary and superficial temporal veins merge in the substance to the parotid and not at the superior border of the parotid as previously recognised. This has particular surgical significance during retromandibular-retroparotid approaches to the mandibular condyle, as the retromandibular vein may not be the first venous structure encountered.

Ethical approval

Informed consent was obtained for research prior to donor donation.

Conflict of interest

There were no conflicts of interest associated with this study.

Author contributions

El Kininy: Data collection, Data analysis, Manuscript writing/editing

Stassen: Protocol/project development

Barry: Manuscript writing/editing, Figure production

Table 1 (in publication). Facial nerve and retromandibular vein variants.

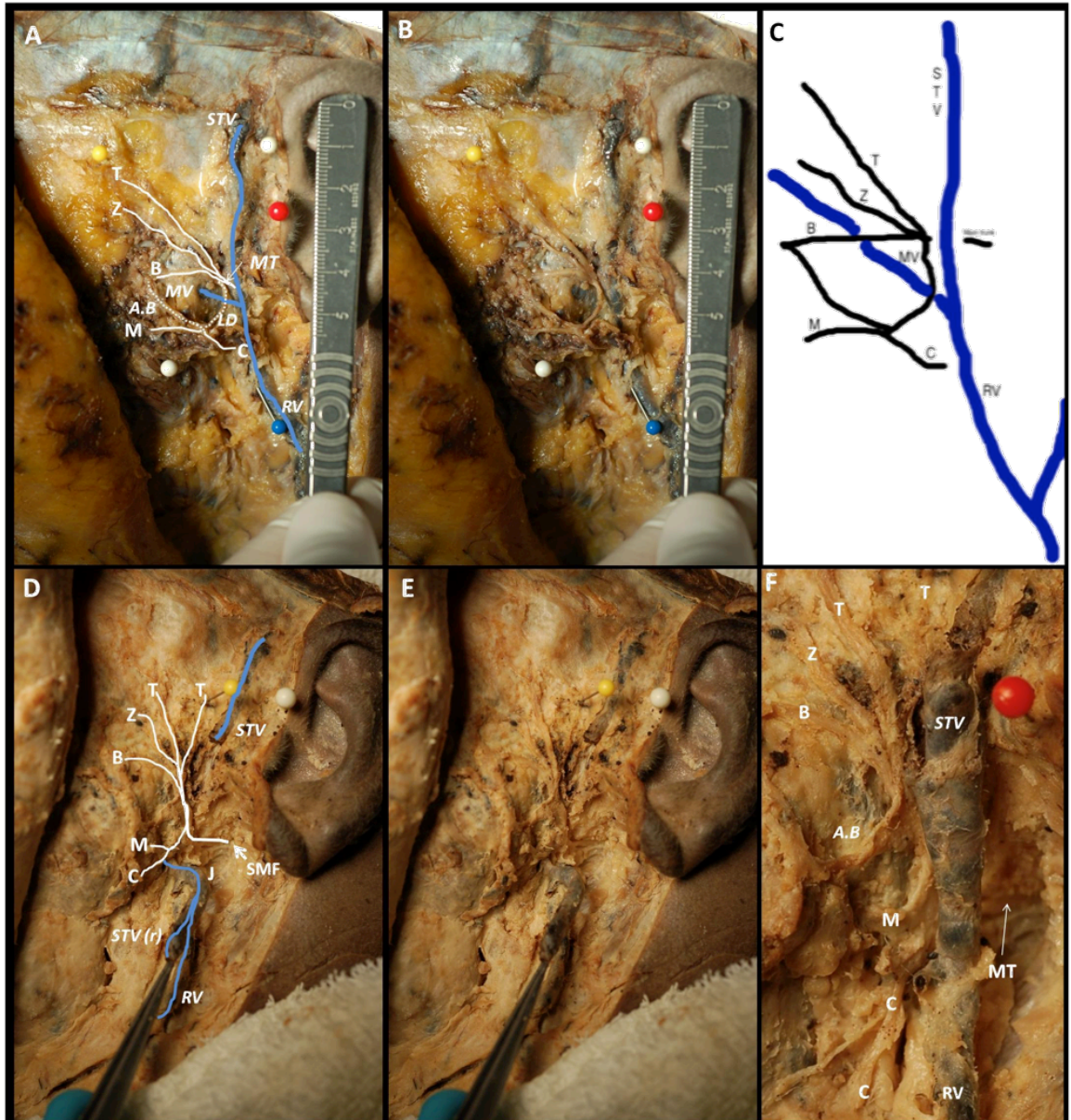
Type 1	Retromandibular vein lay medial (deep) to the facial nerve (65.2%)
Type 2	Retromandibular vein lay lateral (superficial) to the facial nerve (28%)
Types 3-6	Constituted subtypes of type 2

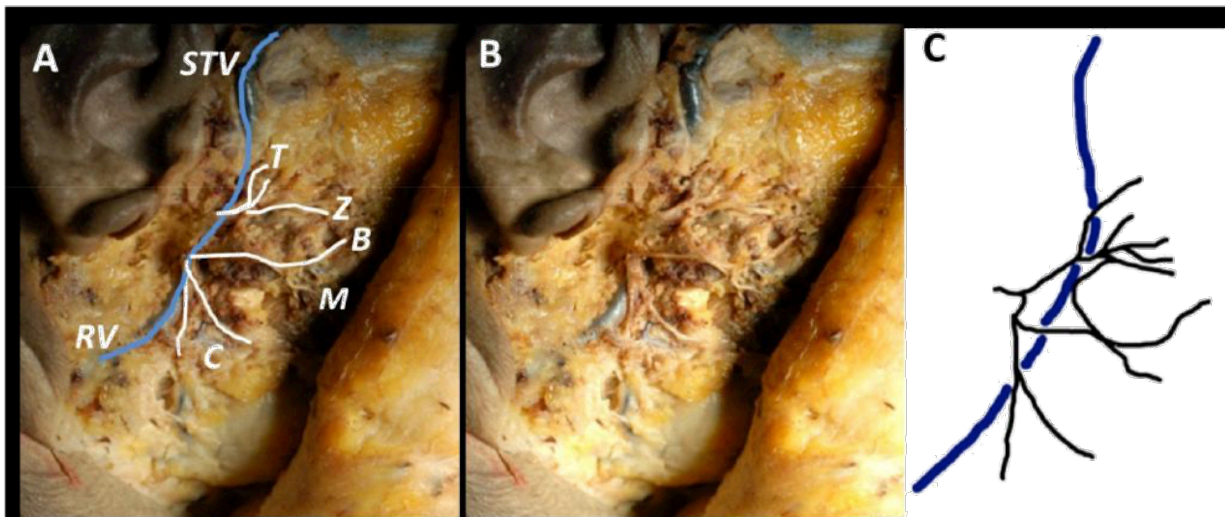
Figure 1 (in publication). Facial nerve variation. (A) Labelled left superficial parotid dissection showing the facial nerve variation in relation to the superficial temporal and maxillary veins with scale.

(B) Unlabelled left sided schematic of facial nerve variation. (C) Schematic of facial nerve variation. (D) Labelled left superficial parotid dissection showing the facial nerve variation with superficial temporal vein reflected inferiorly. (E) Unlabelled left superficial parotid dissection showing the facial nerve variation with superficial temporal vein reflected inferiorly. (F) Enhanced image of left superficial parotid dissection showing the facial nerve trunk deep to superficial temporal vein. STV, Superficial Temporal Vein; RV, Retromandibular vein; MV, Maxillary vein; T, Temporal branch; Z, Zygomatic branch; B, Buccal branch; M, Marginal mandibular branch; C, Cervical branch; SMF, Stylomastoid foramen; J, Junction of STV and MV; RV(r), Retromandibular vein reflected; A.B, Anastomosing branch.

Pins; Upper white, Junction of zygomatic arch and pre auricular dissection line; Lower white, Angle of mandible; Yellow, Temporal branch crossing zygomatic arch; Red, Tragal pointer; Blue, Retromandibular vein.

Figure 2 (in publication). Normal facial nerve anatomy. (A) Labelled right facial nerve dissection showing no variation with the retromandibular vein deep to the facial nerve. (B) Unlabelled right facial nerve dissection showing no variation with the retromandibular vein deep to the facial nerve. (C) Schematic of right facial nerve superficial to retromandibular vein. STV, Superficial Temporal Vein; RV, Retromandibular vein; T, Temporal branch; Z, Zygomatic branch; B, Buccal branch; M, Marginal mandibular branch; C, Cervical branch





Appendix 2 : Dodge Dis-Spray

Revision date: 26/08/2014

Revision: 6

Supersedes date: 04/04/2012



SAFETY DATA SHEET

Dis-Spray

According to Regulation (EC) No 1907/2006, Annex II, as amended by Regulation (EU) No 453/2010

SECTION 1: Identification of the substance/mixture and of the company/undertaking

1.1. Product identifier

Product name Dis-Spray

Product number 505030

1.2. Relevant identified uses of the substance or mixture and uses advised against

Identified uses Embalming Spray

1.3. Details of the supplier of the safety data sheet

Supplier Dodge Company Ltd.
Units 11/15 Ardglan Industrial Estate,
Whitchurch, Hampshire,
RG28 7BB, United Kingdom
+44 (0)1256-893883
+44 (0)1256-893868
enquiries@dodge-uk.com

1.4. Emergency telephone number

Emergency telephone +44 (0)1256 893883 (Mon- Fri 9:00 am - 4:30 pm)

SECTION 2: Hazards identification

2.1. Classification of the substance or mixture

Classification

Physical hazards

Flam. Liq. 2 - H225

Health hazards

Eye Irrit. 2 - H319 Elicitation - EUH208 STOT SE 3 - H336

Environmental hazards

Aquatic Chronic 2 - H411

Classification (67/548/EEC or 1999/45/EC)

F; R11. Xi; R36. N; R51/53. R67

2.2. Label elements

Pictogram



Signal word

Danger

Hazard statements

Dis-Spray

H225 Highly flammable liquid and vapour.

H319 Causes serious eye irritation.

H336 May cause drowsiness or dizziness.

H411 Toxic to aquatic life with long lasting effects.

EUH208 Contains 3-Iodo-2-propynyl butylcarbamate. May produce an allergic reaction.

Precautionary statements

P210 Keep away from heat, hot surfaces, sparks, open flames and other ignition sources. No smoking.

P261 Avoid breathing vapour/spray.

P273 Avoid release to the environment.

P280 Wear protective gloves/protective clothing/eye protection/face protection.

P303+P361+P353 IF ON SKIN (or hair): Take off immediately all contaminated clothing. Rinse skin with water/shower.

P304+P340 IF INHALED: Remove person to fresh air and keep comfortable for breathing.

P305+P351+P338 IF IN EYES: Rinse cautiously with water for several minutes. Remove contact lenses, if present and easy to do. Continue rinsing.

P312 Call a POISON CENTER/doctor if you feel unwell.

P501 Dispose of contents/container in accordance with national regulations.

Contains

propan-2-ol

Supplementary precautionary statements

P240 Ground/bond container and receiving equipment.

P241 Use explosion-proof electrical equipment.

P242 Use only non-sparking tools.

P243 Take precautionary measures against static discharge.

P264 Wash contaminated skin thoroughly after handling.

P271 Use only outdoors or in a well-ventilated area.

P337+P313 If eye irritation persists: Get medical advice/attention.

P370+P378 In case of fire: Use foam, carbon dioxide, dry powder or water fog to extinguish.

P391 Collect spillage.

P403+P233 Store in a well-ventilated place. Keep container tightly closed.

P403+P235 Store in a well-ventilated place. Keep cool.

P405 Store locked up.

2.3. Other hazards

This substance is not classified as PBT or vPvB according to current EU criteria.

SECTION 3: Composition/information on ingredients**3.2. Mixtures**

propan-2-ol	50 - 100%
CAS number: 67-63-0 EC number: 200-661-7 REACH registration number: 01-2119457558-25-XXXX	
Classification	Classification (67/548/EEC or 1999/45/EC)
Flam. Liq. 2 - H225	F; R11. Xi; R36. R67
Eye Irrit. 2 - H319	
STOT SE 3 - H336	

Dis-Spray

ethanediol		0.5 - <1%
CAS number: 107-21-1 EC number: 203-473-3		
Classification		Classification (67/548/EEC or 1999/45/EC)
Acute Tox. 4 - H302		Xn; R22
quaternary ammonium compounds, benzyl-C12-18-alkyldimethyl, chlorides		0.25 - <0.5%
CAS number: 68391-01-5 EC number: 269-919-4		
M factor (Acute) = 1		
Classification		Classification (67/548/EEC or 1999/45/EC)
Acute Tox. 4 - H302		Xn; R22. C; R34. N; R50
Skin Corr. 1B - H314		
Eye Dam. 1 - H318		
Aquatic Acute 1 - H400		
3-iodo-2-propynyl butylcarbamate		0.025 - <0.25%
CAS number: 55406-53-6 EC number: 259-627-5		
M factor (Acute) = 10 M factor (Chronic) = 1		
Classification		Classification (67/548/EEC or 1999/45/EC)
Acute Tox. 4 - H302		Xn; R20/22. Xi; R37, R41. N; R50. R43
Acute Tox. 3 - H331		
Eye Dam. 1 - H318		
Skin Sens. 1 - H317		
STOT RE 1 - H372		
Aquatic Acute 1 - H400		
Aquatic Chronic 1 - H410		
triclosan		0.025 - <0.25%
CAS number: 3380-34-5 EC number: 222-182-2		
M factor (Acute) = 100 M factor (Chronic) = 100		
Classification		Classification (67/548/EEC or 1999/45/EC)
Skin Irrit. 2 - H315		Xi; R36/38. N; R50/53
Eye Irrit. 2 - H319		
Aquatic Acute 1 - H400		
Aquatic Chronic 1 - H410		

The Full Text for all R-Phrases and Hazard Statements are Displayed in Section 16.

SECTION 4: First aid measures**4.1. Description of first aid measures****General information**

If in doubt, get medical attention promptly.

Inhalation

Move affected person to fresh air and keep warm and at rest in a position comfortable for breathing. Get medical attention if any discomfort continues.

Ingestion

Rinse mouth thoroughly with water. Give a few small glasses of water or milk to drink. Get medical attention if any discomfort continues.

Skin contact

Wash skin thoroughly with soap and water. Wash contaminated clothing before reuse. Get medical attention if irritation persists after washing.

Appendix 3 : Dodge Metaflow

Revision date: 08/08/2014

Revision: 3

Supersedes date: 20/04/2012



SAFETY DATA SHEET

Metaflow

According to Regulation (EC) No 1907/2006, Annex II, as amended by Regulation (EU) No 453/2010

SECTION 1: Identification of the substance/mixture and of the company/undertaking

1.1. Product identifier

Product name Metaflow
Product number 340066

1.2. Relevant identified uses of the substance or mixture and uses advised against

Identified uses Embalming Chemical

1.3. Details of the supplier of the safety data sheet

Supplier Dodge Company Ltd.
Units 11/15 Ardglan Industrial Estate,
Whitchurch, Hampshire,
RG28 7BB, United Kingdom
+44 (0)1256-893883
+44 (0)1256-893868
enquiries@dodge-uk.com

1.4. Emergency telephone number

Emergency telephone +44 (0)1256 893883 (Mon- Fri 9:00 am - 4:30 pm)

SECTION 2: Hazards identification

2.1. Classification of the substance or mixture

Classification

Physical hazards

Not Classified

Health hazards

Eye Irrit. 2 - H319

Environmental hazards

Aquatic Chronic 3 - H412

Classification (67/548/EEC or 1999/45/EC)

Xi; R36. R52/53

2.2. Label elements

Pictogram



Signal word Warning

Hazard statements

H319 Causes serious eye irritation.
H412 Harmful to aquatic life with long lasting effects.

Precautionary statements

Metaflow

P264 Wash contaminated skin thoroughly after handling.

P273 Avoid release to the environment.

P280 Wear protective gloves/protective clothing/eye protection/face protection.

P305+P351+P338 IF IN EYES: Rinse cautiously with water for several minutes. Remove contact lenses, if present and easy to do. Continue rinsing.

P337+P313 If eye irritation persists: Get medical advice/attention.

P501 Dispose of contents/container in accordance with national regulations.

2.3. Other hazards

This product does not contain any substances classified as PBT or vPvB.

SECTION 3: Composition/information on ingredients**3.2. Mixtures**

propane-1,2-diol CAS number: 57-55-6 EC number: 200-338-0	10 - <25%
Classification Not Classified	Classification (67/548/EEC or 1999/45/EC)
trisodium 2-(carboxylatomethyl(2-hydroxyethyl)amino)ethyliminodi(acetate) CAS number: 139-89-9 EC number: 205-381-9 M factor (Acute) = 1 M factor (Chronic) = 1	1 - <2.5%
Classification Skin Irrit. 2 - H315 Eye Dam. 1 - H318 Aquatic Acute 1 - H400 Aquatic Chronic 1 - H410	Classification (67/548/EEC or 1999/45/EC) Xi; R41, R38. N; R50/53
Sodium hydroxide CAS number: 1310-73-2 EC number: 215-185-5	<0.025%
Classification Skin Corr. 1A - H314 Eye Dam. 1 - H318	Classification (67/548/EEC or 1999/45/EC) C; R35

The Full Text for all R-Phrases and Hazard Statements are Displayed in Section 16.

SECTION 4: First aid measures**4.1. Description of first aid measures****Inhalation**

Move affected person to fresh air and keep warm and at rest in a position comfortable for breathing. Get medical attention if symptoms are severe or persist.

Ingestion

Rinse mouth. Give a few small glasses of water or milk to drink. Get medical attention if any discomfort continues.

Skin contact

Wash with plenty of water. Wash contaminated clothing before reuse.

Eye contact

Remove any contact lenses and open eyelids wide apart. Rinse cautiously with water for several minutes. Get medical attention if irritation persists after washing.

Appendix 4 : Dodge Rectifiant

Revision date: 11/08/2014

Revision: 3

Supersedes date: 08/10/2012



SAFETY DATA SHEET

Rectifiant

According to Regulation (EC) No 1907/2006, Annex II, as amended by Regulation (EU) No 453/2010

SECTION 1: Identification of the substance/mixture and of the company/undertaking

1.1. Product identifier

Product name Rectifiant
Product number 320008

1.2. Relevant identified uses of the substance or mixture and uses advised against

Identified uses Embalming Chemical

1.3. Details of the supplier of the safety data sheet

Supplier Dodge Company Ltd.
Units 11/15 Ardglan Industrial Estate,
Whitchurch, Hampshire,
RG28 7BB, United Kingdom
+44 (0)1256-893883
+44 (0)1256-893868
enquiries@dodge-uk.com

1.4. Emergency telephone number

Emergency telephone +44 (0)1256 893883 (Mon- Fri 9:00 am - 4:30 pm)

SECTION 2: Hazards identification

2.1. Classification of the substance or mixture

Classification

Physical hazards

Not Classified

Health hazards

Eye Dam. 1 - H318

Environmental hazards

Aquatic Chronic 2 - H411

Classification (67/548/EEC or 1999/45/EC)

Xi; R41. N; R51/53

2.2. Label elements

Pictogram



Signal word

Danger

Hazard statements

H318 Causes serious eye damage.

H411 Toxic to aquatic life with long lasting effects.

Precautionary statements

Rectifiant

P273 Avoid release to the environment.

P280 Wear protective gloves/protective clothing/eye protection/face protection.

P305+P351+P338 IF IN EYES: Rinse cautiously with water for several minutes. Remove contact lenses, if present and easy to do. Continue rinsing.

P310 Immediately call a POISON CENTER/doctor.

P391 Collect spillage.

P501 Dispose of contents/container in accordance with national regulations.

Contains

trisodium 2-(carboxylatomethyl(2-hydroxyethyl)amino)ethyliminodi(acetate)

2.3. Other hazards

This product does not contain any substances classified as PBT or vPvB.

SECTION 3: Composition/information on ingredients**3.2. Mixtures**

trisodium 2-(carboxylatomethyl(2-hydroxyethyl)amino)ethyliminodi(acetate)		5 - <10%
CAS number: 139-89-9 EC number: 205-381-9		
M factor (Acute) = 1 M factor (Chronic) = 1		
Classification	Classification (67/548/EEC or 1999/45/EC)	
Skin Irrit. 2 - H315	Xi; R41, R38, N; R50/53	
Eye Dam. 1 - H318		
Aquatic Acute 1 - H400		
Aquatic Chronic 1 - H410		
propane-1,2-diol		5 - <10%
CAS number: 57-55-6 EC number: 200-338-0		
Classification	Classification (67/548/EEC or 1999/45/EC)	
Not Classified		
Sodium hydroxide		0.025 - <0.25%
CAS number: 1310-73-2 EC number: 215-185-5		
Classification	Classification (67/548/EEC or 1999/45/EC)	
Skin Corr. 1A - H314	C; R35	
Eye Dam. 1 - H318		

The Full Text for all R-Phrases and Hazard Statements are Displayed in Section 16.

SECTION 4: First aid measures**4.1. Description of first aid measures****Inhalation**

Move affected person to fresh air and keep warm and at rest in a position comfortable for breathing. Get medical attention if symptoms are severe or persist.

Ingestion

Rinse mouth. Give a few small glasses of water or milk to drink. Get medical attention if any discomfort continues.

Skin contact

Wash with plenty of water. Wash contaminated clothing before reuse.

Eye contact

Remove any contact lenses and open eyelids wide apart. Rinse cautiously with water for several minutes. Get medical attention immediately.

Appendix 5 : Dodge Introfiant Arterial

Revision date: 05/08/2014

Revision: 5

Supersedes date: 12/07/2013



SAFETY DATA SHEET

Introfiant Arterial

According to Regulation (EC) No 1907/2006, Annex II, as amended by Regulation (EU) No 453/2010

SECTION 1: Identification of the substance/mixture and of the company/undertaking

1.1. Product identifier

Product name Introfiant Arterial
Product number 105028

1.2. Relevant identified uses of the substance or mixture and uses advised against

Identified uses Embalming Chemical

1.3. Details of the supplier of the safety data sheet

Supplier Dodge Company Ltd.
Units 11/15 Ardglan Industrial Estate,
Whitchurch, Hampshire,
RG28 7BB, United Kingdom
+44 (0)1256-893883
+44 (0)1256-893868
enquiries@dodge-uk.com

1.4. Emergency telephone number

Emergency telephone +44 (0)1256 893883 (Mon- Fri 9:00 am - 4:30 pm)

SECTION 2: Hazards identification

2.1. Classification of the substance or mixture

Classification

Physical hazards

Flam. Liq. 3 - H226

Health hazards

Acute Tox. 4 - H302 Acute Tox. 3 - H311 Acute Tox. 3 - H331 Skin Corr. 1B - H314 Eye Dam. 1 - H318 Skin Sens. 1 - H317
Muta. 2 - H341 Carc. 1B - H350 Repr. 1B - H360FD STOT SE 2 - H371 STOT SE 3 - H335

Environmental hazards

Not Classified

Classification (67/548/EEC or 1999/45/EC)

T; R23/24. Xn; R22, R68/20/21/22. C; R34. Xi; R37. Carc. Cat. 2 R45. Muta. Cat. 3 R68. Repr. Cat. 1 R60, R61. R10, R43

2.2. Label elements

Pictogram



Signal word Danger

Hazard statements

Introfiant Arterial

H226 Flammable liquid and vapour.
H302 Harmful if swallowed.
H311+H331 Toxic in contact with skin or if inhaled.
H314 Causes severe skin burns and eye damage.
H317 May cause an allergic skin reaction.
H335 May cause respiratory irritation.
H341 Suspected of causing genetic defects.
H350 May cause cancer.
H360FD May damage fertility. May damage the unborn child.
H371 May cause damage to organs .

Precautionary statements

P201 Obtain special instructions before use.
P210 Keep away from heat, hot surfaces, sparks, open flames and other ignition sources. No smoking.
P280 Wear protective gloves/protective clothing/eye protection/face protection.
P301+P330+P331 IF SWALLOWED: Rinse mouth. Do NOT induce vomiting.
P303+P361+P353 IF ON SKIN (or hair): Take off immediately all contaminated clothing. Rinse skin with water/shower.
P304+P340 IF INHALED: Remove person to fresh air and keep comfortable for breathing.
P305+P351+P338 IF IN EYES: Rinse cautiously with water for several minutes. Remove contact lenses, if present and easy to do. Continue rinsing.
P311 Call a POISON CENTER/doctor.
P333+P313 If skin irritation or rash occurs: Get medical advice/attention.
P501 Dispose of contents/container in accordance with national regulations.

Contains

formaldehyde, Methanol, disodium tetraborate decahydrate

Supplementary precautionary statements

Introfant Arterial

P202 Do not handle until all safety precautions have been read and understood.
 P240 Ground/bond container and receiving equipment.
 P241 Use explosion-proof electrical equipment.
 P242 Use only non-sparking tools.
 P243 Take precautionary measures against static discharge.
 P260 Do not breathe vapour/spray.
 P261 Avoid breathing vapour/spray.
 P264 Wash contaminated skin thoroughly after handling.
 P270 Do not eat, drink or smoke when using this product.
 P271 Use only outdoors or in a well-ventilated area.
 P272 Contaminated work clothing should not be allowed out of the workplace.
 P301+P310 IF SWALLOWED: Immediately call a POISON CENTER/doctor.
 P302+P352 IF ON SKIN: Wash with plenty of water.
 P308+P311 IF exposed or concerned: Call a POISON CENTER or doctor.
 P308+P313 IF exposed or concerned: Get medical advice/attention.
 P312 Call a POISON CENTER/doctor if you feel unwell.
 P321 Specific treatment (see medical advice on this label).
 P361+P364 Take off immediately all contaminated clothing and wash it before reuse.
 P362+P364 Take off contaminated clothing and wash it before reuse.
 P363 Wash contaminated clothing before reuse.
 P370+P378 In case of fire: Use foam, carbon dioxide, dry powder or water fog to extinguish.
 P403+P233 Store in a well-ventilated place. Keep container tightly closed.
 P403+P235 Store in a well-ventilated place. Keep cool.
 P405 Store locked up.

2.3. Other hazards

This product does not contain any substances classified as PBT or vPvB.

SECTION 3: Composition/information on ingredients**3.2. Mixtures**

formaldehyde		25 - <50%
CAS number: 50-00-0 EC number: 200-001-8		
Classification	Classification (67/548/EEC or 1999/45/EC)	
Acute Tox. 3 - H301	T; R23/24/25. C; R34. Xi; R37. Carc. Cat. 2 R45. Muta. Cat. 3 R68. R43	
Acute Tox. 3 - H311		
Acute Tox. 3 - H331		
Skin Corr. 1B - H314		
Eye Dam. 1 - H318		
Skin Sens. 1 - H317		
Muta. 2 - H341		
Carc. 1B - H350		
STOT SE 3 - H335		

Introfiant Arterial

Methanol		5 - <10%
CAS number: 67-56-1 EC number: 200-659-6 REACH registration number: 01-2119433307-44-XXXX		
Classification		Classification (67/548/EEC or 1999/45/EC)
Flam. Liq. 2 - H225		
Acute Tox. 3 - H301		
Acute Tox. 3 - H311		
Acute Tox. 3 - H331		
STOT SE 1 - H370		
disodium tetraborate decahydrate		5 - <10%
CAS number: 1330-43-4 EC number: 215-540-4		
Classification		Classification (67/548/EEC or 1999/45/EC)
Repr. 1B - H360FD		Repr. Cat. 1 R60, R61

The Full Text for all R-Phrases and Hazard Statements are Displayed in Section 16.

SECTION 4: First aid measures**4.1. Description of first aid measures****General information**

In case of accident or if you feel unwell, seek medical advice immediately (show the label where possible).

Inhalation

Move affected person to fresh air and keep warm and at rest in a position comfortable for breathing. If breathing stops, provide artificial respiration. Get medical attention immediately.

Ingestion

Rinse nose and mouth with water. Do not induce vomiting unless under the direction of medical personnel. Get medical attention immediately.

Skin contact

Remove contaminated clothing immediately and wash skin with soap and water. Get medical attention immediately.

Eye contact

Remove any contact lenses and open eyelids wide apart. Rinse immediately with plenty of water. Continue to rinse for at least 15 minutes and get medical attention.

Protection of first aiders

First aid personnel should wear appropriate protective equipment during any rescue.

4.2. Most important symptoms and effects, both acute and delayed**General information**

The severity of the symptoms described will vary dependent on the concentration and the length of exposure. Suspected of causing genetic defects. May cause cancer. The product contains a sensitising substance. May damage fertility or the unborn child. May cause damage to organs .

Inhalation

Chemical burns. May cause respiratory irritation. Symptoms following overexposure may include the following: Headache. Nausea, vomiting.

Ingestion

Causes burns. May cause stomach pain or vomiting. Ingestion of large amounts may cause unconsciousness.

Skin contact

Causes burns. Toxic in contact with skin. May cause an allergic skin reaction.

Eye contact

Contact with concentrated chemical may very rapidly cause severe eye damage, possibly loss of sight.

Appendix 6 : Dodge Restorative

Revision date: 11/08/2014

Revision: 1

Supersedes date: 01/05/2007



SAFETY DATA SHEET

Restorative

According to Regulation (EC) No 1907/2006, Annex II, as amended by Regulation (EU) No 453/2010

SECTION 1: Identification of the substance/mixture and of the company/undertaking

1.1. Product identifier

Product name Restorative
Product number 360015

1.2. Relevant identified uses of the substance or mixture and uses advised against

Identified uses Embalming Chemical

1.3. Details of the supplier of the safety data sheet

Supplier Dodge Company Ltd.
Units 11/15 Ardglan Industrial Estate,
Whitchurch, Hampshire,
RG28 7BB, United Kingdom
+44 (0)1256-893883
+44 (0)1256-893868
enquiries@dodge-uk.com

1.4. Emergency telephone number

Emergency telephone +44 (0)1256 893883 (Mon- Fri 9:00 am - 4:30 pm)

SECTION 2: Hazards identification

2.1. Classification of the substance or mixture

Classification

Physical hazards

Not Classified

Health hazards

Not Classified

Environmental hazards

Aquatic Chronic 3 - H412

Classification (67/548/EEC or 1999/45/EC)

R52/53

2.2. Label elements

Hazard statements

H412 Harmful to aquatic life with long lasting effects.

Precautionary statements

P273 Avoid release to the environment.

P501 Dispose of contents/container in accordance with national regulations.

2.3. Other hazards

This product does not contain any substances classified as PBT or vPvB.

SECTION 3: Composition/information on ingredients

3.2. Mixtures

Restorative

propane-1,2-diol		10 - <25%
CAS number: 57-55-6 EC number: 200-338-0		
Classification	Classification (67/548/EEC or 1999/45/EC)	
Not Classified		
propan-2-ol		2.5 - <5%
CAS number: 67-63-0 EC number: 200-661-7 REACH registration number: 01-2119457558-25-XXXX		
Classification	Classification (67/548/EEC or 1999/45/EC)	
Flam. Liq. 2 - H225	F; R11. Xi; R36. R67	
Eye Irrit. 2 - H319		
STOT SE 3 - H336		
lanolin, ethoxylated polymer		1 - <2.5%
CAS number: 61790-81-6 EC number: —		
Classification	Classification (67/548/EEC or 1999/45/EC)	
Aquatic Chronic 4 - H413	R53	
trisodium 2-(carboxylatomethyl(2-hydroxyethyl)amino)ethyliminodi(acetate)		0.25 - <0.5%
CAS number: 139-89-9 EC number: 205-381-9		
M factor (Acute) = 1 M factor (Chronic) = 1		
Classification	Classification (67/548/EEC or 1999/45/EC)	
Skin Irrit. 2 - H315	Xi; R41, R38. N; R50/53	
Eye Dam. 1 - H318		
Aquatic Acute 1 - H400		
Aquatic Chronic 1 - H410		
Sodium hydroxide		<0.025%
CAS number: 1310-73-2 EC number: 215-185-5		
Classification	Classification (67/548/EEC or 1999/45/EC)	
Skin Corr. 1A - H314	C; R35	
Eye Dam. 1 - H318		

The Full Text for all R-Phrases and Hazard Statements are Displayed in Section 16.

SECTION 4: First aid measures

4.1. Description of first aid measures

Inhalation

Move affected person to fresh air and keep warm and at rest in a position comfortable for breathing. Get medical attention if symptoms are severe or persist.

Ingestion

Rinse mouth. Give a few small glasses of water or milk to drink. Get medical attention if any discomfort continues.

Skin contact

Wash with plenty of water. Wash contaminated clothing before reuse.

Eye contact

Remove any contact lenses and open eyelids wide apart. Rinse cautiously with water for several minutes. Get medical attention if irritation persists after washing.

Appendix 7: DWI Data pre processing

Standardising diffusion input files

DICOM

The output files from the Philips scanner can be DICOM (**Digital Imaging and Communications in Medicine (DICOM)**) files, (this is the global industry standard for handling and communicating medical imaging in clinical contexts ⁹⁷). Each 2D image slice, in DICOM format, has its own file, which results in thousands of separate files in for each individual scan because of the concentration of our diffusion data collection. Processing such a large volume is impracticable and significantly error prone. Thus, often the volume is converted into more manageable formats (two to three files per subject that can contain all the relevant diffusion data) by the Phillips scanner. The latest analysis software tools now routinely output these file types, which include

.par/.rec

A propriety MRI data format developed by Philips (Philips Healthcare, Best, The Netherlands). The .par file contains information about the scan protocol. It is in ASCII text header. The .rec file would incorporate the MR data as a single large binary code file (<http://www.diffusion-imaging.com/2015/10/dti-tutorial-1-from-scanner-to-tensor.html>)

.bval/.bvec/.nii

This format is comprised of a .bval (b value) and .bvec (b vector) pair in addition to a NifTI (Neuroimaging Informatics Technology Initiative) file that contains the MR data. The NifTI (.nii) format is an increasingly popular standard for manipulation and storage and of MR data. It is a combined MR data and meta-data style.

.xml/.rec

A recent development by Phillips is the .xml . (Extensible Markup Language) file to replace the .rec file. (Extensible Markup Language). This file format is usually much larger, but allows the user to read the scan protocol information directly using any typical web browser. (<https://www.w3.org/TR/xml11/#charsets>)

4D NifTI

To enable use of the ExploreDTI program, all source data must be converted into a “4D NifTi” file. This is typically a 3D series with a temporal/diffusion weighted dimension ⁹⁸ which can be achieved by the use of “dcm2nii” tool developed by Chris Rorden (see <http://www.cabiatl.com/mricro/mricron/dcm2nii.html> and <https://www.nitrc.org/projects/dcm2nii/> and <http://brainybehavior.com/neuroimaging/2010/05/converting-dicom-images-to-nifti-images/> for further information). This tool allows for simple, trustworthy and speedy conversion of all three file types already mentioned into a dual 4D NifTi and b matrix text (.txt) files. The B-matrix equals the b-value and the gradient directions used to acquire the scan (in our cases our b-value= 400 - 1500 s/mm² and 61 gradient directions).

Therefore, at the end of this step, each cadaveric subject and our live subjects had a NifTi (.nii) and text (.txt) file that contains all the relevant diffusion data and associated parameters. Of note, each subject also had a T1-weighted image (.nii file) for the purpose of co-registration of the diffusion data in order to allow EPI deformation correction.

Signal Drift

The high toll placed on the system due to the diffusion gradients and echo-planar imaging (EPI) readout can cause heating effects that reduce the scanner's temporal stability (i.e. the

signal ‘drifts’ over the day). This can result in a reduction in global signal intensity in diffusion MRI ⁹⁹. A corrective plugin within ExploreDTI, performs a linear and quadratic correction on the data, which can normalise the data for any signal drift¹⁰⁰.

Gibbs Correction

Gibbs-ringing is a well recognised artefact which manifests as spurious oscillations in the vicinity of sharp gradients within the image at tissue boundaries ¹⁰¹. It can also be corrected with the aid of a plugin in ExploreDTI which applies a total-variation computation - a mathematical correction tool applied across the data which penalises for noise at sharp boundaries in the image ¹⁰², but preserves the useful features of the data.

Converting *.nii/txt to *.mat

ExploreDTI is a Matlab based program. Matlab (Matrix Laboratory) (www.mathworks.com) is an exclusive programming language and multi-paradigm numerical computing environment developed by Mathworks Inc. which allows for matrix controls, plotting of data along with functions and the application of algorithms. All diffusion data collected needed conversion from standard diffusion formats to Matlab readable files. This was done by converting DWI (*.nii) and associated B-matrices (*.txt) files to a single *.mat file, thereby permitting ExploreDTI to consolidate all the relevant diffusion information into one single file for computational operation and visualisation. This conversion was realised through the ExploreDTI data conversion tool (see figure 13).

As can be evidenced from Figure 13, problems with spatial and gradient orientations of the diffusion data (i.e. the three dimensions, inferior – superior, anterior-posterior, right-left) can be rectified (see subsequent section).

Checking Orientation of generated *.mat file

Once generated, each new Mat file needed to analysis to ensure correct orientation by checking directionality of the ‘glyphs’ in specific areas of the brain image obtained. A tensor glyph is a visualisation method that allows appreciation of the overall direction (or vector) of diffusion at each voxel (commonly referred to as the diffusion tensor). This is made possible by our knowledge of the directionality of certain large white matter tracts of the brain (e.g. corpus callosum) thereby enabling the correct assessment of the orientation of the *.mat file by analysing the glyphs directions in these areas. This was performed and verified in all our scans in ExploreDTI by loading the generated *.mat file, locating an appropriate region of interest (ROI) to isolate a well known intra cerebral tract and using the glyph plugin (menu-draw-glyph-object) to verify. The tracts we utilized to analyze the glyph orientation were; a) corpus callosum (across L-R), b) corona radiata (vertical I-S) and c) superior longitudinal fasciculus (lengthways A-P). If the glyph readings did not match the expected direction (e.g. glyphs in the corpus callosum pointing A-P instead of L-R), the *.mat file was corrected and recalculated by the adjustment of the gradient orientations as needed (see previous step and specifically figure 12). This fundamental step ensures correct propagation of the diffusion tensors, essential to form the deterministic streamlines and construct the characteristic fiber tracts that can be analyzed and anatomically verified.

Correcting for eddy currents and Head motion

Magnetic resonance imaging is prone to many artifacts that can affect data acquisition, leading to issues with model parameter estimations (i.e. DT maps) and subsequent difficulties with computed measures (e.g. FA maps). Therefore, artefact correction is of paramount importance in post-acquisition processing¹⁰³.

Two main artefacts, particularly relevant to diffusion acquisitions, that may destroy voxel-wise correspondence across all the diffusion weighted images are head motion and eddy current distortions^{104, 105}.

Eddy currents occur in diffusion weighted imaging as a result of the rapid switching of large diffusion gradient pulses¹⁰⁶. These large swings in magnetic gradients can produce currents within the various conducting surfaces of the MRI scanner resulting in image distortions (generalised shift and shear of images and image contraction in severe cases).

Head motion

Diffusion weighted imaging is very sensitive to motion, as a result of phase shifts produced

- a) microscopically by diffusion-driven molecular displacements of water, and
- b) macroscopically by the effects of normal pulsation, breathing and head motion. This sensitivity increases with rising strength and durations of gradient pulses (b-value)¹⁰⁷.

Rectifying both artefacts required registration to the non-diffusion weighted b0 image. As the diffusion weighted image contrast is both orientation and spatially dependent, the B-matrix (containing the diffusion gradient information) was also adjusted so the orientation remained correctly preserved.

Eddy currents, in general, can be remedied with an affine¹ registration to the non-diffusion weighted b0 image. A further step to rectify the issue of cardiac pulsation is by the use of

¹ In rigid registration, it is the *position* of the diffusion weighted image relative to the b0 image only that changes (allowing translation along the x,y,z axes as well as rotation around the x,y,z axes – 6 degrees of freedom). Affine registration allows change of position *and* geometry of the diffusion weighted image (the 6 degrees of combined

adaptive acquisition sequence timing parameter adjustment to harmonize the data acquisition with the cardiac pulse period; thereby minimising it's effect on the data. In live subject scans, these acquisition and scanning modifications are often very time consuming and thereby are often not included. However, an alternative adjustment is possible in ExploreDTI through the "Correct for Subject Motion and EC" plugin which performs this process post acquisition, hence saving the subject prolonged scanning time during the acquisition phase.

Correcting for EPI deformations

Another artefact that reduces diffusion magnetic resonance data quality is as a result of the so-called susceptibility-induced off-resonance fields. This phenomenon causes non-linear geometric image deformations. The acquisition of additional data during the scan by reversing the polarity of the phase-encoding direction can minimise this artefactual effect. However, once again, duration of scanning and comfort constraints prevented the adoption of this technique for our live subject scans. Rather, by using a specialized plugin in ExploreDTI, which allowed for registration and warping of the diffusion weighted image to the acquired T1 image, the EPI deformations were corrected (T1 images aren't susceptible to the same inhomogeneities in the EPI sequence) ¹⁰⁸

translation and rotation as above, in addition to stretching along the x,y,z axes plus shearing/skewing the xy, yz and xz plane - 12 degrees of freedom).